UNIVERSITY
OF MICHIGAN
FEB 27 1956
CHEMISTRY
LIBRARY

Journal of Research

of the National Bureau of Standards

DECEMBER 1955

VOLUME 55 NUMBER 6

U. S. DEPARTMENT OF COMMERCE
Sinclair Weeks, Secretary
NATIONAL BUREAU OF STANDARDS
A. V. Astin, Director

DECEMBER • 1955
VOLUME • 55
NUMBER • 6

JOURNAL OF RESEARCH

of the

NATIONAL BUREAU OF STANDARDS

PERIODICALS OF THE NATIONAL BUREAU OF STANDARDS

(Published monthly)

The National Bureau of Standards is engaged in fundamental and applied research in physics, chemistry, mathematics, and engineering. Projects are conducted in fifteen fields: electricity and electronics, optics and metrology, heat and power, atomic and radiation physics, chemistry, mechanics, organic and fibrous materials, metallurgy, mineral products, building technology, applied mathematics, data processing systems, cryogenic engineering, radio propagation, and radio standards. The Bureau has custody of the national standards of measurement and conducts research leading to the improvement of scientific and engineering standards and of techniques and methods of measurement. Testing methods and instruments are developed; physical constants and properties of materials are determined; and technical processes are investigated.

JOURNAL OF RESEARCH

The Journal presents research papers by authorities in the specialized fields of physics, mathematics, chemistry, and engineering. Complete details of the work are presented, including laboratory data, experimental procedures, and theoretical and mathematical analyses. Annual subscription: domestic, $4.00; $1.25 additional for foreign mailing.

TECHNICAL NEWS BULLETIN

Summaries of current research at the National Bureau of Standards are published each month in the Technical News Bulletin. The articles are brief, with emphasis on the results of research, chosen on the basis of their scientific or technologic importance. Lists of all Bureau publications during the preceding month are given, including Research Papers, Handbooks, Applied Mathematics Series, Building Materials and Structures Reports, Miscellaneous Publications, and Circulars. Each issue contains 12 or more two-column pages; illustrated. Annual subscription: domestic, $1.00; 35 cents additional for foreign mailing.

BASIC RADIO PROPAGATION PREDICTIONS

The Predictions provide the information necessary for calculating the best frequencies for communication between any two points in the world at any time during the given month. The data are important to all users of long-range radio communications and navigation, including broadcasting, airline, steamship, and wireless services, as well as to investigators of radio propagation and ionosphere. Each issue, covering a period of one month, is released three months in advance and contains 16 large pages, including pertinent charts, drawings, and tables. Annual subscription: domestic, $1.00; 25 cents additional for foreign mailing.

Order all publications from the Superintendent of Documents
U. S. Government Printing Office, Washington 25, D. C.

The printing of this publication has been approved by the Director of the Bureau of the Budget, May 12, 1953.

Journal of Research of the National Bureau of Standards Vol. 55, No. 6, December 1955 Research Paper 2633

The First Spectrum of Barium, Ba I

Henry Norris Russell [1] and Charlotte E. Moore

The analysis of the Ba I spectrum is presented. Although a monograph based on homogeneous observations is needed, this paper has been prepared from existing references, to present unpublished analysis by the senior author and, also, because Ba I is important in the history of atomic spectra. The first regularities attributed to two excited electrons were found in Ba I as well as in Ca I and Sr I.

Three tables are included: A complete term list; a complete line list containing all observed and all classified lines; a table giving the estimated intensities of the observed combinations. There are approximately 390 classified lines.

The limit, derived from well-established series, is 42032.4 K, giving an ionization potential of 5.210 volts.

The Ba I spectrum occupies an important position in the history of atomic spectra. Although regular series terms were reported by Saunders, Paschen-Götze, and Fowler (1920 to 1922) [1][2] the first regularities attributed to two excited electrons were found in Ba I, as well as in Ca I and Sr I, in 1925 [2].

Shenstone and Russell suggested some revisions in the early analysis and discussed the perturbed series of Ba I in 1932 [3]. They adopted as the ionization limit, i. e., the absolute value of the ground state, the value 42032.4 K, giving an ionization potential 5.210 volts.

Although the spectrum has been studied thoroughly, a monograph based on a complete homogeneous line list is needed. In view of the fact that this does not appear to be forthcoming, a complete line list and multiplet array have been prepared from the existing literature references, and from unpublished analysis by the senior author. Uniform notation has been adopted, and the decimals of all energy levels have been revised. Sullivan and Burns (table 2, ref. C) improved the values of a number of energy levels from their interferometric measurements of selected lines. Starting with these three-place values, the rest were revised from a study of all observed combinations.

The complete term list is given in table 1, which is self-explanatory. The terms are listed in the following order:

(1) Terms due to the equivalent electron pairs $6s^2$, $6p^2$, and $5d^2$ so far as known.

(2) The regular series of triplet and singlet terms having as limit the ground term in Ba II $6s\ ^2S_{0\frac{1}{2}}$, given in the order of the running electrons ns, np, nd, and nf.

(3) The triplet and singlet terms produced by two excited electrons, having as limit the term $5d\ ^2D$ in Ba II, arranged in the same order of running electrons. The designations for these terms have primes attached to the running electrons to denote the higher limit term in Ba II.

B. E. Moore observed the Zeeman effect in Ba I in 1908 [4] and, so far as is known to the present authors, his work has never been superseded. His measurements of $\Delta\lambda/\lambda^2$ have been divided by the correction factor 1.09, a factor adopted to reduce them to the theoretical Landé patterns for a very few well-known lines. For unresolved patterns the formulas for blends given by Shenstone and Blair [5] have been used to determine observed g-values. The results obtained from Moore's observations are as follows:

Desig.	Obs. g	Desig.	Obs. g	Desig.	Obs. g	Desig.	Obs. g
$6p^2\ ^3P_2$	1.56	$5d\ ^3D_3$	1.38	$4f\ ^3F_4^?$	1.48	$6p'\ ^3P_2^?$	1.52
$^3P_1$	1.53	$^3D_2$	1.18	$^3F_3^?$	1.09	$^3P_1^?$	1.52
$6p^2\ ^1D_2$	1.21	$^3D_1$	0.53	$^3F_2^?$	0.69	$6p'\ ^1P_1^?$	1.02
$6p\ ^3P_2^?$	1.52	$6d\ ^3D_3$	1.32	$4f\ ^1F_3^?$	0.99	$6p'\ ^3D_3^?$	1.32
$^3P_1^?$	1.45	$^3D_2$	1.11:			$^3D_2^?$	1.16
$6p\ ^1P_1^?$	1.02	$5d\ ^1D_2$	1.00			$^3D_1^?$	0.54
$7p\ ^1P_1^?$	1.07					$6d'\ ^1F_3^?$	1.09
						$6d'\ ^1F_3$	1.50

Table 2 contains all of the observed and classified lines of Ba I. The letter in column 1 indicates the literature reference from which the wavelength in column 2 is quoted. The bibliography of these references is given at the end of this table. Two sets of intensities are quoted in column 3. The left-hand entry is from the reference source indicated in column 1, except for those in parentheses, which are arc intensities estimated by Exner and Haschek (ref. G). The intensities in parentheses are entered for the lines observed with the interferometer by Burns and Sullivan. The right-hand entries in column 3 are the arc intensity and temperature class estimated by A. S. King [6]. Brackets denote King's estimated intensity in the furnace spectrum, in cases where this spectrum gives better resolution than his arc spectrum. Column 4 contains the vacuum wave number in cm^{-1}, labeled K for kayser. It is followed by ΔK, the difference between the observed wave number and the wave number calculated from the energy levels. The last column gives the multiplet designation in the notation of table 1. There are approximately 390 classified lines in table 2.

[1] Princeton University Observatory, Princeton, N. J.
[2] Figures in brackets indicate the literature references at the end of this text.

TABLE 1. Ba I terms

Designation	Level	Interval
$6s^2\ {}^1S_0$	0.00	
$5d^2\ {}^3P_2$	23918.94	438.93
$\quad {}^3P_1$	23480.01	270.90
$\quad {}^3P_0$	23209.11	
$5d^2\ {}^1D_2$	23062.06	
$6p^2\ {}^3P_2$	35616.947	793.527
$\quad {}^3P_1$	34823.420	329.522
$\quad {}^3P_0$	34493.898	
$6p^2\ {}^1D_2$	35344.423	
$6p^2\ {}^1S_0$	34370.78	
$6s(^2S)ns$		
$7s\ {}^3S_1$	26160.284	
$8s\ {}^3S_1$	33905.349	
$9s\ {}^3S_1$	37095.492	
$10s\ {}^3S_1$	38662.91	
$11s\ {}^3S_1$	39624.69:	
$7s\ {}^1S_0$	28230.08	
$8s\ {}^1S_0$	37041.00	
$9s\ {}^1S_0$	38267.59	
$6s(^2S)np$		
$6p\ {}^3P_2^\circ$	*13514.738*	878.122
$\quad {}^3P_1^\circ$	*12636.616*	370.595
$\quad {}^3P_0^\circ$	*12266.021*	
$7p\ {}^3P_2^\circ$	*30987.277*	171.715
$\quad {}^3P_1^\circ$	*30815.562*	72.029
$\quad {}^3P_0^\circ$	*30743.533*	
$6p\ {}^1P_1^\circ$	*18080.264*	
$7p\ {}^1P_1^\circ$	*32547.076*	
$8p\ {}^1P_1^\circ$	*35892.518*	
$9p\ {}^1P_1^\circ$	*37774.50*	
$10p\ {}^1P_1^\circ$	*39308.74*	
$11p\ {}^1P_1^\circ$	*39984.75*	
$12p\ {}^1P_1^\circ$	*40421.23*	
$6s(^2S)nd$		
$5d\ {}^3D_3$	9596.551	381.033
$\quad {}^3D_2$	9215.518	181.533
$\quad {}^3D_1$	9033.985	
$6d\ {}^3D_3$	30818.110	67.441
$\quad {}^3D_2$	30750.669	55.075
$\quad {}^3D_1$	30695.594	
$7d\ {}^3D_3$	35785.302	23.691
$\quad {}^3D_2$	35762.211	52.903
$\quad {}^3D_1$	35709.308	
$8d\ {}^3D_3$	37988.485	14.294
$\quad {}^3D_2$	37974.191	12.272
$\quad {}^3D_1$	37961.919	
$9d\ {}^3D_3$	39185.75	27.86
$\quad {}^3D_2$	39157.89	17.19
$\quad {}^3D_1$	39140.70	

Designation	Level	Interval
$6s(^2S)nd$—continued		
$10d\ {}^3D_3$	39905.15	10.62
$\quad {}^3D_2$	39894.53	2.34
$\quad {}^3D_1$	39892.19	
$11d\ {}^3D_3$	40382.68	2.36
$\quad {}^3D_2$	40380.32	
$\quad {}^3D_1$		
$5d\ {}^1D_2$	11395.382	
$6d\ {}^1D_2$	30236.815	
$7d\ {}^1D_2$	37434.956	
$8d\ {}^1D_2$	38556.18	
$9d\ {}^1D_2$	39334.94	
$6s(^2S)nf$		
$4f\ {}^3F_4^\circ$	*34630.809*	14.126
$\quad {}^3F_3^\circ$	*34616.683*	13.881
$\quad {}^3F_2^\circ$	*34602.802*	
$5f\ {}^3F_4^\circ$	*37524.184*	105.217
$\quad {}^3F_3^\circ$	*37418.967*	24.042
$\quad {}^3F_2^\circ$	*37394.925*	
$6f\ {}^3F_4^\circ$	*38825.265*	6.847
$\quad {}^3F_3^\circ$	*38818.418*	2.683
$\quad {}^3F_2^\circ$	*38815.735*	
$7f\ {}^3F_4^\circ$	*39683.02*	2.40
$\quad {}^3F_3^\circ$	*39680.62*	2.56
$\quad {}^3F_2^\circ$	*39678.06*	
$8f\ {}^3F_4^\circ$	*40244.02*	2.65
$\quad {}^3F_3^\circ$	*40241.37*	2.46
$\quad {}^3F_2^\circ$	*40238.91*	
$9f\ {}^3F_4^\circ$	*40627.78*	5.98
$\quad {}^3F_3^\circ$	*40621.80*	7.64
$\quad {}^3F_2^\circ$	*40614.16*	
$10f\ {}^3F_4^\circ$	*40897.07*	−1.62
$\quad {}^3F_3^\circ$	*40898.69*	3.42
$\quad {}^3F_2^\circ$	*40895.27*	
$11f\ {}^3F_4^\circ$	*41096.50*	−0.38
$\quad {}^3F_3^\circ$	*41096.88*	−3.37
$\quad {}^3F_2^\circ$	*41100.25*	
$12f\ {}^3F_4^\circ$	*41247.58*	0.54
$\quad {}^3F_3^\circ$	*41247.04*	−3.52
$\quad {}^3F_2^\circ$	*41250.56*	
$13f\ {}^3F_4^\circ$	*41364.65*	0.29
$\quad {}^3F_3^\circ$	*41364.36*	
$\quad {}^3F_2^\circ$		
$14f\ {}^3F_{3,2}^\circ$	*41456.78*	
$15f\ {}^3F_{3,2}^\circ$	*41530.65*	
$4f\ {}^1F_3^\circ$	*34736.423*	
$5f\ {}^1F_3^\circ$	*37282.175*	
$6f\ {}^1F_3^\circ$	*38884.00*	
$7f\ {}^1F_3^\circ$	*39705.11*	
$8f\ {}^1F_3^\circ$	*40257.63*	
$9f\ {}^1F_3^\circ$	*40614.15*	
$5d(^2D)ns$		
$7s'\ {}^3D_3$	33526.41	582.81
$\quad {}^3D_2$	32943.60	138.61
$\quad {}^3D_1$	32804.99	
$7s'\ {}^1D_2$	33795.84	

Designation	Level	Interval
$5d(^2S)np$		
$6p'\ {}^3P_2^\circ$	*25956.549*	252.409
$\quad {}^3P_1^\circ$	*25704.140*	61.983
$\quad {}^3P_0^\circ$	*25642.157*	
$7p'\ {}^3P_2^\circ$	*37282.08*	292.06
$\quad {}^3P_1^\circ$	*36990.016*	82.01
$\quad {}^3P_0^\circ$	*36908.01*	
$6p'\ {}^1P_1^\circ$	*28554.257*	
$7p'\ {}^1P_1^\circ$	*38499.852*	
$6p'\ {}^3D_3^\circ$	*24979.859*	448.323
$\quad {}^3D_2^\circ$	*24531.536*	339.479
$\quad {}^3D_1^\circ$	*24192.057*	
$7p'\ {}^3D_3^\circ$	*37540.238*	476.93
$\quad {}^3D_2^\circ$	*37063.31*	567.54
$\quad {}^3D_1^\circ$	*36495.770*	
$6p'\ {}^1D_2^\circ$	*23074.416*	
$7p'\ {}^1D_2^\circ$	*37077.50*	
$6p'\ {}^3F_4^\circ$	*23757.077*	809.639
$\quad {}^3F_3^\circ$	*22947.438*	882.777
$\quad {}^3F_2^\circ$	*22064.661*	
$7p'\ {}^3F_4^\circ$	*37132.084*	620.818
$\quad {}^3F_3^\circ$	*36511.266*	276.408
$\quad {}^3F_2^\circ$	*36234.858*	
$6p'\ {}^1F_3^\circ$	*26816.293*	
$7p'\ {}^1F_3^\circ$	*37739.95*	
$5d(^2D)nd$		
$6d'\ {}^3S_1$	36446.583	
$6d'\ {}^3P_2$	38267.67	244.45
$\quad {}^3P_1$	38023.22	347.38
$\quad {}^3P_0$	37675.84	
$6d'\ {}^1P_1$	36902.55	
$6d'\ {}^3D_3$	36628.87	428.45
$\quad {}^3D_2$	36200.423	266.598
$\quad {}^3D_1$	35933.825	
$6d'\ {}^1D_2$	37837.40	
$6d'\ {}^3F_4$	37732.23	228.21
$\quad {}^3F_3$	37504.02	415.18
$\quad {}^3F_2$	37088.844	
$6d'\ {}^1F_3$	36165.311	
$6d'\ {}^3G_5$	36837.50	488.52
$\quad {}^3G_4$	36348.98	454.70
$\quad {}^3G_3$	35894.28	
$6d'\ {}^1G_4$	38177.10	
$5d(^2D)4f?$		
$4f'\ {}^3F_4^\circ$		
$\quad {}^3F_3^\circ$		
$\quad {}^3F_2^\circ?$	*39765.31*	
?	*39665.451*	

† $J=1$ or 2.

The intensities of the observed combinations in Ba I are recorded in table 3. This table is arranged in two sections: (1) the multiplets produced by transitions from the low even terms $6s^2\ ^1S$, $5d^2\ ^3P$, $5d^2\ ^1D$; $5d\ ^3D$, and $5d\ ^1D$ (more precisely $6s\ 5d\ ^{3,1}D$), to higher odd terms, the latter being given in the same order as in table 1; (2) multiplets representing transitions from $6p\ ^{3,1}P^\circ$ and $6p'\ ^{3,1}P^\circ$, $6p'\ ^{3,1}D^\circ$, $6p'\ ^{3,1}F^\circ$ to higher even terms as given in table 1. All observed combinations are reported in table 3 except the following four, which are omitted to save space:

Desig.	Int.
$6d\ ^3D_3$–$4f\ ^3F_4^\circ$	(20)
$6d\ ^1D$–$4f\ ^1F^\circ$	(20)
$7s\ ^3S$–$7p\ ^3P_2^\circ$	(40)
$7s\ ^3S$–$7p\ ^3P_1^\circ$	(15)

The intensities in table 3 are from column 3 of table 2. King's estimated arc intensity (or furnace intensity in brackets) and temperature class are entered when known. All intensities not by King are given in parentheses. For some lines no estimated intensity is available. In such cases, a "(—)" has been adopted to denote that the combination has been observed.

The present summary of our knowledge of the Ba I spectrum does not serve to replace the monograph needed for this spectrum. Further observations of the Zeeman effect are desirable. With modern infrared detectors the long-wave region beyond the photographic range offers an attractive and worthwhile program. In particular, the even term $5d\ ^2\ ^3F$ remains to be found. The short-wave region likewise needs to be reobserved, and many of the early measurements throughout the spectrum could be improved.

The authors are particularly indebted to W. F. Meggers for the use of his precise observational data in the photographic long-wave region, in advance of publication.

References

[1] F. A. Saunders, Astrophys. J. **51,** 23 (1920); F. Paschen und R Götze, Seriengesetze der Linienspektren, p. 90, (Julius Springer, Berlin, 1922); A. Fowler, Report on Series in Line Spectra, p. 133 (Fleetway Press, London, 1922).

[2] H. N. Russell and F. A. Saunders, Astrophys. J. **61,** 38 (1925).

[3] A. G. Shenstone and H. N. Russell, Phys. Rev. **39,** 415 (1932).

[4] B. E. Moore, Ann. der Phys. [4] **25,** 309 (1908).

[5] A. G. Shenstone and H. A. Blair, Phil. Mag. **8,** 765 (1929); H. N. Russell, Phys. Rev. **36,** 1590 (1930).

[6] A. S. King, Contr. Mt. Wilson Solar Obs. No. 150, Astrophys. J. **48,** 13 (1918); Contr. Mt. Wilson Obs. No. 181; Astrophys. J. **61,** 179 (1920).

TABLE 2. Observed and classified Ba I lines

Symbols in Intensity column

d, Double; *h*, hazy; *u*, diffuse; *n*, nebulous; *w*, wide; *H*, very hazy; *U*, very diffuse; *N*, very nebulous; *W*, very wide; *l*, shaded to longer waves; *s*, shaded to shorter waves; *r*, partial self-reversal; *R*, complete self-reversal.

Lit. ref	I. A.	Intensity		K	ΔK o-c	Desig.	Lit. ref	I. A.	Intensity		K	ΔK o-c	Desig.
		Ref.	King Arc T. C.						Ref.	King Arc T. C.			
A	30933.8	30	.....	3232	0	$5d\ ^3D_1$–$6p\ ^3P_0^\circ$		I. A.					
A	30686.9	20	.....	3258	.....	.....							
A	30468.5	15	.....	3281	.....	.....	B	11884.51	5h	.....	8412.01	−0.05	$6p'\ ^1D_2$–$7s'\ ^1D_2$
A	29790.6	35	.....	3356	.....	.....	B	11697.45	40h	.....	8546.53	−0.02	$6p'\ ^3D_1$–$7s'\ ^3D_1$
A	29223.9	50	.....	3421	0	$5d\ ^3D_2$–$6p\ ^3P_1^\circ$	B	11607.36	30h	.....	8612.86	−0.07	$6p'\ ^3D_1$–$7s'\ ^3D_1$
A	27751.1	30	.....	3602	−1	$5d\ ^3D_1$–$6p\ ^3P_1^\circ$	B	11583.0	1h?	.....	8631.0	+0.1	$6p'\ ^3F_2^\circ$–$6d\ ^3D_1$
A	26221.4	20	.....	3813	0	$6d\ ^3D_1$–$4f\ ^3F_2^\circ$	B	11423.46	20h	.....	8751.52	−0.02	$6p'\ ^1D_2$–$7s'\ ^3D_2$
A	25515.7	50	.....	3918	0	$5d\ ^3D_1$–$6p\ ^3P_2^\circ$	B	11403.92	2	.....	8766.51	.....	.....
A	23255.3	30	.....	4299	0	$5d\ ^3D_2$–$6p\ ^3P_2^\circ$	B	11373.88	5h	.....	8789.67	−0.09	$6p'\ ^3P_1^\circ$–$6p^2\ ^3P_0$
A	22313.4	20	.....	4480	−1	$5d\ ^3D_1$–$6p\ ^3P_2^\circ$	B	11303.04	80	.....	8844.75	0.00	$5d\ ^3D_2$–$6p\ ^1P_1^\circ$
A	22220.8	20	.....	4499	−1	$6d\ ^3D_2$–$4f\ ^1F_3^\circ$	B	11274.77	10	.....	8866.93	+0.06	$6p'\ ^3P_2^\circ$–$6p^2\ ^3P_1$
A	21477.2	15	.....	4655	0	$7s\ ^3S_1$–$7p\ ^3P_1^\circ$	B	11257.3	2H?	.....	8880.7	0.0	$6p'\ ^1P_1^\circ$–$7d\ ^1D_2$
A	20712.0	40	.....	4827	0	$7s\ ^3S_1$–$7p\ ^3P_2^\circ$	B	11118.3	1h?	.....	8991.7	.....	.....
A	19087.9	25	.....	5002	0	$6p\ ^1P_1^\circ$–$5d^2\ ^1D_2$	B	11114.42	50h	.....	8994.85	−0.02	$6p'\ ^1D_2^\circ$–$7s'\ ^3D_1$
A	19074.6	20	.....	5241	−1	$6p'\ ^3P_1^\circ$–$7s'\ ^1D_2$	B	11075.7	3	.....	9026.3	0.0	$5d\ ^3D_1$–$6p\ ^3P_1^\circ$
A	18204.1	15	.....	5492	0	$5d^2\ ^3D_2$–$6p'\ ^1P_1^\circ$	B	11012.69	60hl	.....	9077.95	−0.04	$6p'\ ^1F_3^\circ$–$6d'\ ^3G_3$
A	17182.57	5	.....	5818	+1	$6p'\ ^1P_1^\circ$–$6p^2\ ^1S_0$	B	10962.65	20	.....	9119.39	+0.11	$6p'\ ^3P_1^\circ$–$6p^2\ ^3P_1$
A	17064.8	10	.....	5858	−1	$6p\ ^1P_1^\circ$–$5d^2\ ^3P_2$	B	10914.85	3	.....	9159.32	.....	.....
A	15000.4	40	.....	6665	0	$5d\ ^1D_2$–$6p\ ^1P_1^\circ$	B	10888.65	30	.....	9181.36	+0.10	$6p'\ ^3P_0^\circ$–$6p^2\ ^3P_1$
A	14325.4	25	.....	6979	−1	$6p'\ ^1F_3^\circ$–$7s'\ ^1D_2$	B	10791.25	40hl	.....	9264.23	−0.07	$6p'\ ^1D_2^\circ$–$7s'\ ^1D_2$
A	14159.5	30	.....	7060	−1	$6p'\ ^3F_3^\circ$–$6d\ ^3D_3$	B	10769.2	4h	.....	9283.2	+0.1	$6p'\ ^1P_1^\circ$–$6d'\ ^1D_2$
					−8	$(5d^2\ ^3P_2$–$7p\ ^3P_2^\circ)$	B	10693.7	8hl	.....	9348.8	−0.2	$6p'\ ^1F_3^\circ$–$6d'\ ^1F_3$
A	14077.9	40	.....	7101	0	$6p'\ ^3P_1^\circ$–$7s'\ ^3D_1$	B	10649.10	30h	.....	9387.90	+0.03	$6p'\ ^3P_2^\circ$–$6p^2\ ^1D_2$
A	13956.5	20	.....	7163	0	$6p'\ ^3P_0^\circ$–$7s'\ ^3D_1$	B	10540.10	8	.....	9484.97	−0.05	$5d^2\ ^1D_2$–$7p\ ^1P_1^\circ$
A	13810.5	40	.....	7239	−1	$6p'\ ^3P_1^\circ$–$7s'\ ^3D_2$	B	10487.3	2h	.....	9532.7	0.0	$6p'\ ^1F_3^\circ$–$6d'\ ^3G_4$
A	13207.3	40	.....	7569	−1	$6p'\ ^3P_2^\circ$–$7s'\ ^3D_3$	B	10471.26	100	.....	9547.34	+0.02	$6p\ ^3P_2^\circ$–$5d^2\ ^1D_2$
A	12814.8	10	.....	7801	−2	$6p'\ ^3F_3^\circ$–$6d\ ^3D_2$	B	10409.7	3h	.....	9603.8	0.0	$6p'\ ^1D_2^\circ$–$7s'\ ^1D_2$
A	12554.3	30	.....	7963	−1	$6p'\ ^1D_2^\circ$–$7s'\ ^3D_2$	B	10370.35	10h	.....	9640.23	−0.05	$6p'\ ^3P_1^\circ$–$6p^2\ ^1D_2$
B	12083.60	1h	.....	8273.42	−0.03	$6p'\ ^1D_2^\circ$–$7s'\ ^3D_1$	B	10349.05	8hl	.....	9660.08	−0.32	$6p'\ ^3P_2^\circ$–$6p^2\ ^3P_2$
A	11978.2	15	.....	8346	−2	$6p'\ ^1P_1^\circ$–$6d'\ ^1P_1$	B	10327.4	3	.....	9680.3	.....	.....

TABLE 2—Continued

Lit. Ref.	I. A.	Intensity Ref.	Intensity King Arc T. C.	K	ΔK o-c	Desig.
B	10274.06	50h		9730.59	+0.02	$6p'\ ^1D_2^1-7s'\ ^3D_1$
B	10233.23	400h		9769.41	+0.08	$6p'\ ^3F_4^4-7s'\ ^3D_3$
B	10188.24	50h		9812.55	−0.03	$6p'\ ^1F_3^1-6d'\ ^3D_3$
B	10172.1	3h		9828.1	−0.7	$6p'\ ^3P_2^2-7d\ ^3D_3$
B	10146.9	5*Hd*?		9852.5		
B	10129.70	10		9869.25	+0.07	$6p'\ ^1D_2^1-7s'\ ^3D_2$
B	10115.2	5h		9883.4		
B	10085.5	2h		9912.5	−0.3	$6p'\ ^3P_1^1-6p^2\ ^3P_2$
B	10032.10	200		9965.27	0.00	$6p\ ^3P_2^2-5d^2\ ^3P_1$
B	10001.08	300		9996.18	+0.02	$6p'\ ^3F_3^4-7s'\ ^3D_2$
B	9830.37	500*hl*		10169.77	−0.05	$6p\ ^1P_1^1-7s\ ^1S_0$
B	9821.60	3h		10178.85	+0.21	$6p'\ ^3D_1^1-6p^2\ ^1D_2$
B	9792.91	5h		10208.67	−0.09	$6p'\ ^3P_2^2-6d'\ ^1F_3$
B	9772.62	6h		10229.87	+0.19	$6p'\ ^3P_1^1-6d'\ ^3D_1$
B	9759.35	2h		10243.78	−0.09	$6p'\ ^3P_2^2-6d'\ ^3D_2$
B	9713.75	60		10291.86	+0.19 −0.02	$6p'\ ^3P_1^1-6d'\ ^3D_1$ $(6p'\ ^3D_2^3-6p^2\ ^3P_1)$
B	9704.42	20h		10301.76	−0.08	$6p'\ ^3D_1^1-6p^2\ ^3P_0$
B	9658.8	10*nl*		10350.4		
B	9645.72	100h		10364.45	−0.11	$6p'\ ^3D_1^1-6p^2\ ^1D_2$
B	9608.88	300		10404.19	−0.01	$6p\ ^3P_2^2-5d^2\ ^3P_2$
B	9580.37	150		10425.36	−0.08	$6p\ ^3P_1^1-5d^2\ ^1D_2$
B	9530.30	10h		10489.97	−0.06	$6p'\ ^3P_2^2-6d'\ ^3S_1$
B	9524.70	60h		10496.14	−0.14	$6p'\ ^3P_1^1-6d'\ ^3D_2$
B	9455.92	100		10572.49	0.00	$6p\ ^3P_1^1-5d^2\ ^3P_0$
B	9450.05	15h		10579.05	+0.08	$6p'\ ^3F_3^4-7s'\ ^3D_3$
B	9414.6	4h		10618.9	+0.2	$6p'\ ^3F_4^4-7d\ ^1D_2$
B	9403.53	10		10631.39	+0.03	$6p'\ ^3D_1^1-6p^2\ ^3P_1$
B	9398.8	6h		10636.7	−0.4	$6p'\ ^3D_2^1-6p^2\ ^3P_2$
B	9370.06	500		10669.37	+0.09	$5d\ ^1D_2-6p'\ ^3P_2^2$
B	9367.45	80h		10672.34	+0.02	$6p'\ ^3P_2^2-6d'\ ^3D_3$
B	9324.58	100h		10721.40	−0.02	$6p'\ ^1D_2^1-7s'\ ^1D_2$
B	9308.08	100		10740.41	+0.08	$6p'\ ^3F_2^2-7s'\ ^3D_1$
B	9306.52	10		10742.21	−0.23	$6p'\ ^3P_1^1-6d'\ ^3S_1$
B	9253.08	15h		10804.25	−0.18	$6p'\ ^3P_0^1-6d'\ ^3S_1$
B	9245.6	1h		10813.0	+0.1	$6p'\ ^3D_3^3-6p^2\ ^1D_2$
B	9219.69	100		10843.38	−0.01	$6p\ ^3P_1^1-5d^2\ ^3P_1$
B	9215.42	15h		10848.40	0.00	$6p'\ ^3F_2^2-7s'\ ^1D_2$
B	9189.57	60h		10878.92	−0.02	$6p'\ ^1F_3^1-7s'\ ^3D_2$
B	9159.66	10h		10914.44	+0.02	$6p'\ ^3D_3^3-6d'\ ^3G_3$
B	9133.29	15h		10945.95	−0.05	$6p'\ ^3P_2^2-6d'\ ^1P_1$
B	9101.7	3*lm*		10983.9		
B	9097.8	2h		10988.7		
B	9018.63	3h		11085.12	−0.29	$6p'\ ^3D_2^3-6p^2\ ^3P_2$
B	8975.6	2h		11138.3	−0.6	$6p'\ ^3P_2^2-9s\ ^3S_1$
B	8937.93	10h		11185.20	−0.25	$6p'\ ^3D_1^1-6d'\ ^1F_3$
B	8927.41	7*hl*		11198.39	−0.02	$6p'\ ^3P_1^1-6d'\ ^1P_1$
B	8914.99	150		11213.99	0.00	$6p\ ^3P_2^2-5d^2\ ^3P_1$
B	8909.83	3h		11220.48	−0.08	$6p'\ ^1D_2^1-6d'\ ^3D_2$
B	8860.98	100		11282.33	+0.01	$6p\ ^3P_1^1-5d^2\ ^3P_2$
B	8790.76	100h		11360.83	+0.02	$6p'\ ^1F_3^1-6d'\ ^1G_4$
B	8793.36	3h		11369.10	−0.02	$6p'\ ^3D_1^1-6d'\ ^3G_4$
B	8767.7	1h		11402.4	+0.1	$6p'\ ^3D_2^2-6d'\ ^3D_1$
B	8737.74	9h		11441.47		
B	8710.82	3h		11476.83		
D	8659.30	1		11545.11		
B	8654.07	60		11552.09	+0.03	$5d\ ^1D_2-6p'\ ^3F_3^4$
B	8593.18	4h		11633.54	−0.24	$6p'\ ^3D_3^3-6d'\ ^1F_3$
B	8581.98	50*hl*		11649.13	+0.12	$6p'\ ^3D_3^3-6d'\ ^3D_3$
D	8569.99	1*r*		11665.42		
B	8567.58	40*hl*		11668.70	−0.19	$6p'\ ^3D_2^3-6d'\ ^3D_2$
B	8559.97	600h	4 I	11679.08	+0.05	$5d\ ^1D_2-6p'\ ^1D_2^1$
D	8542.37	1*u*		11703.14		
B	8521.96	8*hl*		11731.17	−0.01	$6p'\ ^3F_4^4-7s'\ ^1D_2$
B	8514.23	30*hl*		11741.82	+0.05	$6p'\ ^3D_1^1-6d'\ ^3D_1$
B	8414.58	4*hr*		11880.87	+0.12	$6p'\ ^3P_2^2-6d'\ ^1D_2$
B	8350.76	2h		11971.67	−0.03	$6p'\ ^3P_1^1-6d'\ ^3P_0$
D	8328.82	3*u*		12003.20		
B	8325.38	20h		12008.27	−0.10	$6p'\ ^3D_1^1-6d'\ ^3D_2$
D	8288.10	1*u*		12062.18		
B	8285.00	6*hr*		12066.69	+0.02	$6p'\ ^3P_2^2-6d'\ ^3P_1$
B	8264.01	3h		12097.34	+0.01	$6p'\ ^3D_2^2-6d'\ ^3D_2$
B	8224.41	5h		12155.59		
C	8210.239	300h	4 III?	12176.570	+0.019	$6p\ ^1P_1^1-6d\ ^1D_2$
B	8161.58	10*hl*		12249.17		
B	8158.12	3h		12254.36	−0.17	$6p'\ ^3D_1^1-6d'\ ^3S_1$
B	8147.78	30h		12269.91	−0.10	$6p'\ ^1D_2^1-6p^2\ ^1D_2$
B	8120.49	30*hr*		12311.15	+0.03	$6p'\ ^3P_2^2-6d'\ ^3P_2$
B	8074.58	1h		12381.14	+0.08	$6p'\ ^3P_1^1-6d'\ ^3P_1$
B	8018.23	10		12468.16	+0.05	$5d\ ^3D_3-6p'\ ^3F_3^3$
B	7982.40	15*hr*		12524.12	−0.04	$6p'\ ^3D_3^1-6d'\ ^3F_3$
B	7961.24	10*hr*		12557.41	+0.10	$6p'\ ^3D_2^1-6d'\ ^3F_2$
B	7957.33	2h		12563.58	+0.05	$6p'\ ^3P_1^1-6d'\ ^3P_2$
B	7939.42	3h		12591.92	+0.02	$6p'\ ^3F_4^4-6d'\ ^1G_4$
C	7911.338	200	3 I.4	12636.616	0.000	$6s^2\ ^1S_0-6p\ ^3P_1^1$
C	7905.751	500	6 III	12645.546	0.000	$6p\ ^3P_2^2-7s\ ^3S_1$
B	7877.93	20*hl*		12690.20	−0.20	$6p\ ^1P_1^1-6d\ ^3D_2$

Lit. Ref.	I. A.	Intensity Ref.	Intensity King Arc T. C.	K	ΔK o-c	Desig.
B	7865.29	1h		12710.60	+0.11	$6p'\ ^3D_1^1-6d'\ ^1P_1$
D	7863.45	1*u*		12713.57		
C	7839.574	60h		12752.292	−0.08	$6p'\ ^1D_2^1-6d'\ ^1F_3$
D	7828.96	2		12769.57		
B	7798.26	5h		12819.85	−0.01	$6p'\ ^1D_2^1-6d'\ ^3G_3$
D	7783.552	1		12844.07		
C	7780.479	400	10 I	12849.148	+0.005	$5d\ ^3D_2-6p'\ ^3F_2^2$
B	7775.37	10h		12857.59	+0.05	$6p'\ ^3D_2^1-6d'\ ^1D_2$
D	7770.26?	0		12866.05		
B	7766.80	10*hl*		12871.78	−0.01	$6p'\ ^3F_4^4-6d'\ ^3D_3$
B	7751.68	40*hr*		12896.88	+0.09	$6p'\ ^3D_1^1-6d'\ ^3F_2$
B	7721.78	10h		12946.82	−0.02	$6p'\ ^3F_3^4-6d'\ ^3G_3$
B	7706.51	50*hr*	1*n* III	12972.48	0.00	$6p'\ ^3D_3^2-6d'\ ^3F_3$
C	7672.092	600	25*r* I	13030.673	−0.003	$5d\ ^3D_1-6p'\ ^3F_2^2$
D	7662.03	3		13047.78		
B	7642.91	200*hl*	4*n* III	13080.42	0.00	$6p'\ ^3F_4^4-6d'\ ^3G_5$
B	7636.90	150*hl*	2*n* III	13090.72	−0.18	$6p'\ ^1D_2^1-6d'\ ^1F_3$
D	7616.55	1*u*		13125.69	−0.32	$6p'\ ^1D_2^1-6d'\ ^3D_2$
C	7610.479	50	2 III.4	13136.167	+0.013	$5d\ ^1D_2-6p'\ ^3D_2^2$
B	7575.22	2h		13197.31	+0.07	$6p'\ ^3D_1^1-6d'\ ^1G_4$
B	7543.48	25h		13252.84	−0.14	$6p'\ ^3F_2^2-6d'\ ^3D_2$
B	7528.20	20h		13279.73	−0.03	$6p'\ ^3F_3^3-6p^2\ ^1D_2$
B	7523.60	20h		13287.85	+0.04	$6p'\ ^3D_1^1-6d'\ ^3P_2$
B	7513.40	3h		13305.89	+0.03	$6p'\ ^3D_2^2-6d'\ ^1D_2$
C	7488.083	200	10 I	13350.882	−0.005	$5d\ ^3D_1-6p'\ ^3F_1^1$
B	7476.21	30h		13372.08	−0.09	$6p'\ ^1D_2^1-6d'\ ^3S_1$
B	7459.78	300*hl*	5*n* III	13401.54	0.00	$6p'\ ^3F_3^4-6d'\ ^3G_4$
C	7417.533	100	5 II	13477.866	+0.001	$5d\ ^3D_2-6p'\ ^1D_2^2$
B	7414.26	4*hl*		13483.81	+0.03	$6p'\ ^3D_1^1-6d'\ ^3P_0$
B	7409.97	30*hr*	1 IV	13491.62	−0.06	$6p'\ ^3D_2^2-6d'\ ^3P_1$
C	7392.411	400	30 II	13523.668	0.000	$6p\ ^3P_1^1-7s\ ^3S_1$
B	7375.59	50*hl*	2*n* III	13554.50	+0.05	$6p'\ ^1D_2^1-6d'\ ^1D_2$
B	7359.29	20	1 III.4	13584.53	+0.05	$5d\ ^1D_2-6p'\ ^1D_2^2$
B	7339.57	4h		13621.03	−0.27	$5d^2\ ^3P_2-7p'\ ^3D_1^1$
B	7326.50	10h		13645.33	−0.01	$6p'\ ^3D_1^1-6d'\ ^1D_2$
D	7319.12	1*u*		13659.08		
B	7307.23	10h		13681.31	−0.12	$6p'\ ^3F_3^4-6d'\ ^3D_3$
B	7304.46	5h		13686.50		
C	7280.298	1000	150*r* II	13731.924	+0.004	$5d\ ^3D_2-6p'\ ^3F_1^1$
B	7272.33	2h		13746.97	+0.03	$6p'\ ^3F_4^4-6d'\ ^3F_3$
E	7229.56	10h		13828.29	+0.16	$6p'\ ^1D_2^1-6d'\ ^1P_1$
B	7228.84	200*hl*	25 III	13829.67	+0.05	$6p'\ ^3F_2^2-6d'\ ^3G_3$
B	7213.56	10	1 III.4	13858.97	+0.07	$5d\ ^3D_2-6p'\ ^1D_2^2$
B	7208.18	20h	1*n* III	13869.31	+0.15	$6p'\ ^3F_2^2-6d'\ ^1D_2$
C	7195.235	200	80 III	13894.263	0.000	$6p\ ^3P_0^1-7s\ ^3S_1$
B	7153.54	80*hr*	5 III	13975.25	+0.10	$6p'\ ^3F_4^4-6d'\ ^3F_4$
B	7133.16	4h		14015.17	−0.27	$5d^2\ ^1D_2-7p'\ ^1D_2^2$
D	7129.56	2		14022.24		
B	7126.60	10h		14028.08		
C	7120.329	800*hr*	200 II	14040.431	0.000	$5d\ ^3D_1-6p'\ ^1D_2^2$
D	7110.24	1*u*		14060.35		
D	7097.99	1		14084.61		
B	7080.01	100*hl*	5*n* III	14100.47	−0.18	$6p'\ ^3F_3^4-6d'\ ^1F_3$
B	7072.38	1h		14135.62	−0.14	$6p'\ ^3F_2^2-6d'\ ^3D_2$
B	7069.43	3		14141.52	+0.11	$6p'\ ^3F_3^3-6d'\ ^3F_2$
C	7059.941	2000	400*r* II	14160.526	0.000	$5d\ ^3D_1-6p'\ ^3F_2^2$
B	6986.79	5		14308.78	+0.02	$5d\ ^1D_2-6p'\ ^3P_1^1$
B	6961.63	2h		14360.50	−0.04	$6p'\ ^1D_2^1-7d\ ^1D_2$
D	6951.35	1*u*		14381.73	−0.19	$6p'\ ^3F_2^2-6d'\ ^3S_1$
B	6932.92	2h		14419.96	−0.06	$6p'\ ^3F_4^4-6d'\ ^3G_4$
D	6874.16	1*u*		14543.22		
B	6867.85	100h	8*n* IV?	14556.59	+0.01	$6p'\ ^3F_3^3-6d'\ ^3F_3$
C	6865.692	200	30 II	14561.164	−0.003	$5d\ ^3D_2-6p'\ ^3P_2^2$
B	6771.85	60h	2*n* III	14762.95	−0.03	$6p'\ ^1D_2^1-6d'\ ^1D_2$
D	6769.60	2*u*		14767.84		
B	6761.86	2h		14784.76	−0.03	$6p'\ ^3F_3^1-6d'\ ^3F_4$
B	6714.03	2h		14890.08	+0.12	$6p'\ ^3F_3^1-6d'\ ^1D_2$
C	6693.842	600	70 I	14934.987	+0.002	$5d\ ^3D_1-6p'\ ^1D_2^2$
C	6675.271	500	80 I	14976.538	−0.001	$5d\ ^3D_2-6p'\ ^3D_1^2$
C	6654.102	50	10 III	15024.183	0.000	$6p'\ ^3F_2^2-6d'\ ^3F_2$
F	6642.40	.....	1*n* III.4	15050.64		
C	6595.326	1000	200 I	15158.075	+0.003	$5d\ ^3D_1-6p'\ ^3D_1^2$
B	6580.73	20h	6 III	15191.70		
D	6565.91	0*u*		15225.98		
B	6564.33	3h	2 III.4	15229.65	−0.01	$6p'\ ^3F_3^1-6d'\ ^3G_4$
D	6544.89	1		15274.88		
C	6527.312	(50R)	250 I	15316.020	+0.002	$5d\ ^3D_2-6p'\ ^3D_2^2$
C	6498.759	(100R)	300*r* II	15383.311	+0.003	$5d\ ^3D_1-6p'\ ^3D_1^2$
C	6482.908	(50R)	200 II	15420.924	+0.013	$5d\ ^3D_2-6p'\ ^3F_1^1$
C	6450.854	(30)	125 I	15497.549	−0.002	$5d\ ^3D_1-6p'\ ^3D_2^2$
G	6411.74	1	4 III.4	15592.08		
E	6411.150	1	.....	15593.52	+0.06	$6p\ ^3P_1^1-7s\ ^1S_0$
E	6353.200	1	.....	15735.75	+0.17	$6p\ ^3P_1^1-7s'\ ^1D_2$
C	6341.682	(50)	150 I	15764.338	−0.003	$5d\ ^3D_2-6p'\ ^3D_2^2$
G	6323.4	1	3 III?	15809.90		
D	6300.30	2*u*	.....	15867.87		
G	6235.3	2*u*	30*n* III	16033.28		

TABLE 2—Continued

Lit. Ref.	I. A.	Intensity Ref.	Intensity King Arc T. C.	K	ΔK o-c	Desig.
D	6174.54	4		16191.06		
D	6140.39	5		16281.11		
H	6129.335	3*u*	3 III	16310.47	−0.05	$6p\ ^1P_1^\circ - 6p^2\ ^1S_0$
C	6110.784	(100R)	300*r* II	16359.994	−0.004	$5d\ ^3D_3 - 6p'\ ^3P_2^\circ$
G	6086.4	1*u*		16425.53	+0.09	$5d^2\ ^3P_1 -$ 39905°
C	6083.402	(5)	5 IIIA	16433.632	−0.002	$6p\ ^1P_1^\circ - 6p^2\ ^3P_0$
C	6063.117	(50R)	200 II	16488.612	−0.010	$5d\ ^3D_2 - 6p'\ ^3P_1^\circ$
D	6035.52	1*u*		16563.99		
C	6019.470	(50)	100 II	16608.170	−0.002	$5d\ ^3D_1 - 6p'\ ^3P_0^\circ$
C	5997.088	(50)	100 II	16670.153	−0.002	$5d\ ^3D_1 - 6p'\ ^3P_1^\circ$
G	5985.2	1*u*		16703.25	0.00	$5d^2\ ^1D_2$–39765°
H	5978.496	2	4 IIIA	16721.98	−0.10	$6p\ ^3P_2^\circ - 6d\ ^1D_2$
C	5971.699	50	100 II	16741.027	−0.004	$5d\ ^3D_2 - 6p'\ ^3P_2^\circ$
H	5964.787	2	5 III	16760.42		
H	5962.445	2	2 IIIA	16767.00		
D	5935.43	1*u*		16843.31	−0.08	$5d^2\ ^1D_2$– 39905°
G	5927.7	1		16865.28		
C	5907.639	(10)	15 IIA	16922.558	−0.006	$5d\ ^3D_1 - 6p'\ ^3P_2^\circ$
G	5859.29	1		17062.19		
G	5849.28	1		17091.38		
C	5826.277	(100)	150 II	17158.874	−0.001	$5d\ ^1D_2 - 6p'\ ^1P_1^\circ$
C	5818.831	(3)	5 IIIA	17180.831	−0.025	$6p\ ^3P_2^\circ - 6d\ ^3D_1$
G	5818.25	1		17182.53		
C	5805.685	(10)	20 II	17219.734	−0.008	$5d\ ^3D_3 - 6p'\ ^1F_3^\circ$
C	5800.229	(100)	100 III	17235.932	+0.001	$6p\ ^3P_2^\circ - 6d\ ^3D_2$
H	5784.105	2*n*	4 III	17283.97	−0.19	$6p\ ^1P_1^\circ - 6p^2\ ^1D_2$
C	5777.622	(500)	400*r* II	17303.372	0.000	$6p\ ^3P_2^\circ - 6d\ ^3D_3$
H	5720.712	1		17475.49		
H	5718.364	1		17482.67		
H	5715.953	1		17490.04		
H	5713.554	2	4 *n*III	17497.39		
H	5709.546	1	2 *n*III	17509.67		
H	5706.042	1		17520.42		
H	5704.820	1		17524.17		
C	5680.184		10 IIIA	17600.192	−0.007	$6p\ ^3P_1^\circ - 6d\ ^1D_2$
C	5679.997		2 IIIA	17600.771	−0.004	$5d\ ^3D_2 - 6p'\ ^1F_3^\circ$
I	5664.3	1*h*		17649.53	+0.49	$6p\ ^1P_1^\circ - 7d\ ^3D_1$
G	5641.1	1*u*		17722.12		
H	5628.938	1*U*		17760.41		
H	5625.701	1*U*		17770.63	+0.08	$5d^2\ ^3P_1 - 12f\ ^3F_2^\circ$
G	5620.4	1*u*	20*n* IV?	17787.39		
G	5620.0	1*u*	4*n* IV?	17788.66		
H	5619.099	1*U*		17791.51		
G	5618.7	1*u*		17792.77		
H	5593.297	3	3 III	17873.58	+0.02	$6p\ ^1P_1^\circ - 6d'\ ^3D_1$
G	5546.1	2*u*		18025.68		
F	5535.86	7		18059.02	+0.04	$6p\ ^3P_1^\circ - 6d\ ^3D_1$
C	5535.484	(100*R*)	1000*R* I	18060.264	0.000	$6s^2\ ^1S_0 - 6p\ ^1P_1^\circ$
C	5519.047	(50)	200 II	18114.052	−0.001	$6p\ ^3P_1^\circ - 6d\ ^3D_2$
H	5473.689	2*n*	3 IIIA	18264.14		
H	5437.393	2*n*	4 IIIA	18386.06	−0.26	$6p\ ^1P_1^\circ - 6d'\ ^3S_1$
C	5424.551	(50*r*)	100 II	18429.597	+0.024	$6p\ ^3P_0^\circ - 6d\ ^3D_1$
H	5416.344	1*U*		18457.51		
H	5404.920	1*u*	5 *n*IIIA	18496.52		
I	5393.25	1*hR*		18536.54		
G	5389.6	1*u*		18549.10		
G	5381.0	1*u*		18578.75		
K	5378.85	(1)		18586.17		
H	5365.383	1*u*		18632.82		
H	5349.621	1*U*		18687.72		
H	5308.952	1*U*	4 IV?	18830.87		
H	5305.758	2*u*	4 IV?	18842.20	−0.09	$6p\ ^1P_1^\circ - 6d'\ ^1P_1$
H	5302.808	3*u*	6 IV?	18852.69		
H	5294.130	2*u*		18883.59		
H	5290.945	1*U*		18894.96		
H	5279.619	1*U*		18935.49		
H	5277.625	1*U*	3 IV?	18942.64		
H	5267.033	4*u*	20 IV?	18980.74	0.00	$6p\ ^1P_1^\circ - 8s\ ^1S_0$
H	5265.566	1*u*		18986.03		
H	5253.807	1*U*		19028.52	−0.06	$6p\ ^1P_1^\circ - 6d'\ ^3F_2$
E	5177.322	(2*u*)	2 IV?	19309.63		
H	5175.619	3*u*	5 IV?	19315.98		
E	5169.490	1		19338.88	+0.14	$5d\ ^3D_2 - 6p'\ ^1P_1^\circ$
C	5159.939	(5)	20*n* IV?	19374.692	0.000	$6p\ ^1P_1^\circ - 7d\ ^1D_2$
G	5093.9	1		19625.87		
H	5054.975	2*u*	5 IV?	19776.98	−0.16	$6p\ ^1P_1^\circ - 6d'\ ^1D_2$
G	4995.72	1		20011.55	−0.12	$6p\ ^3P_2^\circ - 7s'\ ^3D_1$
H	4947.350	3*u*	8 III	20207.20	−0.13 −0.21	$6p\ ^1P_1^\circ - 9s\ ^1S_0$ $6p\ ^1P_1^\circ - 6d'\ ^3P_2$
E	4929.355	1		20280.97	−0.13	$6p\ ^3P_2^\circ - 7s'\ ^1D_2$
H	4902.898	4*r*	15 III	20390.41	−0.20	$6p\ ^3P_2^\circ - 8s\ ^3S_1$
H	4877.650	3*u*	30 *N*III	20495.95	+0.03	$6p\ ^1P_1^\circ - 8d\ ^1D_2$
G	4807.6	1*u*	2 *N*III	20794.59		
G	4739.3	1*u*	5 *N*III	21094.26		
G	4731.8	1*u*	5 *N*III?	21127.70		
C	4726.436	(10)	40 II	21151.692	−0.002	$5d\ ^1D_2 - 7p\ ^1P_1^\circ$
H	4724.742	3	3 III	21159.26	+0.04	$6p\ ^3P_1^\circ - 7s'\ ^1D_2$
C	4700.427	(3)	20 III	21268.729	−0.004	$6p\ ^3P_1^\circ - 8s\ ^3S_1$
F	4699.108		15 *N*III	21274.68	0.00	$6p\ ^1P_1^\circ - 9d\ ^1D_2$
I	4698.10	2*h*		21279.25		
C	4691.617	(8)	35 II	21308.667	−0.015	$6p\ ^3P_2^\circ - 6p^2\ ^3P_1$
J	4674.97			21384.52		
C	4673.619	(3)	30 II	21390.727	+0.001	$5d\ ^3D_1 - 7p\ ^3P_2^\circ$
I	4670.75	1*h*		21403.85		
I	4668.56	1*h*		21413.89		
G	4662.8	1*u*	10 *N*IV?	21440.34		
G	4651.8	1*u*	5 *N*IV?	21491.04		
H	4642.038	2*r*	4 *N*IV?	21536.23		
H	4636.333	3*r*	15 *N*IV?	21562.73		
J	4629.63			21593.95		
C	4628.328	(3)	25*n* III	21600.044	0.000	$5d\ ^3D_2 - 7p\ ^1P_1^\circ$
I	4624.21	1*h*		21619.26		
C	4619.924	(3)	20*n* III	21639.336	+0.008	$6p\ ^3P_0^\circ - 8s\ ^3S_1$
J	4606.38			21702.94		
C	4604.982	(1)	8*n* IIIA	21709.548	0.000	$5d\ ^3D_1 - 7p\ ^3P_0^\circ$
H	4599.751	6*R*	30 III	21734.22	+0.06	$6p\ ^3P_1^\circ - 6p^2\ ^1S_0$
J	4593.16			21765.40		
C	4591.824	(2)	10*n* III	21771.758	−0.001	$5d\ ^3D_3 - 7p\ ^3P_2^\circ$
J	4591.07			21775.31		
C	4589.754	(2)	8*n* IIIA	21781.577	0.000	$5d\ ^3D_1 - 7p\ ^3P_1^\circ$
C	4579.639	(15)	80 II	21829.685	0.000	$6p\ ^3P_2^\circ - 6p^2\ ^1D_2$
C	4573.854	(10)	40 II	21857.293	+0.011	$6p\ ^3P_1^\circ - 6p^2\ ^3P_0$
I	4562.75	1		21910.47		
C	4523.171	(10)	60*n* II	22102.206	−0.003	$6p\ ^3P_2^\circ - 6p^2\ ^3P_2$
K	4512.89	1		22152.54		
C	4505.924	(10)	40 II	22186.803	−0.001	$6p\ ^3P_1^\circ - 6p^2\ ^3P_1$
K	4504.36	1*n*		22194.49	−0.08	$6p\ ^3P_2^\circ - 7d\ ^3D_1$
C	4493.637	(6*r*)	50*n* III	22247.469	−0.004	$6p\ ^3P_2^\circ - 7d\ ^3D_2$
C	4488.977	(8*r*)	60*n* III	22270.564	0.000	$6p\ ^3P_2^\circ - 7d\ ^3D_3$
C	4467.093	(3)	12 III	22379.664	+0.12	$6p\ ^3P_2^\circ - 6d'\ ^3G_3$
K	4459.18	0		22419.36	+0.27	$6p\ ^3P_2^\circ - 6d'\ ^3D_1$
C	4431.894	(10)	40 II	22557.403	+0.004	$6p\ ^3P_0^\circ - 6p^2\ ^3P_1$
K	4430.33	1		22565.35		
C	4413.664	(2)	8 III	22650.573	0.000	$6p\ ^3P_2^\circ - 6d'\ ^1F_3$
H	4406.846	4*r*	15 III	22685.59	−0.09	$6p\ ^3P_2^\circ - 6d'\ ^3D_2$
C	4402.539	(20)	60 II	22707.808	+0.001	$6p\ ^3P_1^\circ - 6p^2\ ^1D_2$
I	4375.88	1*H*		22846.13		
C	4359.527	(2)	5 III	22931.845	0.000	$6p\ ^3P_2^\circ - 6d'\ ^3S_1$
C	4350.328	(15)	80 II	22980.334	+0.003	$6p\ ^3P_1^\circ - 6p^2\ ^3P_2$
C	4332.914	(3)	10*n* III	23072.692	0.000	$6p\ ^3P_1^\circ - 7d\ ^3D_1$
H	4325.152	3	10 III	23114.07	−0.06	$6p\ ^3P_2^\circ - 6d'\ ^3D_3$
C	4323.620			23122.286		
C	4323.001	(3*r*)	20*n* III	23125.597	+0.002	$6p\ ^3P_1^\circ - 7d\ ^3D_2$
I	4305.15	1		23221.46	+0.16	$5d\ ^1D_2 - 4f\ ^3F_3^\circ$
C	4291.158	(5)	12 III	23297.201	−0.008	$6p\ ^3P_1^\circ - 6d'\ ^3D_1$
I	4284.90	1		23331.20	−0.36	$5d\ ^3D_2 - 7p\ ^1P_1^\circ$
C	4283.098	(20)	100 II	23341.041	0.000	$5d\ ^1D_2 - 4f\ ^1F_3^\circ$
I	4278.83	0+		23364.50		
C	4264.418	(2)	15*n* IIIA	23443.286	−0.001	$6p\ ^3P_0^\circ - 7d\ ^3D_1$
I	4252.4	1		23509.51		
C	4242.606	(4)	10 III	23563.807	0.000	$6p\ ^3P_1^\circ - 6d'\ ^3D_2$
C	4239.557	(2)	10*n* III	23580.754	0.000	$6p\ ^3P_2^\circ - 9s\ ^3S_1$
C	4223.962	(5)	12 III	23667.813	+0.009	$6p\ ^3P_0^\circ - 6d'\ ^3D_1$
H	4179.372	2*r*	8*n* IIIA	23920.30	+0.08	$6p\ ^3P_2^\circ - 7d\ ^1D_2$
E	4134.383	1		24180.58	+0.02	$6p\ ^3P_0^\circ - 6d'\ ^3S_1$
C	4132.427	(5)	20 I	24192.054	−0.003	$6s^2\ ^1S_0 - 6p'\ ^3D_1^\circ$
E	4110.23	2	2 III	24322.67	+0.01	$6p\ ^3P_2^\circ - 6d'\ ^1D_2$
H	4087.371	1*U*	8*n* IIIA	24458.70	−0.18 −0.75	$6p\ ^3P_1^\circ - 9s\ ^3S_1$ $6p\ ^3P_2^\circ - 8d\ ^3D_2$
H	4085.322	1*U*		24470.97		
C	4084.862	(1*u*)	30 *N* III	24473.747	0.000	$6p\ ^3P_2^\circ - 8d\ ^3D_3$
G	4080.9	1*u*	6*n* III	24497.5	+0.4	$5d\ ^1D_2 - 8p\ ^1P_1^\circ$
E	4057.833	1Pb?		24636.74	+0.21	$6p\ ^3P_0^\circ - 6d'\ ^1P_1$
E	4038.797	0		24752.85	−0.08	$6p\ ^3P_2^\circ - 6d'\ ^3P_2$
E	4031.415	0*h*		24798.18	−0.16	$6p\ ^3P_1^\circ - 7d\ ^1D_2$
G	4026.40	1*r*	2*n* IV?	24829.06	−0.41	$6p\ ^3P_0^\circ - 9s\ ^3S_1$
G	3997.90	1	3 III	25006.06	−0.19	$5d\ ^3D_3 - 4f\ ^3F_3^\circ$
C	3995.656	(5)	30 III	25020.131	−0.001	$5d\ ^3D_3 - 4f\ ^3F_4^\circ$
C	3993.401	(100)	80 II	25034.258	0.000	$5d\ ^3D_2 - 4f\ ^3F_3^\circ$
E	3992.255	3*u*		25041.42	−0.02	$6p\ ^3P_2^\circ - 8d\ ^1D_2$
C	3982.878	(1)	2 III	25100.399	+0.011	$5d\ ^1D_2 - 7p'\ ^3D_1^\circ$
K	3980.42	2*n*		25115.87	−0.01	$5d\ ^1D_2 - 7p'\ ^3F_2^\circ$
C	3975.365	(1*u*)	4*n* III	25147.834	−0.34	$6p\ ^3P_2^\circ - 10s\ ^3S_1$
C	3947.507	(1*u*)	5 *N* III	25325.303	0.000	$6p\ ^3P_1^\circ - 8d\ ^3D_1$
C	3945.595	—	10 *N* III	25337.575	0.000	$6p\ ^3P_1^\circ - 8d\ ^3D_2$
C	3937.870	(8)	20 III	25387.279	−0.005	$5d\ ^3D_2 - 4f\ ^3F_2^\circ$
C	3935.717	(50)	50 II	25401.165	0.000	$5d\ ^3D_2 - 4f\ ^3F_3^\circ$
K	3917.26	8	4 III	25520.82	−0.08	$5d\ ^3D_2 - 4f\ ^1F_3^\circ$
C	3909.910	(50*r*)	40 II	25568.821	+0.004	$5d\ ^3D_1 - 4f\ ^3F_2^\circ$
E	3905.986	2*h*	2 III	25594.48	−0.15	$5d\ ^1D_2 - 7p'\ ^3P_1^\circ$
G	3900.41	1	2 III	25631.07	+0.02	$6p\ ^3P_1^\circ - 6d'\ ^1P_2$
I	3898.58	0		25643.10	−0.05	$6p\ ^3P_2^\circ - 9d\ ^3D_2$

TABLE 2—Continued

Lit. Ref.	I. A.	Intensity Ref.	Intensity King Arc T. C.	K	ΔK o-c	Desig.
C	3894.345	1h	.....	25671.013	+3.08	$5d\ ^1D_2 - 7p'\ ^3D_3^0$
					0.00	$6p\ ^3P_2^0 - 9d\ ^3D_3$
H	3892.653	2u	20 III	25682.14	+0.02	$5d\ ^1D_2 - 7p'\ ^1D_2^0$
I	3890.57	0	.....	25695.89	−0.01	$6p\ ^3P_0^0 - 8d\ ^3D_1$
C	3889.326	(8)	20 II	25704.140	0.000	$6s^2\ ^1S_0 - 6p'\ ^3P_1^0$
E	3881.319	2	.....	25757.14	−0.06	$6p\ ^3P_0^0 - 6d'\ ^3P_1$
H	3861.905	2u	15 III	25886.62	−0.08	$5d\ ^1D_2 - 7p'\ ^3P_2^0$
					−0.17	$5d\ ^1D_2 - 5f\ ^1F_3^0$
I	3841.15	1h	.....	26026.49	+0.20	$6p\ ^3P_1^0 - 10s\ ^3S_1$
I	3828.93	—	.....	26109.55	−0.40	$6p\ ^3P_0^0 - 11s\ ^3S_1$
H	3794.771	5r	15 III	26344.57	0.00	$5d\ ^1D_2 - 7p'\ ^1F_3^0$
J	3790.27	0	.....	26375.85	.....	.....
I	3789.72	−nl	.....	26379.68	−0.11	$6p\ ^3P_2^0 - 10d\ ^3D_2$
					+0.56	$5d\ ^1D_2 - 9p\ ^1P_1^0$?
I	3788.18	—	.....	26390.41	0.00	$6p\ ^3P_2^0 - 10d\ ^3D_3$
I	3787.23	—	.....	26397.03	+0.14	$6p\ ^3P_0^0 - 10s\ ^3S_1$
I	3771.93	—	.....	26504.10	+0.02	$6p\ ^3P_1^0 - 9d\ ^3D_1$
I	3769.48	—	.....	26521.32	+0.05	$6p\ ^3P_1^0 - 9d\ ^3D_2$
I	3767.4	0H	.....	26535.96	.....	.....
I	3721.17	—	.....	26865.63	+0.05	$6p\ ^3P_2^0 - 11d\ ^3D_2$
I	3720.85	—	.....	26867.94	0.00	$6p\ ^3P_2^0 - 11d\ ^3D_3$
I	3719.92	—	.....	26874.65	−0.03	$6p\ ^3P_0^0 - 9d\ ^3D_1$
I	3704.23	—	.....	26988.48	+0.41	$6p\ ^3P_1^0 - 11s\ ^3S_1$
H	3701.716	2u	3 III	27006.81	.....	.....
K	3699.94	2	.....	27019.78	+0.44	$5d\ ^3D_2 - 7p'\ ^3F_3^0$
H	3688.473	3r	20N III	27103.78	−0.69	$5d\ ^1D_2 - 7p'\ ^1P_1^0$
C	3675.310	(1)	2 III	27200.873	0.000	$5d\ ^3D_1 - 7p'\ ^3F_2^0$
I	3667.93	—	.....	27255.57	+0.01	$6p\ ^3P_1^0 - 10d\ ^3D_1$
I	3667.60	—	.....	27258.02	+0.11	$6p\ ^3P_1^0 - 10d\ ^3D_2$
H	3664.598	1u	3 III	27280.35	+0.10	$5d\ ^3D_2 - 7p'\ ^3D_3^0$
C	3662.535	(3)	15 III	27295.748	0.000	$5d\ ^3D_2 - 7p'\ ^3F_3^0$
C	3640.391	(3)	10 III	27461.780	−0.005	$5d\ ^3D_1 - 7p'\ ^3D_2^0$
F	3639.715	.....	2 III	27466.85	+0.09	$5d\ ^3D_3 - 7p'\ ^3D_3^0$
F	3636.832	.....	40N III	27488.62	0.00	$5d\ ^1D_2 - 6f\ ^1F_3^0$
C	3630.640	(10)	40 III	27535.533	0.000	$5d\ ^3D_2 - 7p'\ ^3F_4^0$
C	3610.957	.....	15n III	27685.624	0.000	$5d\ ^3D_3 - 5f\ ^1F_3^0$
					+0.09	$5d\ ^3D_3 - 7p'\ ^3P_2^0$
I	3603.40	—	.....	27743.65	−0.05	$6p\ ^3P_1^0 - 11d\ ^3D_2$
C	3599.402	(3)	15 III	27774.499	+0.001	$5d\ ^3D_2 - 7p'\ ^3P_1^0$
I	3596.33	(1u)	.....	27798.19	−0.18	$5d\ ^3D_3 - 5f\ ^3F_3^0$
C	3593.204	(1)	15n III	27822.406	−0.010	$5d\ ^3D_3 - 5f\ ^3F_4^0$
F	3589.950	.....	3 IIIA	27847.59	−0.20	$5d\ ^3D_2 - 7p'\ ^3D_2^0$
F	3588.099	.....	10 III	27861.96	−0.02	$5d\ ^3D_2 - 7p'\ ^1D_2^0$
C	3586.549	(2)	10 III	27874.031	0.00	$5d\ ^3D_1 - 7p'\ ^3P_0^0$
C	3579.665	(20r)	80n III	27927.633	0.000	$5d\ ^3D_3 - 5f\ ^3F_4^0$
F	3577.615	.....	30 III	27943.60	−0.09	$5d\ ^3D_3 - 7p'\ ^3D_3^0$
F	3576.036	.....	10 III	27955.94	−0.09	$5d\ ^3D_1 - 7p'\ ^3P_1^0$
I	3571.8	1h	.....	27989.10	.....	.....
F	3566.660	.....	10 III	28029.43	+0.10	$5d\ ^3D_1 - 7p'\ ^3D_2^0$
F	3561.942	.....	10 III	28066.56	−0.10	$5d\ ^3D_2 - 5f\ ^1F_3^0$
					0.00	$5d\ ^3D_2 - 7p'\ ^3P_2^0$
I	3552.3	1h	.....	28142.74	.....	.....
C	3547.680	(3)	20n III	28179.415	+0.008	$5d\ ^3D_2 - 5f\ ^3F_3^0$
C	3544.655	(20r)	80n III	28203.462	+0.013	$5d\ ^3D_2 - 5f\ ^3F_2^0$
I	3540.72	1	.....	28234.77	.....	.....
F	3531.345	.....	30N III	28309.73	0.00	$5d\ ^1D_2 - 7f\ ^1F_3^0$
C	3529.480	(3)	15 III	28324.720	0.000	$5d\ ^3D_2 - 7p'\ ^3D_3^0$
C	3524.973	(20r)	80n III	28360.935	−0.005	$5d\ ^3D_1 - 5f\ ^3F_2^0$
K	3523.92	0n	.....	28369.38	−0.55	$5d\ ^1D_2 - 39765°$?
C	3501.107	(50)	200R II	28554.257	0.000	$6s^2\ ^1S_0 - 6p'\ ^1P_1^0$
F	3463.741	.....	[40] III	28862.25	0.00	$5d\ ^1D_2 - 8f\ ^1F_3^0$
F	3427.85	.....	3n III	29164.44	.....	.....
F	3426.453	.....	4n III?	29176.33	.....	.....
F	3421.476	.....	[30n] III	29218.77	0.00	$5d\ ^1D_2 - 9f\ ^1F_3^0$
					−0.19	$(5d\ ^1D_2 - 9f\ ^3F_3^0)$
F	3421.008	.....	[25] III	29222.77	+0.90	$5d\ ^3D_3 - 6f\ ^3F_3^0$
C	3420.316	(8r)	[70R] III	29228.714	0.000	$5d\ ^3D_3 - 6f\ ^3F_4^0$
F	3413.835	.....	3n III	29284.17	−0.16	$5d\ ^3D_2 - 7p'\ ^1P_1^0$
F	3377.391	.....	[20] III	29600.15	−0.07	$5d\ ^3D_2 - 6f\ ^3F_3^0$
C	3377.081	(5r)	[60R] III	29602.900	0.000	$5d\ ^3D_2 - 6f\ ^3F_2^0$
C	3356.800	(4r)	80N III	29781.750	0.000	$5d\ ^3D_1 - 6f\ ^3F_2^0$
F	3323.058	.....	[10] III	30084.11	+0.04	$5d\ ^3D_3 - 7f\ ^3F_4^0$
F	3322.797	.....	[50r] III	30086.47	0.00	$5d\ ^3D_3 - 7f\ ^3F_3^0$
F	3315.753	.....	8n III	30150.39	.....	.....
G	3298.2	1r	.....	30310.84	.....	.....
F	3281.772	.....	[15] III	30462.56	+0.02	$5d\ ^3D_2 - 7f\ ^3F_2^0$
F	3281.503	.....	[40r] III	30465.06	−0.04	$5d\ ^3D_2 - 7f\ ^3F_3^0$
F	3272.405	.....	2n III	30549.76	−0.03	$5d\ ^3D_2 - 39765°$
F	3270.115	.....	4n III	30571.15	.....	.....
F	3262.336	.....	[60P] III	30644.05	−0.03	$5d\ ^3D_1 - 7f\ ^3F_2^0$
F	3261.961	.....	[50r] III	30647.57	+0.10	$5d\ ^3D_1 - 8f\ ^3F_2^0$
F	3253.067	.....	5n III	30731.36	+0.03	$5d\ ^3D_1 - 39765°$
J	3244.20	—	.....	30815.35	−0.21	$6s^2\ ^1S_0 - 7p\ ^3P_1^0$
F	3222.441	.....	[8] III	31023.42	+0.03	$5d\ ^3D_2 - 8f\ ^3F_2^0$
F	3222.188	.....	[40] III	31025.85	0.00	$5d\ ^3D_2 - 8f\ ^3F_3^0$
F	3221.630	.....	[30] III	31031.23	0.00	$5d\ ^3D_2 - 9f\ ^3F_4^0$
F	3203.700	.....	25N III	31204.89	−0.01	$5d\ ^3D_1 - 8f\ ^3F_2^0$
F	3193.967	.....	[5] III	31299.98	.....	.....
F	3193.912	.....	[10] III	31300.52	0.00	$5d\ ^3D_3 - 10f\ ^3F_4^0$
F	3183.96	.....	[15] III	31398.35	−0.29	$5d\ ^3D_2 - 9f\ ^3F_3^0$
F	3183.156	.....	[30] III	31406.28	0.00	$5d\ ^3D_2 - 9f\ ^3F_2^0$
F	3173.69	.....	[15n] III	31499.95	0.00	$5d\ ^3D_3 - 11f\ ^3F_4^0$
F	3165.598	.....	[25] III	31580.47	+0.29	$5d\ ^3D_1 - 9f\ ^3F_2^0$
F	3158.54	.....	[12N] III	31651.03	0.00	$5d\ ^3D_2 - 12f\ ^3F_4^0$
F	3158.046	.....	[12] III	31655.99	.....	.....
F	3155.673	.....	[10] III	31679.79	+0.04	$5d\ ^3D_2 - 10f\ ^3F_3^0$
F	3155.336	.....	[10] III	31683.17	0.00	$5d\ ^3D_2 - 10f\ ^3F_2^0$
I	3146.90	—	.....	31768.10	0.00	$5d\ ^3D_3 - 13f\ ^3F_4^0$
I	3137.80	—	.....	31860.23	0.00	$5d\ ^3D_3 - 14f\ ^3F^0$
F	3137.700	.....	[10] III	31861.25	−0.04	$5d\ ^3D_1 - 10f\ ^3F_2^0$
G	3135.72	—	[8n] III	31881.36	0.00	$5d\ ^3D_2 - 11f\ ^3F_3^0$
F	3132.602	.....	[8] III	31913.10	.....	.....
I	3130.6	—	.....	31933.50	0.00	$5d\ ^3D_1 - 15f\ ^3F^0$
I	3121.02	—	.....	32031.52	0.00	$5d\ ^3D_2 - 12f\ ^3F_3^0$
F	3119.202	.....	3N III	32050.19	.....	.....
F	3117.638	.....	[3n] III	32066.27	0.00	$5d\ ^3D_1 - 11f\ ^3F_2^0$
F	3117.34	.....	[3n] III	32069.33	.....	.....
I	3109.63	—	.....	32148.84	0.00	$5d\ ^3D_2 - 13f\ ^3F_3^0$
F	3108.21	.....	10n III	32163.53	.....	.....
I	3103.1	—	.....	32216.49	−0.09	$5d\ ^3D_1 - 12f\ ^3F_2^0$
C	3071.583	(20)	100R III	32547.076	0.000	$6s^2\ ^1S_0 - 7p\ ^1P_1^0$
C	2785.276	(2)	15 IV	35892.518	0.000	$6s^2\ ^1S_0 - 8p\ ^1P_1^0$
H	2739.243	4	3 IV	36495.64	−0.13	$6s^2\ ^1S_0 - 7p'\ ^3D_1^0$
C	2702.632	(2)	8 IV	36990.016	0.000	$6s^2\ ^1S_0 - 7p'\ ^3P_1^0$
I	2646.50	1h	.....	37774.50	0.00	$6s^2\ ^1S_0 - 9p\ ^1P_1^0$
C	2596.637	(1)	8n IV	38499.852	0.000	$6s^2\ ^1S_0 - 7p'\ ^1P_1^0$
I	2592.30	.....	.....	38564.25	.....	.....
I	2543.2	—	.....	39308.74	0.00	$6s^2\ ^1S_0 - 10p\ ^1P_1^0$
I	2500.2	—	.....	39984.75	0.00	$6s^2\ ^1S_0 - 11p\ ^1P_1^0$
I	2473.20	0h	.....	40421.23	0.00	$6s^2\ ^1S_0 - 12p\ ^1P_1^0$
H	2373.109	3	.....	42125.95	.....	.....
H	2216.577	2	.....	45100.56	.....	.....
H	2214.639	2	.....	45140.02	.....	.....

REFERENCES

A, H. M. Randall, Astrophys. J. **42,** 195 (1915).
B, W. F. Meggers, B. S. J. Research **10,** 680 (1933) RP 558; and unpublished material (Jan. 1935).
C, F. Sullivan and K. Burns, Science Studies, St. Bonaventure Coll. **9,** No. 3, 7 (1941).
D, E. Lorenser, see H. Kayser und H. Konen, Handbuch der Spectroscopie **7,** 79 (1934).
E, H. N. Russ ll, unpublished material (1933?).
F, A. S. King, Contr. Mt. Wilson Solar Obs. No. 150; Astrophys. J. **48,** 13 (1918); and letter (July 1940).
G, F. Exner und E. Haschek, see H. Kayser und H. Konen, Handbuch der Spectroscopie **7,** 79 (1934).
H, K. Schmitz, see H. Kayser und H. Konen, Handbuch der Spectroscopie **7,** 79 (1934).
I, see F. A. Saunders, Astrophys. J. **51,** 23 (1920); see also H. Kayser und H. Konen, Handbuch der Spectroscopie **7,** 79 (1934).
J, see A. Fowler, Report on Series in Line Spectra, p. 133 (Fleetway Press, London, 1922).
K, see H. N. Russell and F. A. Saunders, Astrophys. J. **61,** 38 (1925).

TABLE 3. Intensities of Ba I combinations

	$6s^2\ ^1S_0$	$5d^2\ ^3P_2$	$5d^2\ ^3P_1$	$5d^2\ ^3P_0$	$5d^2\ ^1D_2$	$5d\ ^3D_3$	$5d\ ^3D_2$	$5d\ ^3D_1$	$5d\ ^1D_2$
$6p\ ^3P_2^\circ$		(300)	(200)		(100)	(50)	(30)	(20)	
$^3P_1^\circ$	3 I.A	(100)	(100)	(100)	(150)		(50)	(30)	
$^3P_0^\circ$			(150)					(30)	
$7p\ ^3P_2^\circ$						30 II	10*n* III		
$^3P_1^\circ$	(−)						25*n* III	8*n* III.A	
$^3P_0^\circ$								8*n* III.A	
$6p\ ^1P_1^\circ$	1000*R* I	(10)			(25)		(80)	(3)	(40)
$7p\ ^1P_1^\circ$	100*R* III				(8)		(1)		40 II
$8p\ ^1P_1^\circ$	15 IV								6*n* III
$9p\ ^1P_1^\circ$	(1*h*)								(−)*nl**
$10p\ ^1P_1^\circ$	(−)								
$11p\ ^1P_1^\circ$	(−)								
$12p\ ^1P_1^\circ$	(0*h*)								
$4f\ ^3F_4^\circ$						80 II			
$^3F_3^\circ$						30 III	50 II		(1)
$^3F_2^\circ$						3 III	20 III	40 II	
$5f\ ^3F_4^\circ$						80*n* III			
$^3F_3^\circ$						15*n* III	80*n* III		
$^3F_2^\circ$						(1*n*)	20*n* III	80*n* III	
$6f\ ^3F_4^\circ$						[70*R*] III			
$^3F_3^\circ$						[25] III	[60*R*] III		
$^3F_2^\circ$							[20] III	80*N* III	
$7f\ ^3F_4^\circ$						[50*r*] III			
$^3F_3^\circ$						[10] III	[40*r*] III		
$^3F_2^\circ$							[15] III	[60*R*] III	
$8f\ ^3F_4^\circ$						[50*r*] III			
$^3F_3^\circ$							[40] III		
$^3F_2^\circ$							[8] III	25*N* III	
$9f\ ^3F_4^\circ$						[30] III			
$^3F_3^\circ$							[30] III		
$^3F_2^\circ$							[15] III	[25] III	
$10f\ ^3F_4^\circ$						[10] III			
$^3F_3^\circ$							[10] III		
$^3F_2^\circ$							[10] III	[10] III	
$11f\ ^3F_4^\circ$						[15*n*] III			
$^3F_3^\circ$							[8*n*] III		
$^3F_2^\circ$								[3*n*] III	
$12f\ ^3F_4^\circ$						[12*N*] III			
$^3F_3^\circ$							(−)		
$^3F_2^\circ$			(1*U*)					(−)	

	$6s^2\ ^1S_0$	$5d^2\ ^3P_2$	$5d^2\ ^3P_1$	$5d^2\ ^3P_0$	$5d^2\ ^1D_2$	$5d\ ^3D_3$	$5d\ ^3D_2$	$5d\ ^3D_1$	$5d\ ^1D_2$
$13f\ ^3F_4^\circ$						(−)			
$^3F_3^\circ$							(−)		
$^3F_2^\circ$									
$14f\ ^3F^\circ$						(−)			
$15f\ ^3F^\circ$						(−)			
$4f\ ^1F^\circ$							4 III		100 II
$5f\ ^1F^\circ$						15*n* III*	10 III*		15 III*
$6f\ ^1F^\circ$									40*N* III
$7f\ ^1F^\circ$									30*N* III
$8f\ ^1F^\circ$									[40] III
$9f\ ^1F^\circ$									[30*n*] III
$6p'\ ^3P_2^\circ$						300*r* II	100 II	15 II.A	30 II
$^3P_1^\circ$	20 II						200 II	100 II	(5)
$^3P_0^\circ$								100 II	
$7p'\ ^3P_2^\circ$						15*n* III*	10 III*		15 III*
$^3P_1^\circ$	8 IV						15 III	10 III	2 III
$^3P_0^\circ$								10 III	
$6p'\ ^1P_1^\circ$	200*R* II				(15)		(1)		150 II
$7p'\ ^1P_1^\circ$	8*n* IV						3*n* III		20*N* III
$6p'\ ^3D_3^\circ$						300*r* II	150 I		1 III.A
$^3D_2^\circ$						70 I	250 I	125 I	2 III.A
$^3D_1^\circ$	20 I						80 I	200 I	
$7p'\ ^3D_3^\circ$		(4*h*)				30 III	15 III		
$^3D_2^\circ$						2 III	3 III.A	10 III	(1*h*)*
$^3D_1^\circ$	3 IV						3 III	10 III	2 III
$6p'\ ^1D_2^\circ$						5 II	1 III.A	200 II	4 I
$7p'\ ^1D_2^\circ$					(4*h*)		10 III		20 III
$6p'\ ^3F_4^\circ$						400*r* II			
$^3F_3^\circ$						10 I	150*r* II		(60)
$^3F_2^\circ$						(10)	10 I	25*r* I	(500)
$7p'\ ^3F_4^\circ$						40 III			
$^3F_3^\circ$							15 III		(2*n*)
$^3F_2^\circ$							(2)	2 III	
$6p'\ ^1F_3^\circ$						20 II	2 III.A		200 II
$7p'\ ^1F_3^\circ$									15 III
39765$\frac{1}{2}$					(1*u*)		2*n* III	5*n* III	(0*n*)
39905$_{1,2}$			(1*u*)		(1*u*)				

* Blend.

TABLE 3. Intensities of Ba I combinations—Continued

	$6p\ ^3P_2^1$	$6p\ ^3P_1^1$	$6p\ ^3P_0^1$	$6p\ ^1P_1^1$	$6p'\ ^3P_2^1$	$6p'\ ^3P_1^1$	$6p'\ ^3P_0^1$	$6p'\ ^1P_1^1$	$6p'\ ^3D_3^1$	$6p'\ ^3D_2^1$	$6p'\ ^3D_1^1$	$6p'\ ^1D_2^1$	$6p'\ ^3F_4^1$	$6p'\ ^3F_3^1$	$6p'\ ^3F_2^1$	$6p'\ ^1F_3^1$
$6p^2\ ^3P_2$	60*n* II	80 II	.....	.....	(8*hl*)	(2*h*)	.....	.....	(6*h*)	(3*h*)	.....	.....	.....	.....	.....	.....
$^3P_1$	35 II	40 II	40 II	.....	(10)	(20)	(30)	.....	.....	(=)	(10)	.....	.....	.....	.....	.....
$^3P_0$	.....	40 II	.....	5 IIIA	.....	(5*h*)	.....	.....	.....	.....	(20*h*)	.....	.....	.....	.....	.....
$6p^2\ ^1D_2$	80 II	60 II	.....	4 III	(30*h*)	(10*h*)	.....	.....	(100*h*)	(1*h*)	(3*h*)	(30*h*)	.....	.....	20*h*	.....
$6p^2\ ^1S_0$	.....	30 III	.....	3 III	.....	.....	.....	(5)	.....	.....	.....	.....	.....	.....	.....	.....
$7s\ ^3S_1$	6 III	30 II	80 III	.....	.....	.....	.....	.....	.....	.....	.....	.....	.....	.....	.....	.....
$8s\ ^3S_1$	15 III	20 III	20*n* III	.....	.....	.....	.....	.....	.....	.....	.....	.....	.....	.....	.....	.....
$9s\ ^3S_1$	10*n* III	8*n* IIIA*	2*n* IV?	.....	(2*h*)	.....	.....	.....	.....	.....	.....	.....	.....	.....	.....	.....
$10s\ ^3S_1$	4*n* III	(1*h*)	(—)	.....	.....	.....	.....	.....	.....	.....	.....	.....	.....	.....	.....	.....
$11s\ ^3S_1$	(—)	(—)	.....	.....	.....	.....	.....	.....	.....	.....	.....	.....	.....	.....	.....	.....
$7s\ ^1S_0$	.....	(1)	.....	(500*hl*)	.....	.....	.....	.....	.....	.....	.....	.....	.....	.....	.....	.....
$8s\ ^1S_0$	.....	.....	.....	20 IV?	.....	.....	.....	.....	.....	.....	.....	.....	.....	.....	.....	.....
$9s\ ^1S_0$	.....	.....	.....	8 III*	.....	.....	.....	.....	.....	.....	.....	.....	.....	.....	.....	.....
$6d\ ^3D_3$	400*r* II	.....	.....	.....	.....	.....	.....	.....	.....	.....	.....	.....	(30)	.....	.....	.....
$^3D_2$	100 III	200 II	.....	(20*hl*)	.....	.....	.....	.....	.....	.....	.....	.....	.....	(10)	.....	.....
$^3D_1$	5 IIIA	(7)	100 II	.....	.....	.....	.....	.....	.....	.....	.....	.....	.....	.....	(1*h*?)	.....
$7d\ ^3D_3$	60*n* III	.....	.....	.....	(3*h*)	.....	.....	.....	.....	.....	.....	.....	.....	.....	.....	.....
$^3D_2$	50*n* III	20*n* III	.....	.....	.....	.....	.....	.....	.....	.....	.....	.....	.....	.....	.....	.....
$^3D_1$	(1*n*)	10*n* III	15*n*IIIA	(1*h*)	.....	.....	.....	.....	.....	.....	.....	.....	.....	.....	.....	.....
$8d\ ^3D_3$	30*N* III	.....	.....	.....	.....	.....	.....	.....	.....	.....	.....	.....	.....	.....	.....	.....
$^3D_2$	8*n* IIIA*	10*N* III	.....	.....	.....	.....	.....	.....	.....	.....	.....	.....	.....	.....	.....	.....
$^3D_1$	.....	5*N* III	(0)	.....	.....	.....	.....	.....	.....	.....	.....	.....	.....	.....	.....	.....
$9d\ ^3D_3$	(1*h*)*	.....	.....	.....	.....	.....	.....	.....	.....	.....	.....	.....	.....	.....	.....	.....
$^3D_2$	(0)	(—)	.....	.....	.....	.....	.....	.....	.....	.....	.....	.....	.....	.....	.....	.....
$^3D_1$	.....	(—)	(—)	.....	.....	.....	.....	.....	.....	.....	.....	.....	.....	.....	.....	.....
$10d\ ^3D_3$	(—)	.....	.....	.....	.....	.....	.....	.....	.....	.....	.....	.....	.....	.....	.....	.....
$^3D_2$	(—*nl*)*	(—)	.....	.....	.....	.....	.....	.....	.....	.....	.....	.....	.....	.....	.....	.....
$^3D_1$	.....	(—)	.....	.....	.....	.....	.....	.....	.....	.....	.....	.....	.....	.....	.....	.....
$11d\ ^3D_3$	(—)	.....	.....	.....	.....	.....	.....	.....	.....	.....	.....	.....	.....	.....	.....	.....
$^3D_2$	(—)	(—)	.....	.....	.....	.....	.....	.....	.....	.....	.....	.....	.....	.....	.....	.....
$^3D_1$	.....	.....	.....	.....	.....	.....	.....	.....	.....	.....	.....	.....	.....	.....	.....	.....
$6d\ ^1D_2$	4 IIIA	10 IIIA	.....	4 III?	.....	.....	.....	*2II*?	.....	.....	.....	.....	.....	.....	.....	.....
$7d\ ^1D_2$	8*n* IIIA	(0*h*)	.....	20*n* IV?	.....	.....	.....	.....	.....	.....	.....	(2*h*)	.....	.....	.....	(4*h*)
$8d\ ^1D_2$	(3*n*)	.....	.....	30*N* III	.....	.....	.....	.....	.....	.....	.....	.....	.....	.....	.....	.....
$9d\ ^1D_2$	.....	.....	.....	15*N* III	.....	.....	.....	.....	.....	.....	.....	.....	.....	.....	.....	.....
$7s'\ ^3D_3$	(1)	.....	.....	.....	(40)	.....	.....	.....	(40*h*)	(50*h*)	.....	.....	(400*h*)	(15*h*)	.....	.....
$^3D_2$	.....	.....	.....	.....	.....	(40)	.....	.....	(30)	(5*h*)	(20*h*)	(10)	.....	(300)	(60*h*)	.....
$^3D_1$	.....	.....	.....	.....	.....	(40)	(20)	.....	.....	(1*h*)	(30*h*)	(50*h*)	.....	.....	(100)	.....
$7s'\ ^1D_2$	(1)	3 III	.....	(1)	.....	.....	.....	(20)	.....	(40*hl*)	(3*h*)	(100*h*)	.....	(15*h*)	(8*hl*)	(25)
$6d'\ ^3S_1$	5 III	.....	(1)	4 IIIA	(10*h*)	(10)	(15*h*)	.....	.....	.....	(3*h*)	(30*h*)	.....	.....	(1*n*)	.....
$6d'\ ^3P_2$	(0)	2 III	.....	8 III*	(30*hr*)	(2*h*)	.....	.....	(20*h*)	.....	.....	.....	.....	.....	.....	.....
$^3P_1$	.....	.....	(2)	.....	(6*hr*)	.....	(1*h*)	.....	.....	(30*hr*) IV	.....	.....	.....	.....	.....	.....
$^3P_0$	.....	.....	.....	.....	.....	(2*h*)	.....	.....	.....	.....	(4*hl*)	.....	.....	.....	.....	.....
$6d'\ ^1P_1$	.....	.....	(1) *Ph*?	4 IV?	(15*h*)	(7*hl*)	.....	(15)	.....	.....	(1*h*)	(10*h*)	.....	.....	.....	.....
$6d'\ ^1D_2$	10 III	.....	.....	.....	(80*h*)	.....	.....	.....	(50*hl*)	(3*h*)	.....	2*n* III	(10*hl*)	(10*h*)	.....	(50*h*)
$^1D_2$	15 III	10 III	.....	.....	(2*h*)	(60*rh*)	.....	.....	(3*h*)	(40*hl*)	(20*h*)	(1*n*)	.....	(25*h*)	(1*h*)	.....
$^1D_1$	(0)	12 III	12 III	3 III	.....	(6*h*)	(60)	.....	.....	(1*h*)	(30*hl*)	.....	.....	.....	1*n*III	.....
$6d'\ ^1D_2$	2 III	.....	.....	5 IV?	(4*hr*)	.....	.....	(4*h*)	(10*h*)	(3*h*)	(10*h*)	2*n* III	.....	(2*h*)	.....	.....
$6d'\ ^3F_4$	.....	.....	.....	.....	.....	.....	.....	.....	(60*h*)	.....	.....	.....	5 III	(2*h*)	.....	.....
$^3F_3$	.....	.....	.....	.....	.....	.....	.....	.....	(15*hr*)	(50*hr*)	.....	.....	(2*h*)	8*n* IV?	.....	.....
$^3F_2$	.....	.....	.....	(1*n*)	.....	.....	.....	.....	.....	(10*hr*)	(40*hr*)	.....	.....	(3)	10 III	.....
$6d'\ ^1F_3$	8 III	.....	.....	.....	(5*h*)	.....	.....	.....	(10*h*)	(4*hl*)	.....	2*n* III	.....	.....	5*n* III	(8*hl*)
$6d'\ ^3G_5$	≙	.....	.....	.....	.....	.....	.....	.....	.....	.....	.....	.....	4*n* III	.....	.....	.....
$^3G_4$	.....	.....	.....	.....	.....	.....	.....	.....	(3*h*)	.....	.....	.....	(3*h*)	5*n* III	.....	(2*h*)
$^3G_3$	.....	.....	.....	.....	.....	.....	.....	.....	(10*h*)	.....	.....	(5*h*)	.....	(10*h*)	25 III	(60*hl*)
$6d'\ ^1G_4$	.....	.....	.....	.....	.....	.....	.....	.....	(2*h*)	.....	.....	.....	(2*h*)	2 IIIA	.....	(100*h*)

*Blend.
=Masked.

WASHINGTON, February 18, 1955.

Journal of Research of the National Bureau of Standards Vol. 55, No. 6, December 1955 Research Paper 2634

Compressibilities of Long-Chain Normal Hydrocarbons

C. E. Weir and J. D. Hoffman

Measurements were made of the compressions of n-$C_{18}H_{38}$, n-$C_{20}H_{42}$, n-$C_{24}H_{50}$, n-$C_{26}H_{54}$, n-$C_{28}H_{58}$, and n-$C_{30}H_{62}$ in the crystalline state at 21° C. The pressure range used was from 1,000 to 10,000 atmospheres. Within the experimental error, which was fairly large because of the small size of sample, no significant variation of the compression with chain length was observed. The average compression of all the hydrocarbons studied may be represented by the equation

$$-\Delta V/V_0 = 0.1717 \log_{10} (2{,}500 + P) - 0.6272.$$

The average compressibility of the hydrocarbons extrapolated to 1 atmosphere was calculated to be 29.8×10^{-6} atm^{-1} at 21° C.

1. Introduction

Considerable interest has been exhibited in the properties of the normal long-chain hydrocarbons, as indicated by numerous reports on studies of these materials. As pointed out earlier [1],[1] there is need for data on the compressibilities of these materials, the only data available on the crystalline materials appearing to be those of Müller [2] obtained from X-ray measurements on n-$C_{23}H_{48}$ and n-$C_{29}H_{60}$. Data on the liquids containing between 5 and 10 carbon atoms were reported by Bridgman [3], and Cutler, Schiessler, and Webb [4] have recently reported measurements on n-$C_{12}H_{26}$, n-$C_{15}H_{32}$, and n-$C_{18}H_{38}$ in the liquid state.

In the present report, data are given for compressions at 21° C for some of the crystalline normal hydrocarbons containing between 18 and 30 carbon atoms.

Because of the small amount of each hydrocarbon available, the errors of measurement were necessarily rather large. Accordingly, the present results are of a somewhat exploratory nature, and will probably be subject to slight revision when data on much larger samples are obtained.

2. Experimental Method

It was considered desirable to measure the compressibilities at low pressures, i. e., 1 to 1,000 atm, but efforts to do this with the present samples in this pressure range, using piezometric techniques, were unsuccessful. The errors in such measurements were so large as to render the data of dubious value. These errors were probably the result of interfacial effects arising from the fact that the only confining liquids considered inert toward the specimens were water and mercury—both nonwetting liquids. After vacuum impregnation of the specimens with either liquid, unfilled capillary spaces were visible. Presumably these were filled at elevated pressures, thus giving rise to the erratic compressions observed. Attempts to fill the voids permanently at 10,000 atm were unsuccessful because the visible capillaries emptied partially in an irreproducible manner on reduction of the pressure. It was decided, therefore, to measure the compressions at high pressures, where errors arising from void spaces are negligible. The basic techniques and equipment used in such studies have been described earlier [5].

Certain modifications of the procedures were devised to permit study of the small specimens. Each hydrocarbon was fused and recrystallized in a small Pyrex tube, open at one end. The filled tubes were placed, open end down, in a stainless-steel container, open at one end. A steel spring under compression served to hold the open end of the glass tube in contact with the bottom of the steel container. This assembly was evacuated for ½ hr, using a mechanical pump, and the stainless-steel container filled with clean mercury while under vacuum. To minimize danger of contamination of the pressure vessel with mercury, the mercury-filled assembly was placed in a somewhat larger telescoping steel container designed to catch any mercury inadvertently spilled from the inner container. This unit, consisting of telescoping tubes, glass, mercury, spring, and hydrocarbon, represented the compression specimen and was immersed in a light petroleum distillate (Varsol) in the pressure vessel. For a comparison standard the same assembly was used, except that the glass tube contained no hydrocarbon. The comparison material for the hydrocarbon, therefore, consisted of a similar volume of mercury.

Compression data were calculated by means of a generalization of the equation of Adams [6], as follows:

$$k-k' = \frac{S}{V_0}\Big\{\Delta L(1+\alpha P)+\Delta l'\alpha(P-P')+\Big[\nabla l'(1+\alpha P_0)+\sum_{n=1}^{n=m-1}\frac{V'_n - V'_{nr}}{S}\Big]\frac{k-k'_l}{1-k'_l}\Big\}+\sum_{n=1}^{n=m-2}(k_n-k'_n)\Big(\frac{V_{nr_0}-V_{n_0}}{V_0}\Big). \quad (1)$$

P denotes pressure in atmospheres and V, volume; subscript zero denotes 1 atm, and subscripts r and l refer to measurements made with reference material and pressure-transmitting liquid, respectively. Primes denote the experimental reference pressure

[1] Figures in brackets indicate the literature references at the end of this paper.

of 2,000 atm. The compression $k=-(V-V_0)/V_0=-\Delta V/V_0$ at pressure P; k' is the corresponding compression at 2,000 atm, i. e., $-(V'-V_0)/V_0$. S is the area of the bore of the vessel at 1 atm; α is the pressure coefficient of this area $(1/S)\ (dS/dP)$; ΔL is the difference in travel of the piston at pressure P in the measurements on the reference specimen and the unknown specimen calculated from 2,000 atm; $\Delta l'$ is the difference of the positions of the piston at 2,000 atm in the two measurements. The generalization is contained in the two summations, the first being carried out over all m components in the vessel except the pressure-transmitting liquid, and the second for all except the specimen and the liquid.

All components of the compression specimen were weighed and the required volumes calculated from the weights. Known densities of steel and mercury were used, whereas that of the glass was determined by hydrostatic weighing. Volumes of the hydrocarbons were obtained from the weights by use of specific volume-temperature data of Templin [7]. All these data were extrapolated to 21° C, and some uncertainty (probably not exceeding 1%) exists in the specific volumes used. The values used were, in cubic centimeters per gram, 1.070 for $C_{18}H_{38}$; 1.060 for $C_{20}H_{42}$; and 1.050 for all other specimens. The latter value agrees with a flotation density of n-$C_{29}H_{60}$ obtained by Müller [8]. The error introduced through inaccuracies in these values is believed to be less than the precision of the compression measurements.

All glass tubes used were prepared from a single length of tubing, and all were annealed simultaneously. The compression of glass used was that reported by Adams and Gibson [9]. The compression of mercury was also taken from the data of Adams [10] and represents only a slight modification of his published data [6]. The compression of steel did not enter the calculations because the volume of steel was the same in all measurements.

About 1 cm_3 of each of the following hydrocarbons was available for study: n-$C_{18}H_{38}$, n-$C_{20}H_{42}$, n-$C_{24}H_{50}$, n-$C_{26}H_{54}$, n-$C_{28}H_{58}$, and n-$C_{30}H_{62}$. The melting points, which were sharp, are given in table 1.

3. Results and Discussions

The results of the compression measurements on the hydrocarbons are given in table 1. Values of compression, $-\Delta V/V_0$, referred to 2,000 atm are tabulated for each 1,000-atm interval; measurements at 1,000 atm appear as negative values because the data are based on the reference point at 2,000 atm. The data at 1,000 atm are less reliable than those at the higher pressures and are not considered in the following discussion. Two independent measurements, obtained at different times, were made on each specimen, and these data are tabulated as runs 1 and 2. The averages of the two measurements on each specimen are also tabulated.

By inspection of the duplicate measurements it is apparent that the errors are large. The increased error [11] is to be expected as the specimen has a volume of only about 1 cm^3 out of a total of 25 cm^3 of material in the pressure vessel. Ordinarily a 10- to 12-cm^3 specimen is used. In view of the decreased precision a statistical analysis of the data was carried out. This analysis corroborated a standard deviation of ± 0.0040 in $-\Delta V/V_0$ and showed that, for a given pressure, no really significant difference exists between the compressions of the different hydrocarbons within experimental error. On this basis the data of table 1 (excluding those taken at 1,000 atm) have been averaged, with the results given in the last column of the table. These average data are considered to be representative of all specimens studied. To obtain compressibility data, the average compressions of table 1 were fitted to the Tait equation [12] by means of least squares. The resulting equation,

$$-\Delta V/V_0=0.1717\ \log_{10}(2{,}500+P)-0.6272, \quad (2)$$

with P in atmospheres, reproduces the average compression data within ± 0.0005, which is well within the experimental error. The fit of eq 2 with the experimental data as averaged at each pressure is shown in figure 1. The corresponding values of the

TABLE 1. *Compressions of normal hydrocarbons*

Compression, $-\Delta V/V_0$

Pressure	n-$C_{18}H_{38}$ (mp=28.1° C)			n-$C_{20}H_{42}$ (mp=36.5° C)			n-$C_{24}H_{50}$ (mp=50.6° C)			n-$C_{26}H_{54}$ (mp=56.1° C)			n-$C_{28}H_{58}$ (mp=61.1° C)			n-$C_{30}H_{62}$ (mp=65.4° C)			Average of all
	1	2	Average	1	2	Average	1	2	Average	1	2	Average	1	2	Average	1	2	Average	
atm																			
10,000	0.0764	0.0748	0.0756	0.0761	0.0736	0.0748	0.0757	0.0816	0.0786	0.0682	0.0773	0.0728	0.0822	0.0712	0.0767	0.0750	0.0791	0.0770	0.0759
9,000	.0695	.0701	.0698	.0702	.0667	.0684	.0701	.0780	.0740	.0602	.0708	.0655	.0769	.0672	.0720	.0695	.0745	.0720	.0703
8,000	.0643	.0617	.0630	.0619	.0600	.0610	.0632	.0695	.0664	.0566	.0647	.0606	.0680	.0600	.0640	.0635	.0659	.0647	.0633
7,000	.0552	.0531	.0542	.0554	.0549	.0552	.0534	.0619	.0576	.0494	.0567	.0536	.0604	.0516	.0560	.0562	.0570	.0566	.0554
6,000	.0431	.0468	.0450	.0467	.0472	.0470	.0463	.0553	.0508	.0368	.0490	.0429	.0512	.0444	.0478	.0500	.0490	.0495	.0472
5,000	.0342	.0378	.0360	.0384	.0390	.0387	.0343	.0447	.0395	.0307	.0389	.0348	.0410	.0351	.0380	.0390	.0394	.0392	.0377
4,000	.0263	.0277	.0270	.0294	.0262	.0278	.0253	.0345	.0299	.0227	.0284	.0256	.0298	.0261	.0280	.0307	.0284	.0296	.0280
3,000	.0145	.0149	.0147	.0156	.0147	.0152	.0150	.0190	.0170	.0081	.0159	.0120	.0161	.0143	.0152	.0113	.0159	.0136	.0146
2,000	.0000	.0000	.0000	.0000	.0000	.0000	.0000	.0000	.0000	.0000	.0000	.0000	.0000	.0000	.0000	.0000	.0000	.0000	.0000
1,000	−.0218	−.0141	−.0180	−.0069	.....	−.0069	.....	.....	.....	−.0121	−.0124	−.0122	.....	−.0153	−.0153	−.0108	−.0164	−.0136	−.0137

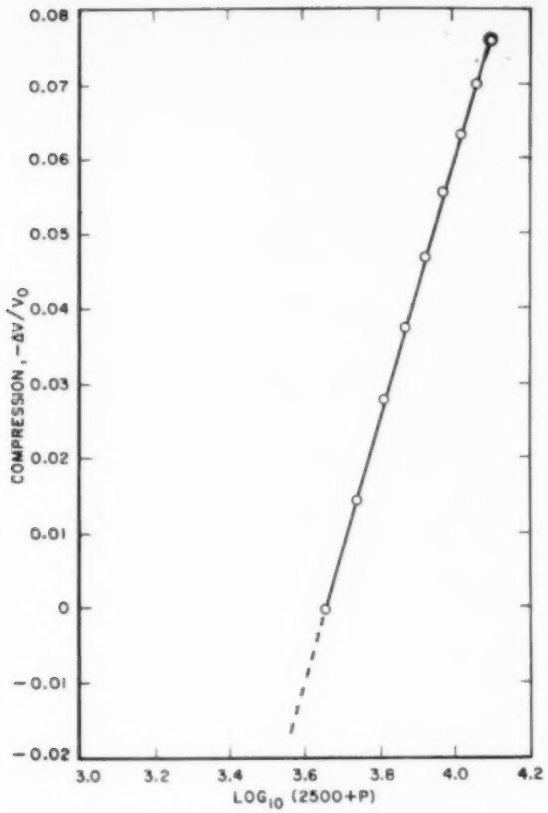

FIGURE 1. *Plot of Tait equation for normal hydrocarbon.*

compressibility at the various pressures are given in figure 2.

It has been noted by Gibson [12] that the Tait equation reproduces both volume and compressibility data on many materials with great accuracy over a wide pressure range (see also [4]). Of immediate interest is the fact that this equation, although empirical, has been used very successfully in extrapolating from low to high pressures. The reverse process is used here, as data are desired at low pressures. From the derivative of eq 2 it is found that the compressibility is given by the equation

$$-\frac{dV}{V_0 dP}=\frac{0.1717}{2.303\ (2{,}500+P)}. \tag{3}$$

If $P \ll 2{,}500$ atm, the volume compressibility is found to be 29.8×10^{-6} atm^{-1}. Statistical analysis of the data indicates that the standard deviation in the value is 0.4×10^{-6} atm^{-1}. The true value may, of course, lie outside these limits.

It is interesting to compare the present results with those of Müller [2], who measured the change in X-ray spacings with pressure for the odd-carbon compounds n-$C_{23}H_{48}$ and n-$C_{29}H_{60}$. In making this comparison, it should be remembered that the even- and odd-carbon hydrocarbons have different crystal structures at room temperature, so that close agreement of the compressibility values is not necessarily to be expected. At room temperature the odd-carbon compounds from n-$C_{21}H_{44}$ to n-$C_{29}H_{60}$ are orthorhombic, whereas the even-carbon compounds from n-$C_{18}H_{38}$ through n-$C_{24}H_{50}$ are triclinic; n-$C_{28}H_{58}$ and n-$C_{30}H_{62}$ are monoclinic [13]. Both the monoclinic and triclinic forms appear simultaneously in n-$C_{26}H_{54}$ [1, 13]. Using Müller's finding [2] that the compressibility is essentially a two-dimensional effect,[2] the linear compressibility values quoted in Müller's paper are equivalent to volume compressibilities of 21×10^{-6} atm^{-1} for n-$C_{23}H_{48}$, and 5.5×10^{-6} atm^{-1} for n-$C_{29}H_{60}$. These values represent the average compressibility at 500 atm; our value at the same pressure for the even-carbon compounds is 25.5×10^{-6} atm^{-1}.

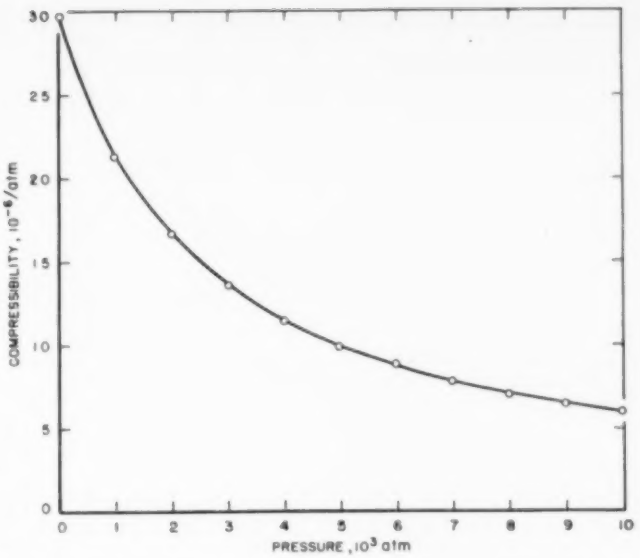

FIGURE 2. *Average compressibility-pressure relationship in normal hydrocarbon.*

The effects arising at chain ends lead to the expectation that the compressibility should decrease slightly with increasing chain length in the normal hydrocarbons. Bridgman's data on the liquid hydrocarbons [3] up to n-$C_{10}H_{22}$ show this effect. The data of Cutler, Schiessler, and Webb [4] on n-$C_{12}H_{26}$, n-$C_{15}H_{32}$, and n-$C_{18}H_{38}$ in the liquid state also show a slight decrease of compressibility with length of chain. However, in the latter study it is clear that the effect decreases with increasing chain length and pressure, as would be expected. Bridgman [14] has reported data on polyethylene of three different average molecular weights in the range 14,000 to 38,000 that show no significant effect of molecular weight on compressibility, and verify the belief that the effect of chain ends on compressibility becomes negligible as the chain length increases in this partially amorphous and partially crystalline (monoclinic) polymer. The fact that no effect of chain length on compressibility is shown by the present

[2] The changes with pressure of the X-ray spacings found by Müller were stated to be almost entirely a result of the hydrocarbon chains moving closer together laterally.

data on the crystalline hydrocarbons implies that such an effect is smaller than the experimental error of the measurements. Similarly, there does not appear to be any large difference in the compressibilities of the triclinic and monoclinic forms of the even-carbon hydrocarbons because the results for materials with 18 to 24 carbon atoms do not differ greatly from those for materials with 28 and 30 carbon atoms per molecule.

The authors are indebted to J. Mandel for advice in connection with the statistical analyses of the experimental data.

WASHINGTON, September 7, 1955.

4. References

[1] J. D. Hoffman and Buelah F. Decker, J. Phys. Chem. **57,** 520 (1953).
[2] A. Müller, Proc. Roy. Soc. (London) [A] **178,** 227 (1941).
[3] P. W. Bridgman, The physics of high pressure (G. Bell & Sons, Ltd., London, 1949).
[4] W. G. Cutler, R. W. Schiessler, and W. Webb, Bul. Am. Phys. Soc. [3] **30,** 38 (1955).
[5] C. E. Weir, J. Research NBS **45,** 468 (1950) RP2160.
[6] L. H. Adams, J. Am. Chem. Soc. **53,** 3769 (1931).
[7] P. R. Templin, M. S. Thesis, University of Pittsburgh (1954).
[8] A. Müller, Proc. Roy. Soc. (London) [A] **120,** 437 (1928).
[9] L. H. Adams and R. E. Gibson, J. Wash. Acad. Sci. **21,** 381 (1931).
[10] L. H. Adams (private communication).
[11] C. E. Weir, J. Research NBS **52,** 247 (1954) RP2496.
[12] R. E. Gibson, J. Am. Chem Soc. **59,** 1521 (1937).
[13] A. A. Schaerer, C. J. Busso, A. E. Smith, and L. B. Skinner, J. Am. Chem. Soc. **77,** 2017 (1955).
[14] P. W. Bridgman, Proc. Am. Acad. Arts Sci. **76,** 55 (1948)

Journal of Research of the National Bureau of Standards Vol. 55, No. 6, December 1955 Research Paper 2635

Absolute Calibration of the National Bureau of Standards Photoneutron Standard: II. Absorption in Manganese Sulfate

James De Juren [1] and Jack Chin

An absolute method of calibrating a neutron source by determining the neutron absorption rate in a manganese sulfate bath is described. In this method slightly more than one liter of solution from the bath is irradiated in a strong neutron flux. The absolute activity of manganese in an aliquot of this activated solution is determined with a 4π flow proportional counter. Concurrently, one liter of this solution is added to the inactive bath and after stirring, the counting rate is measured with a dip counter. As the number of radioactive manganese nuclei contained in the liter is obtained from the aliquot activity, the dip counter is calibrated for a known manganese activity. Then the bath is irradiated by the source and the dip counting rate at saturation yields the neutron capture rate by the manganese. From a knowledge of the neutron capture cross sections and the manganese sulfate concentration, the fraction of neutrons captured by manganese is determined. As a result, the total neutron capture rate in the bath at saturation is obtained. A value of $Q=1.25_0\times10^6$ neutrons per second was obtained for the National Bureau of Standards source (1954). The standard error is ±2 percent.

1. Introduction

As wide discrepancies between international neutron standards [1] [2] have been revealed by intercomparisons, it was thought advisable to use two different methods for the calibration of the NBS standard neutron source. Both the emission rate of the NBS standard neutron source [2] and the thermal neutron density in a moderator [3] have already been determined by methods in which the key measurement is the absolute counting rate of alpha particles from thin boron films. The purpose of the present work was to develop an independent method having an accuracy equal to or better than that obtained previously. In the method selected the key measurement is the determination of the absolute activity of an aliquot from an activated manganese sulfate solution.

Two previous absolute calibrations of neutron sources have been made elsewhere in which manganese sulfate $(MnSO)_4$ solutions were employed to moderate and absorb the emitted neutrons. O'Neal and Sharff Goldhaber [4] used a simple method. The activity of a tank of manganese sulfate solution is measured with a dip counter after irradiation to saturation with a neutron source and thorough stirring of the active solution. Powdered manganese is added to the solution and the mixture again irradiated to saturation. After removal of the powder, the activity of the solution is measured and the absolute activity of the powder determined. The total activity of the powder is equal to $(1-f)Q$, where f is the ratio of the solution counting rates from irradiations with and without the powder, and Q is the emission rate of the source. When the irradiation is made with the powder present, f is the fraction of the emitted neutrons captured by the solution.

The Swiss standard source has been calibrated in a similar manner [5]. Instead of using manganese powder, the activity of the solution is measured at two different concentrations to determine the ratio of the captures in manganese sulfate to water (hydrogen). A solution of manganese sulfate is activated in an intense neutron flux from the D-D reaction. The activity of the solution is measured, as before, with a dip counter. Part of the solution is precipitated as manganese carbonate and the absolute activity of a dried sample of this powder determined with a layer counter [6]. This measurement calibrates the dip counter arrangement for this concentration in terms of the manganese activity present. Both methods require the determination of the absolute beta activity of a fairly thick layer of powder and the precision in the neutron emission rates claimed is of the order of 8 percent.

In brief, the NBS standard Ra-Be (γ,n) source consists of a beryllium sphere, 4 cm in diameter, at the center of which a one curie capsule of $RaBr_2$ is placed. As only gamma rays can enter the beryllium, the neutron emission rate is quite constant, unlike a Ra-Be (α,n) source, which has an initial growth of about 0.5 percent a year.

2. Experimental Method

2.1. Outline of General Method

In the present method the unknown source is suspended at the center of a cylindrical tank (approximately 1 m in both diameter and depth) filled with manganese sulfate solution. After irradiation to saturation and thorough stirring, the activity of the solution is measured with a dip counter. Then in a

[1] Present address: Westinghouse Electric Corp., AFD, Pittsburgh, Pa.
[2] Figures in brackets indicate the literature references at the end of this paper.

later experiment, slightly more than 1 liter of tank solution is irradiated in a strong neutron flux. A small aliquot (usually 0.075 ml) of this activated solution is pipetted onto a plastic film and its absolute activity determined with a 4π counter. One liter of this solution is added to the inactive solution in the tank, the mixture stirred, and the activity measured with the dip counter. The number of radioactive manganese nuclei initially present in the tank is obtained from the absolute activity of the aliquot after correction for decay to the same arbitrary reference time. Then the ratio of the saturated dip counting rate from the neutron source irradiation to the counting rate for the known manganese activity yields the saturated neutron counting rate in manganese. This counting rate is converted to total neutron capture rate by a factor expressing the ratio of the total capture cross section per millimeter in the bath to the manganese cross section per millimeter. Let

(1) C_s be the dip counting rate of the tank solution at saturation from the source irradiation,

(2) C_a be the dip counting rate when the liter of activated solution is added to the tank,

(3) $C_{4\pi}$ be the absolute counting rate of the aliquot of volume 0.075 ml.

Then the ratio of the absolute manganese activity in the tank to the dip counting rate when the liter of activated solution is added to the tank and stirred is

$$R=\frac{1000}{0.075}\times\frac{C_{4\pi}}{C_a}. \tag{1}$$

R may be interpreted as the absolute manganese activity in the tank per unit dip counting rate. The number of neutrons from the source captured per second by the manganese, Q_{Mn}, is

$$Q_{Mn}=RC_s. \tag{2}$$

If all the absorbing nuclei in the tank solution had capture cross sections varying inversely with the neutron velocity, the number of captures per second in the tank, Q, would be

$$Q=\frac{N_{Mn}(\sigma_{Mn}+\sigma_S)+N_H\sigma_H}{N_{Mn}\sigma_{Mn}}\,Q_{Mn}, \tag{3a}$$

where N_{Mn} is the number of manganese (and sulfur) nuclei per millimeter N_H is the number of hydrogen nuclei per millimeter, and σ_{Mn}, σ_S, and σ_H are the capture cross sections of manganese, sulfur, and hydrogen for thermal neutrons. Neutron capture in oxygen is negligible for the photoneutron source. Manganese is not a strict $1/v$ absorber in the epithermal region and a small ($\sim 1\%$) correction is given in the appendix. Including the correction term the equation is

$$Q=\frac{1.012\,N_{Mn}\sigma_{Mn}+N_{Mn}\sigma_S+N_H\sigma_H}{1.012\,N_{Mn}\sigma_{Mn}}\,RC_s \tag{3b}$$

for the concentration used.

A thin-walled Geiger counter, which had proved very reliable, was used as the dip counter.

2.2. Description of the 4π Counter

A 4π flow counter using a 90-percent argon, 10-percent carbon dioxide gas mixture was used for the absolute measurement of the specific activity. The counter has two hemicylindrical collecting volumes separated by a plastic film 7.3 by 12.1 cm. Stainless-steel wires, 0.0025 cm in diameter and 2.5 cm above and below the plastic film, extend parallel to the cylinder axes and are supported by kovar seals projecting through the cylinder bases. One-quarter mil mylar films, coated on both sides with 5 to 10 $\mu g/cm^2$ of aluminum, were mounted on a slide, which slipped into position between the hemicylinders (fig. 1).

Pulses from the collecting wires were separately fed by cathode followers to Chase-Higinbotham nonoverloading amplifiers operating at a gain of approximately 30,000. The amplified pulses from each half of the chamber and the coincidence counting rate were recorded with a coincidence circuit having a resolving-time gate width of 2 μsec. Several tests were made of the performance of the counter. An activated gold foil, 1 cm^2 in area, was used to measure the relative counting efficiencies at different positions on the mylar support. When the source was confined to a central region with boundaries 2.5 cm from the bases and 0.8 cm from the walls of the hemicylinders, the measured activities, corrected for decay, agreed within the standard deviation of 0.3 percent. A calibrated Na^{22} source (supplied by H. Seliger of the NBS Radioactivity Section) was measured with this 4π counter. The counting rate obtained, when corrected for decay and absorption in the mylar, was in agreement (within the experimental errors) with the original calibration.

The counting rate as a function of collecting wire voltage and counting rate as a function of (integral) discriminator voltage characteristics of the chamber were investigated with neutron irradiated manganese foils. A collecting voltage of 1,950 v was selected in the center of a voltage plateau of more than 200 v.

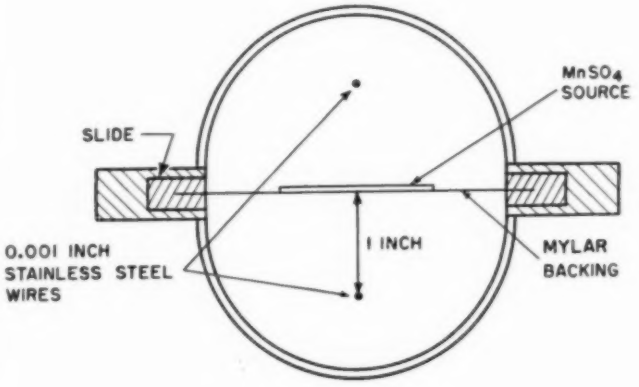

FIGURE 1. *Four π counter.*

The decay of the manganese foils was followed for several half-lives on six separate occasions. These measurements yielded a value of 223.7 ± 0.2 min for the mean life, which is in good agreement with published values [7].

The 4π counting rate is equal to the sum of the individual counting rates from each half of the chamber minus the coincidence counting rate. Usually the collecting wires are connected together so that the 4π counting rate is obtained directly; however, knowledge of the individual counting rates gives more information regarding improper operation of the chamber. If a source is not thoroughly dried or the chamber not thoroughly flushed, the trouble is usually quickly detected by observation of the individual counting rates.

2.3. Preparation of 4π Sources

Considerable difficulty was initially experienced in preparing 4π sources, which, after drying, would adhere well to the mylar backing without flaking. The following technique proved the most satisfactory. An area 25 cm^2 in extent was wet with a water solution containing 1.5 percent of polyvinyl alcohol and 0.2 percent of triton X–100. Triton X–100 is a potent spreading and wetting agent and the polyvinyl alcohol an excellent binding material. An ultramicroburet, accurate to 1 part in a thousand, delivered 0.075 ml of the activated manganese sulfate solution onto the prepared area. The slide containing the manganese sulfate and a beaker of ammonium hydroxide were placed under a bell jar for a few minutes until the manganese was precipitated. Then the beaker was removed and the bell jar evacuated through a cold trap to dry the film. The mass of one of these sources, determined by weighing, was 25.6 mg, giving a value of about 1.0 mg/cm^2 for the average source thickness.

3. Experimental Data

Five measurements were taken of the absolute counting rate of the 0.075-ml aliquots with a ¼-mil mylar backing, and one measurement was made with the aliquot sandwiched between two coated mylar films. For the backing alone a typical set of measurements, corrected for decay, was as follows:

(1) Single-chamber counting rate ~2,000 counts per minute

(2) Coincidence counting rate ~500 counts per minute. The top side of the chamber (facing the uncovered source) had a counting rate of about 6 percent greater than the bottom half. Table 1 gives the pertinent data for these six cases.

Measurements were made of the 4π counting rate as a function of mylar absorber thickness. To obtain a statistically significant effect, aluminum-coated sheets of mylar 7.5 mg/cm^2 thick were added above and below the manganese sulfate source deposited on ¼-mil mylar film. The absorption data are shown in figure 2. A ¼-mil (~1 mg/cm^2) mylar absorber causes

TABLE 1. *Calibration data*

Source—	4π counting rate	Absorption correction	Absolute counting rate, $C_{4\pi}$	Dip counting rate, C_s	[a] $R=\frac{1{,}000\ C_{4\pi}}{0.075\times C_s}$
	Counts/min		*Counts/min*	*Counts/min*	
On ¼-mil mylar backing	2662.8	1.014	2700.1	205.7	1.750×10^5
Do	.....	1.014	3068.6	237.4	1.724
Do	3294.4	1.014	3340.5	252.6	1.763
Do	3336.9	1.014	3383.6	257.2	1.754
Do	3170.9	1.014	3215.3	246.6	1.738
In ¼-mil mylar sandwich	3077.6	1.020	3139.3	241.7	1.732
Average					1.744×10^5

[a] Each measurement of R, not including the error in the absorption factor, has a statistical accuracy of about ±0.9 percent, and the error in the average value of R is ±0.4 percent. The indicated uncertainties are expressed in terms of the standard error of the mean.

a reduction of $(0.6 \pm 0.1\%)$ in the counting rate. As the manganese sulfate source thickness is also about 1 mg/cm^2, the correction for self-absorption will be of equal size; however, to allow for nonuniformity in the source thickness and variation in the area covered by different sources, the source self-absorption has been taken as $(0.8 \pm 0.4\%)$. All sources used should have self-absorption corrections falling within these bounds. For the sources deposited on the mylar backing with no cover, the total absorption correction is $(1.4 \pm 0.4\%)$. At the concentration used and for the cross sections listed in the appendix, eq 3b becomes

$$Q = 2.861\ RC_s. \tag{3c}$$

Using the average value of R from table 1,

$$Q = 4.990 \times 10^5 C_s. \tag{4}$$

With the manganese sulfate bath-dip counter system calibrated in this manner, the absolute calibration of the neutron emission rate from any source is obtained

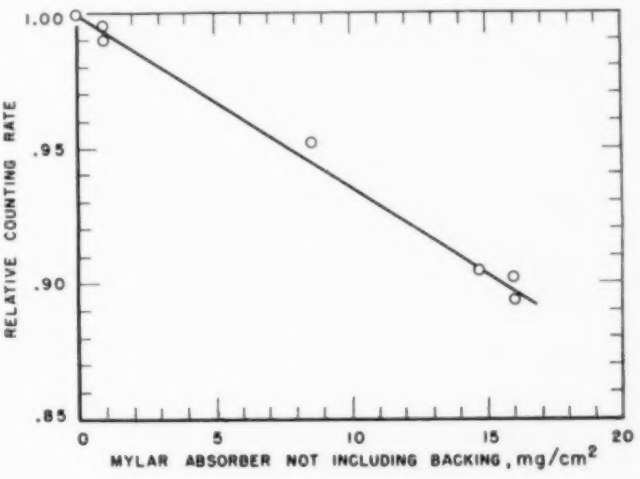

FIGURE 2. *Absorption of* Mn^{56} *beta particles in mylar absorber.*

from the dip counting rate at saturation. A small correction must be made for the self-absorption of thermal neutrons by the source when in the bath.

When the NBS standard Ra-Be (γ,n) source was placed in the bath, the saturated dip counting rate was 2.49_8 ($\pm 1\%$) counts per second, giving a value $Q=1.24_8\times 10^6$ neutron captures per second in the bath. In pure water the source self-absorption [2] amounted to $6{,}000\pm 2{,}000$ neutrons per second. For the manganese sulfate solution used, the slowing down length is about 4 percent longer than in water, and the mean life of a thermal neutron is only two-thirds of the life in water. As a result, the thermal neutron density in the vicinity of the source in the manganese sulfate solution is 60 percent of the value in water, reducing the source self-capture to $3{,}600\pm 1{,}500$ neutrons per second. Finally, the total emission rate from the source is $(1.25_0\pm 0.02_5)\times 10^6$ neutrons per second.

4. Discussion

The major part of the final standard error in the calibration stems from the uncertainties in the capture cross-section values for manganese and hydrogen, which cause a standard error of 1.2 percent in the capture factor. Recent measurements of the hydrogen cross section by the pulsed neutron decay method yield a value of 0.333 ± 0.003 barn [8], compared with the earlier value of 0.321 ± 0.005 barn [9]. The value of 0.333 barn, combined with the value of 0.329 ± 0.004 barn obtained by Hamermesh, Ringo, and Wexler [10] and 0.332 ± 0.007 barn obtained by Harris et al. [11], would give a "best average" of 0.332 barn, compared with the 0.328 barn used. Further work on the decay method is planned by von Dardel in order to resolve some of the uncertainties. However, an increase of 1.2 percent in the hydrogen cross section causes an increase of only 0.8 percent in the value of the neutron emission rate for the concentration of manganese sulfate used.

A value of 13.2 barns was used for the thermal-neutron absorption cross section of manganese. As manganese has only one isotope, the activation cross section is equal to the absorption cross section. The activation cross section of manganese was measured [12] by exposing a small cell of manganese sulfate solution in a known thermal neutron flux. After irradiation, the absolute activity of an aliquot of the solution was determined by 4π counting (with the same equipment used in the present experiment), and $\sigma_{act}=13.1_9\pm 0.3_0$ barns was obtained. In the second supplement of AECU–2040 (neutron cross-section compilation) an absorption cross section of 13.2 ± 0.4 barns is listed for the thermal-neutron absorption cross section of manganese and 13.4 ± 0.3 barns for the activation cross section (the latter based on a gold absorption cross section of 98 barns). The weighted average of the three values is accurate to 0.1_9 barn.

Actually, systematic errors partially compensate each other, when our own measured value of the manganese activation cross sections is used. Any systematic error in the 4π counting technique, which causes an error in the value of $C_{4\pi}$, causes a similar percentage error in the manganese cross-section result. These effects tend to oppose each other, and the net error in the source emission rate is only one-third of the systematic error.

The emission rate of $(1.25_0\pm 0.02_5)\times 10^6$ neutrons per second obtained in this calibration agrees well with the value of $(1.26_3\pm 0.03_7)\times 10^6$ neutrons per second obtained by a different method [2]. These two results give a weighted average of $(1.25_5\pm 0.02_1)\times 10^6$ neutrons per second for the emission rate of the standard.

The only American neutron source compared with a foreign source is the Los Alamos source. It was compared with the British standard at Harwell in 1951 by three different methods [13]. As two of these comparisons differed by more than 4 percent, the exact ratio of the source strengths is not precisely known. In an effort to improve this situation, additional international comparisons are planned.

A photoneutron source such as Sb-Be (γ,n) could probably be calibrated absolutely to an accuracy within 1 percent by a modification of the present technique. As the gamma-ray energies are less than the photoneutron threshold of deuterium, a bath of manganese sulfate in heavy water could be used. Over 96 percent of the captures would be in manganese, and the error introduced by the cross-section values would be negligible.

The authors express their appreciation to H. A. Bright, NBS Analytical Chemistry Section, for the chemical analyses of manganous sulfate solutions; to H. H. Seliger for the use of his ultramicroburet and Na-22 source; and to R. Tilley and W. Bailey for assistance in performing the experiments.

5. Appendix. Neutron Capture Above the Cadmium Cutoff Energy

Manganese is not a strict $1/v$ neutron absorber in the epithermal region; however, the resonances in the region above the cadmium cutoff energy are principally due to scattering [14], and the epithermal neutron absorption by manganese in solution during the slowing down process is small. Walker has measured the neutron distribution from an Ra-Be (α,n) source in water by means of manganese foils with and without 0.020-in. cadmium covers [15]. For the space integrals ($\int$ activity$\times r^2dr$) Walker's measurements give a ratio of ($1.5\ \pm 0.1\%$) for the integral with cadmium covers to that with bare foils. A small BF_3 chamber gave a value of 0.71 percent for the same ratio. As both boron and hydrogen are good $1/v$ absorbers, 0.71 percent of the neutrons from the source are captured by the hydrogen in water above the cadmium cutoff energy. Manganese, therefore, has about twice the epi-cadmium absorption of a $1/v$ detector.

The resonance escape integral, P_r, may be used to evaluate the epicadmium captures.

$$P_r = \exp - \int_{E_{Cd}}^{E_0} \frac{\sum \sigma_{at} C_t}{\sum \sigma_{st} C_t} \frac{dE}{\xi E}, \tag{5}$$

where P_r is the probability of a neutron escaping capture in slowing down from initial energy E_0 to the cadmium cutoff energy, E_{Cd}; C_t, σ_{at} and σ_{st} are the concentration, absorption cross section, and scattering cross section, respectively of the ith element in the medium and ξ is the average logarithmic energy loss per neutron collision. In water and in manganese sulfate solution the slowing down from elastic collisions is almost entirely due to hydrogen, so the equation may be written

$$P_r = \exp - \int_{E_{Cd}}^{E_0} \frac{\sum \sigma_{at} C_t}{\sigma_{sH} C_H} \frac{dE}{E}, \tag{6}$$

with $\xi = 1$ (for hydrogen).
The integral is sensitive to the value used for the cadmium energy (usually taken as 0.3 to 0.5 ev).

Bothe has derived an expression [16] for the probability of absorption, α, of a neutron from an isotropic flux passing through a foil of thickness d and absorption cross section σ:

$$\alpha = 1 - e^{-n\sigma d}(1 - n\sigma d) + (n\sigma d)^2 EI(-n\sigma d), \tag{7}$$

where n is the number of nuclei per cubic centimeter. A graph of this function is given in figure 3 for 0.020-in. cadmium; where $\sigma_a(E) = \sigma_t(E) - 7.0$ barns is used for the absorption cross section of cadmium and $\sigma_t(E)$, the total cross section, is obtained from AECU–2040. From the graph, $E = 0.5$ ev appears to be the best choice for the cadmium cutoff energy. For water, letting

$$\sigma_{aH}(E) = \sigma_{aH}(\text{th})[E_{\text{th}}/E]^{1/2},$$

and

$$P_r = \exp - \int_{E_{Cd}}^{E_0} \frac{\sigma_{aH}(\text{th})}{\sigma_{sH}} \frac{E_{\text{th}}^{1/2}}{E^{3/2}} dE$$

$$P_r = \exp - \frac{2\sigma_{aH}(\text{th}) E_{\text{th}}^{1/2}}{\sigma_{sH}} \left[\frac{1}{E_{Cd}^{1/2}} - \frac{1}{E_0^{1/2}} \right]. \tag{8}$$

Using $E_{\text{th}} = 0.025$ ev, $E_0 \sim 10^6$ ev, $\sigma_{aH}(\text{th}) = 0.328$ barn, and $\sigma_{sH} = 20.0$ barns, the value of $P_r = 0.9927$. Thus 0.73 percent of the emitted neutrons are captured by hydrogen in the epicadmium region. This figure is in good agreement with Walker's result for water.

The concentration of the manganese sulfate used in the measurements was $MnSO_4$: 1.435 moles per liter, H_2O: 53.33 moles per liter.
The thermal neutron absorption cross sections used are $\sigma_{aMn}(\text{th}) = 13.2 \pm 0.2$ barns, and $\sigma_{aS}(\text{th}) = 0.49 \pm 0.02$ barn. For this case, the escape probability is

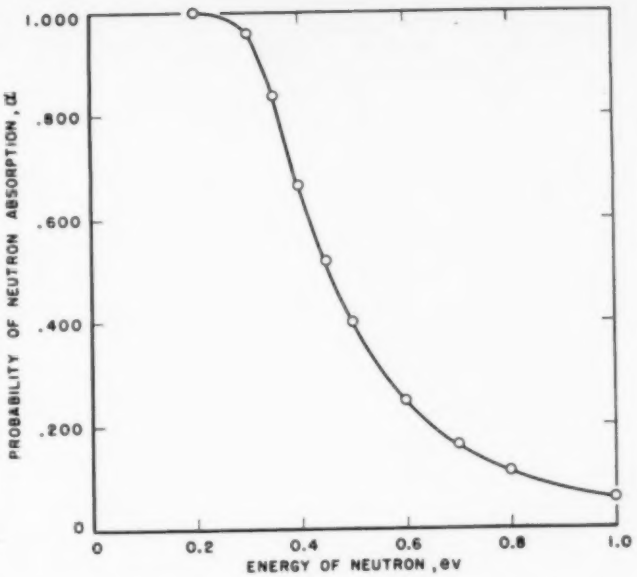

FIGURE 3. *Probability of neutron absorption from an isotropic flux passing through 0.020 in. of cadmium.*

$$P_r = \exp - \int_{E_{Cd}}^{E_0} \frac{\sigma_{aH} C_H + \sigma_{aMn} C_{Mn} + \sigma_{aS} C_S}{\sigma_{sH} C_H} \frac{dE}{\xi E}, \tag{9a}$$

$$P_r = \left[\exp - \int_{E_{Cd}}^{E_0} \frac{\sigma_{aH}}{\sigma_{sH}} \frac{dE}{E} \right] \left[\exp - \int_{E_{Cd}}^{E_0} \frac{\sigma_{aMn} C_{Mn}}{\sigma_{sH} C_H} \frac{dE}{E} \right] \left[\exp - \int_{E_{Cd}}^{E_0} \frac{\sigma_{aS} C_S}{\sigma_{sH} C_H} \frac{dE}{E} \right]. \tag{9b}$$

where $\xi = 1$.
Assuming that the thermal-capture cross sections vary as $1/E^{1/2}$, the following values are obtained for the three factors comprising P_r, respectively,

$$P_r = (0.9927) \quad (0.99604) \quad (0.99985).$$

Manganese would capture 0.396 percent of the neutrons from the source in the epicadmium region, if it were a perfect $1/v$ absorber. From the manganese foil measurements, the manganese in solution will actually capture $(1.5/0.72) \times 0.396\% = 0.825\%$ of the emitted neutrons in the epicadmium region; hence 0.43 percent of the neutrons will undergo resonance captures in the manganese. From the thermal cross section data and the manganese sulfate concentration, 34.68 percent of the remaining neutrons or 34.53 percent of the emitted neutrons are "$1/v$" captured by manganese. Finally, (the sum of the $1/v$ and resonance captures) 34.96 percent of the emitted neutrons are captured by the manganese in the bath. For the concentration used, the manganese captures 1.2 percent more of the emitted neutrons than a perfect $1/v$ absorber. If this correction were neglected, the resulting error in the emission rate of the source would be 0.8 percent.

6. References

[1] D. J. Hughes, Pile Neutron Research, p. 79 (Addison-Wesley Publishers Inc., Cambridge, Mass., 1953).
[2] J. A. De Juren, D. W. Padgett, and L. F. Curtiss, J. Research NBS 55, **63** (1955) RP2605.
[3] J. A. De Juren and H. Rosenwasser, J. Research NBS **52**, 93 (1954) RP2477.
[4] R. D. O'Neal and G. Sharff Goldhaber, Phys. Rev. **69**, 368 (1946).
[5] F. Alder and P. Huber, Helv. Phys. Acta **22**, 368 (1949).
[6] F. Metzger, F. Alder, and P. Huber, Helv. Phys. Acta **21**, 278 (1948).
[7] H. H. Hopkins, Jr., Phys. Rev. **77**, 717 (1950); E. Rabinowicz, Proc. Phys. Soc. (London) **63** [A], 1040 (1950); R. Schumann and A. Camilli, Phys. Rev. **84**, 158 (1951); L. M. Silver, Phys. Rev. **76**, 589 (1949).
[8] G. von Dardel and N. G. Sjostrand, Phys. Rev. **96**, 1566 (1954).
[9] G. von Dardel and A. W. Waltner, Phys. Rev. **91**, 1284 (1953).
[10] B. Hamermesh, G. Ringo, and S. Wexler, Phys. Rev. **90**, 603 (1953).
[11] S. P. Harris et al., Phys. Rev. **91**, 125 (1953).
[12] J. A. De Juren and J. Chin, Phys. Rev. **99**, 1 (1955).
[13] D. J. Littler, E. E. Lockett, A. D. McRonald, P. W. Mummery, and P. R. Tunnicliffe, British Atomic Energy Research Establishment Report, AERE R/R 776 (1951).
[14] S. P. Harris, C. T. Hibdon, and C. O. Muelhause, Phys. Rev. **80**, 1014 (1950).
[15] R. L. Walker, U. S. Atomic Energy Commission Document, MDDC 414 (Oct. 22, 1946).
[16] W. Bothe, Z. Physik **120**, 437 (1943).

WASHINGTON, June 9, 1955.

Journal of Research of the National Bureau of Standards Vol. 55, No. 6, December 1955 Research Paper 2636

A New Bunsen-Type Calorimeter

Ralph S. Jessup

A new Bunsen-type calorimeter, using diphenyl ether as the calorimetric substance, is described. Tests of this calorimeter show that it can be used to measure quantities of heat of the order of 38 calories with a precision of about 0.05 percent.

1. Introduction

A new Bunsen-type [1][1] calorimeter for use in measurements of small quantities of heat, such as heats of mixing of polymers and solvents is described. The calorimeter uses diphenyl ether (phenyl ether, phenoxybenzene) as the calorimetric substance instead of water. The data reported in the literature indicate that Bunsen calorimeters using organic compounds as calorimetric substances have considerably higher sensitivity than that reported for the ice calorimeter [2, 3]. The organic compounds that have been used for this purpose include acetic acid [4], anethole [5], diphenylmethane [6, 8, 9] naphthalene [10,11], phenol [7, 12], benzalacetone [13], and diphenyl ether [14, 15, 16, 21]. The last-named substance has the important advantages that it is quite stable, it can be easily prepared in a state of high purity, and its melting point (26.87° C) is conveniently near room temperature.

2. Description of Calorimeter

The calorimeter is shown schematically in figure 1. It is similar in design to the ice calorimeter described by Ginnings, Douglas, and Ball [3], but has a larger central well to accommodate a "reaction vessel" for use in measurements of heats of reaction or heats of mixing.

The central well of the calorimeter was made from a piece of 1¾ in. stainless-steel pipe that was turned down to a wall thickness of 0.02 in. at the upper end to reduce thermal leakage, and is hard soldered to a copper insert in the jacket cover, *K*, and to the brass piece, *I*, which constitutes the top of the calorimeter proper. The brass bottom of the well is hard-soldered to the stainless-steel pipe. The copper fins, *F*, which are soldered to the outer wall of the well are partly to improve thermal contact between the well and the diphenyl ether, and partly for supporting the solid diphenyl ether, which is denser than the liquid. The copper spacers, *C*, between the fins at the lower end of the well are to promote uniformity in the vertical distribution of heat transferred between the well and the diphenyl ether outside of it. The outer shell, *E*, of the calorimeter is of stainless steel 1/16 in. in thickness and is soft-soldered to the brass piece, *I*. The diphenyl ether occupies the space enclosed by the shell, *E*, the top, *I*, and central well of the calorimeter, with the exception of the space occupied by the pool, *H*, of mercury in the bottom of *E*.

An electric heater having a resistance of about 30 ohms is wound on the outside of the cylindrical part of shell *E* of the calorimeter, and a heater of about 10 ohms is wound on the hemispherical part of the bottom. Both heaters are cemented to the shell with glyptal lacquer, and are covered with aluminum foil to reduce radiation. They can be used separately or in series. The use of these heaters is described in section 4.

When the calorimeter is in use the outer surface of the central well is covered by a mantle of solid diphenyl ether. Heat transferred between the central well and the diphenyl ether causes partial melting or freezing, with a consequent change in volume of the diphenyl ether and a flow of mercury into or out of the calorimeter through the platinum tube, *W*, and the stainless steel tube, *J*, so as to keep the total volume of liquid plus solid in *E* constant.[2] The quantity of heat is measured by the volume or weight of mercury so transferred. If this is small, it can be determined from the displacement of the mercury meniscus in the 40-cm graduated glass capillary, *G*, the steel valve, *V*, being kept closed. If the volume of mercury is large it can be determined from the combination of the change in weight of the contents of the beaker, *B*, and the change in position of the meniscus in the capillary.

The capillary, *G*, is horizontal so that the changes in the position of the mercury meniscus in it do not affect the pressure on the diphenyl ether in the calorimeter. Changes in barometric pressure might be large enough to affect the position of the meniscus significantly. To reduce any such effect the open end of capillary *G* is connected to a 1-liter flask immersed in oil in a Dewar flask. The pressure in this system is adjusted to atmospheric at the beginning of an experiment and has been shown by measurements with a closed-end mercury manometer to remain practically constant during the time of an experiment.

The T-joint in the stainless-steel tube near the valve, *V*, and the connections to the valve and the glass capillary, *G*, are made with Apiezon wax.

The interchange of heat between the calorimeter and its environment is reduced to a minimum by

[1] Figures in brackets indicate the literature references at the end of this paper.

[2] The calorimeter was originally constructed with the stainless-steel tube *J*, extending nearly to the bottom of the pool of mercury. Difficulties were encountered due to creeping of the diphenyl ether past the mercury seal between diphenyl ether and the stainless-steel tube. This was overcome by replacing the lower end of the stainless-steel tube with the platinum tube, *W* [17]. The nickel sleeve connecting tubes *J* and *W* is sealed to them with a low-melting-point glass made of equal parts by weight of soda glass, borax, and zinc oxide.

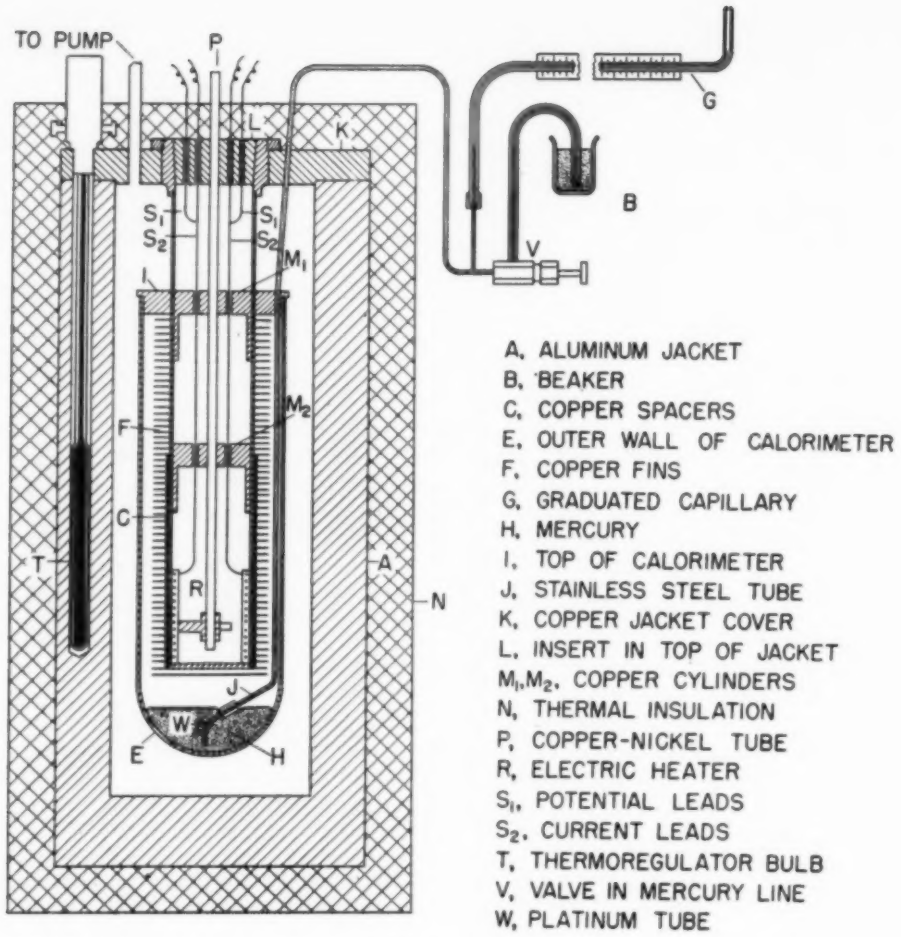

FIGURE 1. *Schematic drawing of calorimeter.*

surrounding the calorimeter with the aluminum jacket, A, with its copper cover K. The jacket is maintained at the temperature of the calorimeter within ± 0.001 deg C by means of thermoregulator T. The temperature difference between the top of the calorimeter, I, and the copper jacket cover, K, is measured by means of a 10-junction copper-constantin thermocouple (not shown in fig. 1) and a Diesselhorst potentiometer. The coefficient of thermal leakage between calorimeter and jacket is reduced by radiation shields (not shown in fig. 1) of aluminum foil and by evacuating the space between calorimeter and jacket to a pressure of about 1μ.

The 100-ohm electric heater, R, the $^3/_{16}$-in. copper-nickel tube, P, the cylindrical copper pieces, M_1 and M_2, and the conical copper piece, L, form a unit, the lower part of which fits closely inside the central well. This unit, which is used only for calibrating the calorimeter, can be removed and replaced by a similar unit having a reaction vessel instead of the heater, R, together with suitable tubes for introducing reactants. The purpose of copper pieces M_1 and M_2 is to provide zones of good thermal contact with the wall of the well, and thereby trap heat that would otherwise escape by conduction along the leads, or by radiation and convection. The conical piece, L, fits into a conical hole in the jacket cover and forms a part of the jacket cover, and M_1 forms part of the top of the calorimeter proper.

The heater leads are brought out in such a manner that they are in intimate thermal contact with jacket L and calorimeter M_1. The potential leads are connected to the current leads midway between L and M_1. As the total resistance of the current leads between L and M_1 is approximately 0.01 ohm, or 0.01 percent of the heater resistance, the uncertainty in the heat developed between calorimeter and jacket is negligible.

The current through the heater was turned on and off by a double-pole double-throw switch similar to one described by Osborne, Stimson, and Fiock [20]. It is operated by a spring and a release that is actuated by second signals from a standard clock.

3. Filling the Calorimeter With Diphenyl Ether

3.1. Diphenyl Ether

The diphenyl ether used was purified under the direction of F. L. Howard by fractional freezing and distillation in the Engine Fuels Section of the Bureau. The purity was determined by R. E. McCoskey and G. T. Furukawa from measurement of the equilibrium temperature of a solid-liquid mixture for various known values of the mass ratio of solid to liquid. The value reported for the purity is 99.9985 mole percent and that for the triple-point temperature is 300.03° K. It was later found [18] that the purity of this sample of diphenyl ether after heating to about 360° K in a tin-lined calorimeter had decreased to 99.9926 mole percent.

3.2. Cleaning the Calorimeter

Before shell E (fig. 1) was soldered to brass piece I, it was washed internally, and the central well and attached vanes were washed externally with organic solvents to remove traces of oil or grease. After shell E was soldered in place, the interior surfaces were washed repeatedly with boiling distilled water until tests showed only a slight change in the resistivity of the water after such washings. The system was then heated internally and externally to a temperature somewhat lower than the melting point of the soft solder, and was evacuated for about a week at a pressure less than 10^{-4} mm of mercury to remove water and other adsorbed materials.

3.3. Introducing Diphenyl Ether and Mercury into the Calorimeter

The method of introducing diphenyl ether and mercury into the calorimeter can best be explained by reference to figure 2. The liquid diphenyl ether was first put into a 1-liter spherical flask, F, and slowly frozen under vacuum. This process was repeated several times until most of the dissolved gas was removed. Then with the diphenyl ether frozen the flask was disconnected from the vacuum system and sealed to the 2-in. glass tube, T (fig. 2), and connecting tubing, and connected to a vacuum pump and to the calorimeter as indicated. The system was then evacuated to a pressure less than 10^{-4} mm of mercury.

During this procedure the end of glass capillary G (fig. 1) was sealed, and beaker B (fig. 1) was replaced by a short glass test tube containing mercury and closed at the top by a rubber stopper with a hole of the proper size to fit the glass capillary leading to valve V. This tube was evacuated through a side tube above the mercury surface. Valve V was then opened so that the pressure in it and the glass capillary above it was reduced to that in the calorimeter

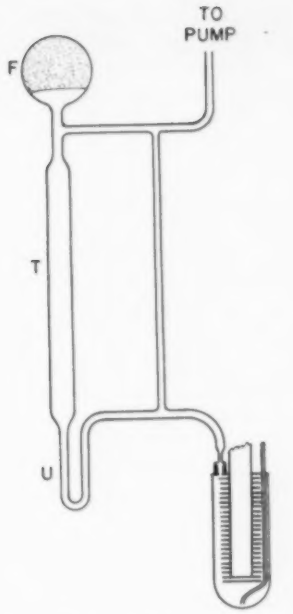

FIGURE 2. *Schematic diagram to illustrate method of introducing diphenyl ether into calorimeter.*

(less than 10^{-4} mm). Valve V was then closed, and air admitted to the glass tube, which replaced beaker B, thus filling the valve and connecting glass capillary completely with mercury. The beaker, B, containing a weighed amount of mercury, was then replaced in its normal position, as shown in figure 1.

An attempt was made to remove any residual gas in the diphenyl ether before introducing it into the calorimeter, as follows:

With the vacuum pump operating, a small amount of diphenyl ether in flask F (fig. 2) was melted and allowed to run down into tube T, where it was refrozen by surrounding the tube with ice. The diphenyl ether in T was then remelted and allowed to run down into the U-tube at the lower end of T. After this the U-tube was kept in an ice bath to prevent any premature flow of diphenyl ether into the calorimeter. The procedure of melting a small amount of the diphenyl ether in F, freezing it in T, and finally remelting it and allowing it to flow to the bottom of T, was followed repeatedly until the entire amount had been transferred from F into T.

Valve V (fig. 1) was then opened, and the desired amount of mercury was introduced into the calorimeter. After this, the temperature of the room was raised above the melting point of diphenyl ether, the entire amount of diphenyl ether in tube T (fig. 2) and in the U-tube at the bottom was melted, and the liquid allowed to flow into the calorimeter. When the flow stopped, a small amount of liquid remained in the tube connecting to the calorimeter. Air was then admitted to the system through the line to the vacuum pump, raising the pressure to atmospheric. The connection to the calorimeter was then removed and the small opening

into the calorimeter was closed by a conical stainless-steel pin forced into the opening by means of a screw-cap. Holes in ths screweap permitted washing out any diphenyl ether remaining outside the calorimeter proper in the space around the conical pin.

It is believed that by the above procedure the diphenyl ether introduced into the calorimeter was substantially free from dissolved gases. Unfortunately, however, a small amount of air was later introduced into the system due to failure of the room thermostat during a weekend, resulting in an excessively low room temperature and consequent freezing of enough diphenyl ether to draw all the mercury from beaker B (fig. 1), together with a small amount of air, into the calorimeter. The part of the air that was trapped in valve V and tube J was easily removed, but that which actually got into the calorimeter could not be removed without a major operation, which it seemed desirable to avoid. The air is normally dissolved in the liquid diphenyl ether and apparently does not seriously reduce the accuracy of measurements with the calorimeter, but it does cause considerable inconvenience in the use of the instrument.

4. Forming a Mantle of Solid Diphenyl Ether

The inconvenience in the use of the calorimeter resulting from dissolved air in the diphenyl ether has been greatest in attempts to form a satisfactory mantle of solid around the central wall. Because it is not possible to see into the calorimeter, some parts of the following discussion were inferred from the observed behavior of the calorimeter.

Because diphenyl ether may undercool several degrees, it is necessary to cool some part of the material in the calorimeter several degrees below its melting point to start freezing. This is done most conveniently by pressing a piece of ice against the wall of the central well. If any considerable amount of diphenyl ether is frozen in this way, air in the gas phase accumulates in the calorimeter, as shown by the fact that the change with pressure in the position of the mercury meniscus in the capillary, G, increases by a factor of as much as five in some cases. The excess sensitivity to pressure disappears due to solution of air in the remaining liquid, but mantles formed entirely by cooling with ice have never given satisfactorily consistent results in calibration experiments. It is inferred that this is due to air entrapped inside the solid in such a manner that it did not contribute appreciably to the apparent compressibility of the diphenyl ether, but that it dissolved in the liquid when the adjacent solid is melted in a calibration experiment, thus causing the observed increase in volume of the system to be low.

In some cases the freezing of the diphenyl ether was started with ice, and the central well was then filled with water and freezing continued slowly by bubbling air through the water. This procedure did not always lead to satisfactory precision in the calorimetric experiments. In some cases it appeared that in this procedure the mantle did not spread uniformly over the central well, but tended to grow over only a small area, and finally to bridge over the space between the central well and shell E (fig. 1) of the calorimeter.

The most satisfactory results were obtained with the following procedure: (1) A small amount of diphenyl ether was frozen by cooling with ice, and the calorimeter was left overnight to permit any gaseous air to redissolve. (2) The central well was filled with water, which was stirred by bubbling air through it; heat was supplied by means of the heaters wound on the outer shell E (fig. 1) of the calorimeter, and small pieces of ice were added periodically to the water in the central well. By proper adjustment of the heating current and the rate of addition of ice, the rate of freezing of diphenyl ether could be made as low as desired, and the temperature of the water could be maintained from 0.5 to 2 deg below the freezing point. Under these conditions it was expected that the mantle would spread over the central well so as to form a more or less uniform layer.

After the above procedure had been followed for about 1.5 hr, the addition of ice to the central well was stopped, and the current through the heaters was reduced gradually to zero as the temperature of the water in the well rose to the melting point of the diphenyl ether. Slow freezing of the diphenyl ether was then continued over a period of 2 or 3 days by bubbling air through the water in the central well, at first with the well filled with water up to the top of the calorimeter proper, and finally with about half of this amount in order to make the mantle thicker in the lower part where heat was to be added to it. During this slow freezing a small current was passed through the electric heaters on the outside of shall E.

Even with a mantle formed in the manner indicated, it was necessary to melt part of it by means of the heater, R, before consistent results could be obtained. It seems probable that the part of the solid diphenyl ether which was frozen with ice contained entrapped gaseous air, and this part must be melted and the air dissolved in order to obtain satisfactory results.

It is believed that the difficulties encountered in forming a satisfactory mantle are due to the air in the system, and that if no air were present, a mantle could be formed much more quickly and easily.

5. Thermal Leakage

The results of typical experiments to determine the thermal-leakage coefficient of the calorimeter are plotted in figure 3. The slope of the straight line corresponds to a thermal leakage of 0.0042 j (0.0010 cal) per minute for a temperature difference of 0.001 deg C between calorimeter and jacket. That part of the thermal leakage due to conduction along metallic connections between calorimeter and jacket has been calculated to be approximately half of the observed total, so that the other half may be assumed to be due to radiation.

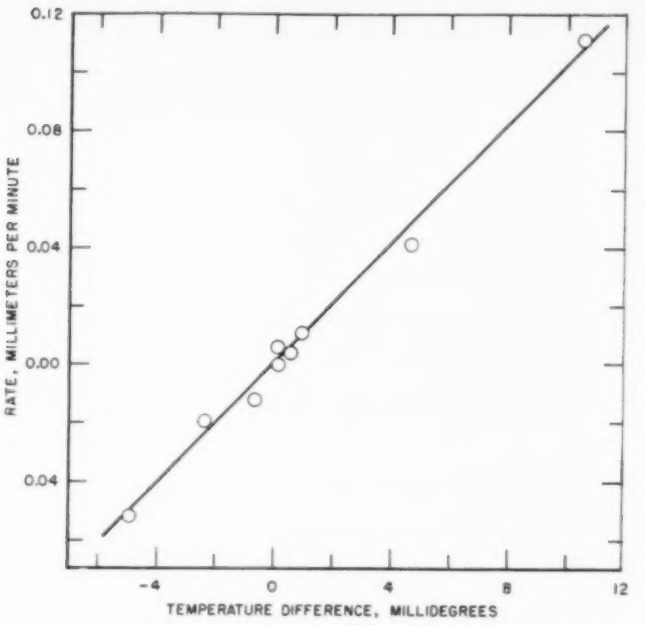

FIGURE 3. *Thermal leakage between calorimeter and jacket.*

Ordinate represents the rate change of position of the mercury meniscus in the graduated capillary tube. (1 mm is approximately equivalent to 0.1 cal) Abscissa represents temperature difference between calorimeter and jacket.

The observed thermal-leakage coefficient is a little larger than is desirable for measurements to a precision of one or two hundredths of a calorie. The "reaction period" for an electrical calibration experiment is about 30 min, and the temperature of the jacket varies in an irregular manner over a range of a few ten thousandths of a degree up to 0.001 deg. It is found, however, that the observed rate of heat transfer remains more nearly constant over periods of 1 or 2 hr than would be expected on the basis of the curve in figure 3 and the observed variation in jacket temperature. This is undoubtedly due to damping of the effect of fluctuations in jacket temperature by the radiation shields between calorimeter and jacket, the relatively heavy calorimeter wall, and the layer of liquid between the calorimeter wall and the mantle of solid diphenyl ether. Although this damping of the effect of fluctuations in jacket temperature probably reduces the uncertainty in the thermal leakage, this uncertainty nevertheless is very probably one of the major sources of error in the calorimeter, particularly in experiments extending over long periods of time.

6. Calibration of the Calorimeter

The graduated capillary, G (fig. 1), was calibrated by observing at various points along the capillary the lengths of 2- and 8-cm mercury threads with reference to the scale etched on the capillary, and by weighing the mercury removed from the capillary when the reading of the meniscus changed from 40 cm to zero. Corrections found for nonuniformity of the capillary bore did not exceed 0.2 mm (0.02 cal), and the mass of mercury required to fill the capillary was found to be $0.05239_8 \pm 0.000004_2$ (sdm) g/cm. This corresponds to an average capillary diameter of 0.71 mm.

TABLE 1. *Electrical calibration experiments*

Series	Experiment	Calibration factor	Deviation from mean for series	Deviation from mean of all experiments
		j/cm	*j/cm*	*j/cm*
1	1	4.1435	−0.0021	−0.0012
	2	4.1452	−.0004	+.0005
	3	4.1458	+.0002	+.0011
	4	4.1473	+.0017	+.0026
	5	4.1433	−.0023	−.0014
	6	4.1485	+.0029	+.0038
Mean		4.1456		
Standard deviation of mean			$\pm 0.0008_4$	
2	1	4.1461	+0.0021	+0.0014
	2	4.1438	−.0002	−.0009
	3	4.1418	−.0022	−.0029
	4	4.1421	−.0019	−.0026
	5	4.1444	+.0004	−.0003
	6	4.1450	+.0010	+.0003
	7	4.1443	+.0003	−.0004
	8	4.1449	+.0009	+.0001
Mean		4.1440		
Standard deviation of mean			$\pm 0.0005_2$	
3	1	4.1470	+0.00025	+0.0023
	2	4.1448	+.00003	+.0001
	3	4.1436	−.00009	−.0011
	4	4.1448	+.00003	+.0001
	5	4.1425	−.00020	−.0022
Mean		4.1445		
Standard deviation of mean			$\pm 0.0007_5$	
Mean of all results		4.1447		
Standard deviation of mean				$\pm 0.0004_6$

Table 1 shows that the results of each series of experiments are in satisfactory agreement among themselves, the maximum deviation from the mean in any one series being about 0.07 percent, which corresponds to about 0.11 j (0.02_7 cal) in the 159 j supplied to the calorimeter. However, the mean of

The calorimeter was calibrated electrically, using the 100-ohm heater, R, shown in figure 1, a Wolff-Diesselhorst potentiometer, a Wolff 0.1-ohm standard resistor, a 20000/20-ohm volt box, and a saturated cadmium standard cell maintained at a constant temperature of about 32.8° C by means of a temperature-control box [19]. The potentiometer, volt box, standard resistor, and standard cell were calibrated in the Electricity and Electronics Division of the Bureau immediately following the calibration experiments reported.

The results of three series of calibration experiments are given in table 1, expressed in absolute joules per centimeter displacement of the mercury meniscus in the graduated capillary, G. The results of each series were obtained on a separate mantle formed in the manner described in section 5. The amount of heat supplied to the calorimeter in each experiment was approximately 159 j (38 cal).

the results of the first series differs from the means for the other two series by somewhat more than would be expected in view of the precision attained in the separate series. This suggests that perhaps the method of forming a mantle of solid does not entirely prevent the entrapment of air in the solid, and that the amount entrapped in different mantles may be significantly different, but that in any one mantle it is small enough and distributed uniformly enough through the solid to permit a relatively high precision in measurements with that mantle. It is to be expected, therefore, that to obtain a precision of the order of 0.1 j in the measurement of a small quantity of heat with the calorimeter it will be necessary to make a new calibration of the calorimeter for each new mantle.

If the individual results of all three series are averaged, the maximum deviation from the mean result so obtained of the mean for any one series is about 0.02 percent, corresponding to 0.03_5 j (0.01cal), but the maximum deviation of individual results from this mean is now 0.09_5 percent (0.15 j, or 0.04 cal).

Combination of the calibration factor 4.1447 j/cm with the value 0.05239_8 g/cm for the mercury required to fill the capillary yields the calibration factor 79.10 ± 0.010 (sdm) j/g of mercury. This may be compared with the value 270.46 j/g of mercury reported by Ginnings, Douglas, and Ball [3] for the calibration factor of the ice calorimeter. The sensitivity of the diphenyl ether calorimeter is thus about 3.4 times that of the ice calorimeter.

Combination of the value 79.10 j/g of mercury for the calibration factor with the value 300.06° K for the freezing point of diphenyl ether under the pressure (114 cm of mercury) in the calorimeter yields the value $-\Delta H/T\Delta V = 35.6_6$ bars per deg C. This value is subject to some uncertainty because of the fact that the observed value of $\Delta H/\Delta V$ may be affected by gaseous air in the solid diphenyl ether.

It is of interest to compare the calibration factor obtained in the present work with those reported by other investigators—who have reported their results in terms of weight (or volume) of mercury expelled per calorie. The results on this basis are as follows:

Author	Calibration factor
	g Hg/*cal*
Sachse [14]	0.0364
Holmberg [15]	.0488
Klemm, Tilk, and Jacobi [16]	.0528
Giguère, Morissette, and Olmos [21]	.05260
Present work	$.05289_3$

7. References

[1] R. Bunsen, Pogg. Ann. **141,** 1 (1870).
[2] D. C. Ginnings and R. J. Corruccini, J. Research NBS **38,** 583 (1947) RP1796.
[3] D. C. Ginnings, T. B. Douglas, and A. F. Ball, J. Research NBS **45,** 23 (1950) RP2110.
[4] L. E. O. de Visser, Z. physik. Chem. **9,** 767 (1892).
[5] V. Grassi, Soc. Linc. (5) **221,** 494 (1913).
[6] A. N. Shchukarev, I. P. Krivobalko, and L. A. Shchukareva, Physik. Z. Sowjetunion **5,** 722 (1934).
[7] A. N. Shchukarev, T. V. Ass, and N. I. Putilin, Méd. exptl. (Ukraine), **1936,** No. 6, 114.
[8] K. S. Evstrop'ev, J. Phys. Chem. (USSR) **8,** 130 (1936).
[9] M. M. Gordon, Zentralblatt **1938,** II 561.
[10] C. C. Coffin, J. C. Devine, J. R. Dingle, J. H. Greenblatt, T. R. Ingraham, and S. Schrage, Can. J. Research [B] **28,** 579 (1950).
[11] A. Thomas, Faraday Soc. Trans. **47,** 569 (1951).
[12] S. J. Gregg, J. Chem. Soc. **1927,** 1494.
[13] E. J. Caule and C. C. Coffin, Can. J. Research [B] **28,** 639 (1950).
[14] H. Sachse, Z. physik. Chem. [A] **143,** 94 (1929).
[15] Toivo Holmberg, Soc. Sci. Fennica, Commentationes Phys.-Math. **9,** No. 17 (1938).
[16] W. Klemm, W. Tilk, and H. Jacobi, Z. anorg. allgem. Chem. **207,** 187 (1932).
[17] R. S. Jessup, J. App. Phys. **23,** 543 (1952).
[18] G. T. Furukawa, D. C. Ginnings, R. E. McCoskey, and R. A. Nelson, J. Research NBS **46,** 195 (1951) RP2191.
[19] E. F. Mueller and H. F. Stimson, J. Research NBS **13,** 699 (1934) RP739.
[20] N. S. Osborne, H. F. Stimson, and E. F. Fiock, BS J. Research **5,** 429 (1930) RP209.
[21] P. A. Giguère, B. G. Morissette, and A. W. Olmos, Can. J. Chem. **33,** 657 (1955).

WASHINGTON, August 16, 1955.

Journal of Research of the National Bureau of Standards Vol. 55, No. 6, December 1955 Research Paper 2637

Mass Spectra of Thermal Degradation Products of Polymers

Paul Bradt and Fred L. Mohler

Polymers are degraded or evaporated from a tube furnace directly into the mass spectrometer, and mass spectra recorded as the temperature of the sample is increased. Polyethylene degrades into paraffins, olefins, and diolefins and at 386° C the mass spectrum extends to mass 684, $C_{49}H_{96}$. Polyvinyl chloride degrades in two stages. From 127° to 300° C it loses HCl and some benzene, and above 300° C it evolves a great variety of hydrocarbons.

The heavy fraction from rubber degradation evaporates over a wide temperature range, and molecules containing from 3 to 16 units of the monomer, C_5H_8, are recorded. The heaviest ion is $C_{80}H_{127}$ of mass 1,087. Degradation of polyxylylene gives molecules containing from 1 to 9 units of the monomer, C_8H_8, the heaviest ion being $C_{72}H_{71}$ of mass 935. A low polymer of polyphenyl was evaporated and molecules containing 2 to 11 monomer units were recorded. The heaviest ion was $C_{66}H_{46}$ of mass 838.

1. Introduction

The products of thermal degradation of polymers have been a subject of systematic research by S. L. Madorsky [1, 2, 3][1] and his colleagues in the NBS Polymer Structure Section. In Madorsky's researches the volatile products of thermal degradation have been analyzed by mass spectrometer, and in most cases the average molecular weight of the nonvolatile degradation product has been evaluated by standard methods. In a few instances, notably polymethylmethacrylate and polytetrafluoroethylene, the degradation product is almost pure monomer, and these techniques give a complete description of the degradation product. In most cases the nonvolatile fraction is an appreciable part of the degradation product, and existing information on this is fragmentary and incomplete.

In a previous publication by the authors [4] on polystyrene degradation, a technique is described for degrading and evaporating the products of degradation directly into the ionization chamber of a mass spectrometer and recording mass spectra of all the products that are volatile at the temperature of degradation. The same technique has been applied to record the mass spectra of molecules of perfluoropolyphenyl, which evaporates without degradation [5].

The present paper gives a survey of mass spectra obtained when various other polymers are evaporated or degraded directly into the mass spectrometer.

2. Experimental Method

A small tube furnace extends to the entrance port in the ionization chamber of a mass spectrometer, and the sample to be studied is in a short length of capillary tubing supported in the tube furnace by a thermocouple, which measures the temperature of the sample. The amount of sample is of the order of 1 mg. The mass spectrometer is a Nier-type 60° instrument of 6-in. radius of curvature, and the spectrum is recorded with a pen recorder by varying the magnetic field. The mass scale can be extended as required by lowering the ion-accelerating voltage, which is normally 2,500 for molecular weights less than 300. The resolving power is about 1 in 300, which does not resolve unit mass in the high mass range encountered in these studies. Partial resolution sufficient to identify individual ions of hydrocarbons extended to about mass 600. Ion currents are expressed in arbitrary units of scale divisions on the record at the maximum sensitivity used in each series of measurements.

In each experiment, after obtaining a good vacuum, the temperature was increased step by step, and at each step the mass spectrum was recorded. It required about 2 hr to cover the full range of spectrum at optimum recording speed. A higher speed was often used for a quick survey to see whether there was anything to measure. Each experiment extended over several days, and after the sample was exhausted the ionization chamber was dismantled and thoroughly cleaned.

3. Results

3.1. Polymethylene

A pure grade of polymethylene, made by decomposing diazomethane in the presence of a catalyst, was supplied by the Polymer Structure Section. This polymer is similar to polyethylene, except that there should be no branched hydrocarbon chains. Madorsky and Straus [3] find that this degrades by breaking at random C—C bonds to give *n*-paraffins, 1-*n*-olefins, and diolefins. About 97 percent of the degradation product is not volatile at room temperature and has an average molecular weight of 692, corresponding to about 50 carbon atoms.

The sample of polymethylene began to degrade into volatile compounds at about 335° C. At 352° C the hydrocarbon spectrum extended to mass 253, $C_{18}H_{37}$. The maximum peak was 179 scale divisions. At 369° C the ion currents were much larger but unsteady because of bubble formation. The mass spectrum extended to 460, $C_{33}H_{64}$. As the sample became depleted the ion current became steady and at 386° C the heaviest ions appeared. Table 1 gives some of the larger peaks in this spectrum,

[1] Figures in brackets indicate the literature references at the end of this paper.

TABLE 1. *Mass spectrum of degradation products of polymethylene at 386° C*

m/e	Ion	Relative abundance
43	C_3H_7	65
57	C_4H_9	100
71	C_5H_{11}	66
83	C_6H_{11}	57
85	C_6H_{13}	48
97	C_7H_{13}	90
111	C_8H_{15}	53
125	C_9H_{17}	25
139	$C_{10}H_{19}$	7.0
141	$C_{10}H_{21}$	12
155	$C_{11}H_{23}$	8.0
169	$C_{12}H_{25}$	7.5
183	$C_{13}H_{27}$	7.0
197	$C_{14}H_{29}$	7.0
211	$C_{15}H_{31}$	5.5
225	$C_{16}H_{33}$	4.5
239	$C_{17}H_{35}$	5.5
253	$C_{18}H_{37}$	3.5
267	$C_{19}H_{39}$	4.0
281	$C_{20}H_{41}$	2.5
295	$C_{21}H_{43}$	3.0
306	$C_{22}H_{42}$	2.5
309	$C_{22}H_{45}$	2.5
320	$C_{23}H_{44}$	3.0
323	$C_{23}H_{47}$	2.5
334	$C_{24}H_{46}$	3.0
.....	C_nH_{2n-2} from $n=25$ to $n=45$	3.0
642	$C_{46}H_{90}$	3.0
656	$C_{47}H_{92}$	2.0
670	$C_{48}H_{94}$	1.5
684	$C_{49}H_{96}$	1.5
698	$C_{50}H_{98}$	<0.2

which extended to mass 684, $C_{49}H_{96}$. The maximum peak, at mass 57, was 103 scale divisions.

The mass spectrum of table 1 shows a remarkably regular succession of peaks at intervals of 14 mass units from mass 253 to mass 684. For ions containing less than 22 carbon atoms the larger peaks in each carbon group are, with a few exceptions, the alkyl ions $C_nH^+_{2n+1}$. In ions with more than 22 carbon atoms the ions $C_nH^+_{2n-2}$ become larger. The latter come presumably from the diolefin spectra. The spectra gave no evidence as to the mass distribution in the degradation products except that there are molecules with 49 or 50 carbon atoms.

The spectrum of table 1 was obtained from a sample that was nearly exhausted and this spectrum differs from the preceding spectrum at 369° C in the relative intensity of the pair of peaks C_nH_{2n-2} and C_nH_{2n+1} in each carbon group. The $2n-2$ peak is larger in the spectrum at 386° C, and the difference becomes conspicuous at the heavy end of the spectrum. This indicates that the polymethylene becomes depleted in hydrogen in the process of degradation.

3.2. Polyvinyl Chloride

A sample of polyvinyl chloride, "Geon 101", was supplied by the Bureau's Plastics Section. Polyvinyl chloride degrades in a complicated manner. At low temperatures evolution of HCl by the following reaction is predominant:

$$\begin{matrix} H & H & H & H \\ -C- & -C- & -C- & -C- \\ H & Cl & H & Cl \end{matrix} \rightarrow -CH=CH-CH=CH- \ldots + n\,HCl.$$

Some benzene is also evolved in this temperature range. At temperatures above 300° C the CH chain degrades to give a mixture of hydrocarbons.

TABLE 2. *Summary of mass spectra of degradation products of polyvinyl chloride*

Ion currents in scale divisions				
Temperature ° C	HCl ($m=36$)	Benzene ($m=78$)	C_7H_7 ($m=91$)	Maximum (m/e)
127	7	.....	.....	.....
179	218	12.5	.....	.....
194	440	48.0	.....	128
220	2,300	244.0	4	179
220	915	66.0	2	179
Overnight at 217° C				
250	1,015	45.0	.....	.....
280	1,290	43.0	13	179
306	126	51.0	72	192
335	59	37.0	123	253
Overnight at 320° C				
368	15	40.0	250	520
389	3.5	11.5	89	596

Table 2 lists the series of spectra obtained in one experiment in the range 127° to 389° C. It includes molecule ion peaks of HCl and benzene and the benzyl radical, and in the last column lists the heaviest ion recorded in each spectrum. Peak heights are given in scale divisions.

The evolution of HCl began at about 127° C, and at 220° C the rate of evolution of gas reached the maximum amount for satisfactory measurement. The sample was held overnight near this temperature, and then the temperature was slowly increased. Above 300° C the evolution of HCl and benzene became small and a complicated hydrocarbon spectrum appeared. The maximum peak in this spectrum was the benzyl radical ion of mass 91. Above 389° C the evolution of vapor decreased and a carbonized residue was left in the sample tube.

Table 3 gives the larger peaks in the mass spectra obtained at four temperatures. Below 300° C benzene is by far the most abundant hydrocarbon. The small peaks extending to mass 179 are heavier aromatics. The largest of these, at mass 128, is the molecule ion of naphthalene. The peak at mass 178 may be the molecule ion of anthracene, but peaks at 179 and 167 come from something else. At the highest temperature there are peaks at every mass number above 78, and beyond mass 200 all peaks become of the same order of magnitude. From mass 400 to mass 596 the spectrum of the partially resolved peaks appears as a very uniform sine wave with maxima at even mass numbers. The upper limit is set by resolving power, and the ion current is measurable beyond mass 596.

TABLE 3. *Partial mass spectrum of degradation products of polyvinyl chloride*

m/e	Ion	Ion currents in scale divisions			
		220° C	306° C	335° C	389° C
36	HCl	2,294	126	59	3.5
78	C_6H_6	244	51	37	11.5
79	C_6H_7	.....	22	36	37
89	C_6H_9	.....	.....	.....	35
91	C_7H_7	4	72	123.0	89
93	C_7H_9	.....	.....	18.0	25
95	C_7H_{11}	.....	.....	.....	25
104	C_8H_8	1.0	16	31	9
105	C_8H_9	.....	12	37	55.0
115	C_9H_7	6.5	36	75	40.0
117	C_9H_9	3.5	22.5	51	21.0
119	C_9H_{11}	2.0	.....	11	21.0
128	$C_{10}H_8$	14	40	67	21.0
129	$C_{10}H_9$	4.5	24	57	49
131	$C_{10}H_{11}$	.....	.....	20	38
141	$C_{11}H_9$	4.0	22.5	54	46.0
143	$C_{11}H_{11}$	.....	6.0	38	33.0
152	$C_{12}H_8$	1.7	10.0	24	21.0
153	$C_{12}H_9$	1.7	10.0	24	22.0
154	$C_{12}H_{10}$	1.5	13.0	18	12.0
155	$C_{12}H_{11}$	.....	5.5	20	38
165	$C_{13}H_9$	3.5	15	45	47.0
167	$C_{13}H_{11}$	2.0	10.5	28	35
178	$C_{14}H_{10}$	3.5	10.5	9.0	31
179	$C_{14}H_{11}$	2.5	6.0	26.0	41
191	$C_{15}H_{11}$	.....	2.5	13.5	28
193	$C_{15}H_{13}$	.....	3.0	12.0	22
203	$C_{16}H_{11}$	.....	.....	10	28
215	$C_{17}H_{11}$	.....	.....	14	36
229	$C_{18}H_{13}$	.....	.....	5	32
239	$C_{19}H_{11}$	.....	.....	2.5	27
253	$C_{20}H_{13}$	.....	.....	2.0	27
254 to 596	.....	.....	.....	.....	(*)

* At 389° C there are peaks of the same magnitude at every mass number.

3.3. Crepe Rubber

Crepe-rubber degradation has been studied by Straus and Madorsky [2]. The degradation products at 350° C are about 4 percent of monomer, 13 percent of dimer, and 83 percent of heavier compounds with an average molecular weight of 616. The monomer is isoprene, 2-methyl-1,3-butadiene, of molecular weight 68, and the maximum peak is at mass 67. The dimer is mostly the cyclic compound dipentene, and the maximum peak is at mass 68 [8].

Crepe rubber degraded in the range 236° to 353° C. The mass spectrum extended to mass 271 and by comparison with the known mass spectra of the monomer and dimer, the product appeared to be monomer, dimer, trimer, and tetramer in roughly comparable amounts. The experiment was not entirely successful because the ion currents were small. Failure to find the heavy molecules reported by Straus and Madorsky [2] may be ascribed to inadequate sensitivity.

A sample of the heavy fraction of the degradation product with monomer and dimer removed was supplied by Straus. This was evaporated into the mass spectrometer and 25 mass spectra were recorded in the range 80° to 460° C. Table 4 gives some of the peaks in six of these mass spectra. These mass spectra are complicated, but, except for peaks at masses 69 and 81, the larger peaks come at intervals

TABLE 4. *Partial mass spectrum of the heavy fraction obtained from rubber pyrolysis*

m/e	Ion	Relative intensity at temperature of evaporation					
		80° C	130° C	138° C	209° C	209° C	264° C
69	C_5H_9	70	60	52	53	48	.....
81	C_6H_9	100	100	100	100	100	100
135	$C_{10}H_{15}$	41	65	64	100	48	26
203	$C_{15}H_{23}$	6	16	15	30	13.5	14.5
271	$C_{20}H_{31}$	.....	5.3	4.4	12	4.5	9.5
339	$C_{25}H_{39}$	.....	2.9	1.5	9.0	2.7	5.5
407	$C_{30}H_{47}$	.....	2.5	2	6.3	2.1	5.0
475	$C_{35}H_{55}$	.....	2.6	2	2.3	1.8	4.0
543	$C_{40}H_{63}$	.....	.....	2	2.7	1.5	3.0
611	$C_{45}H_{71}$	.....	.....	6.0	7.5	1.8	2.8
679	$C_{50}H_{79}$	.....	.....	3.0	12.0	2.3	1.8
747	$C_{55}H_{87}$	.....	.....	.....	2.7	5.1	2.2
815	$C_{60}H_{95}$	.....	.....	.....	0.25	8.6	2.5
883	$C_{65}H_{103}$	.....	.....	.....	.....	2.3	2.7
951	$C_{70}H_{111}$	.....	.....	.....	.....	.....	2.5
1,019	$C_{75}H_{119}$	.....	.....	.....	.....	.....	0.6
1,087	$C_{80}H_{127}$	.....	.....	.....	.....	.....	.4
Scale divisions at mass 81		150	738	59	696	656	100

of 68 mass units, and have masses one unit less than the molecular weight of polymers of isoprene. Table 4 gives the abundances of these peaks relative to the mass 81 peak. The last row of table 4 gives the height of the 81 peak in scale divisions. This is a measure of the rate of evaporation.

At 80° C the vapor is mostly trimer. The peaks at masses 69, 81, and 135 are present but are relatively small in the dimer spectrum and must come primarily from ionization of the trimer. At 130° C the rate of evaporation is high, and molecules with 4, 5, 6, and 7 monomer units appear. After these evaporate, molecules with 8, 9, and 10 units appear. At 209° C there is rapid evaporation of molecules with 10 monomer units. These quickly evaporate and in the next spectrum record, molecules with 11, 12, and 13 units appear. The heaviest ions were recorded at 264° C. Peaks at 1,019 and 1,087 are barely visible and could possibly be accidental fluctuations. A comparison with the experiment on rubber degradation indicates that at 264° C there may be some thermal degradation of the sample, but at the lower temperatures this is negligible. The larger peaks in the lower molecular weight range must come almost entirely from ionization of the heavier molecules.

3.4. Polyxylylene

An experimental polymer, polyparaxylylene,

$$CH_2\text{-}C_6H_4\text{-}CH_2\text{-}CH_2\text{-}C_6H_4\text{-}CH_2 \ldots,$$

was supplied by the Polaroid Corporation. Experiments by Madorsky and Straus [6] showed that about 4 percent of the degradation product was volatile at room temperature and the heavy fraction had an average molecular weight of 661. Mass-spectrometer analysis of the volatile fraction gave 78 mole percent of xylene, 7 percent of methylethylbenzene, 4 percent of methylstyrene, 8 percent of toluene, and 3 percent of benzene.

When this polymer was degraded directly into the

TABLE 5. *Partial mass spectrum of degradation products of polyxylylene at 310° C.*

Mass	Ion[a]	Relative intensity
104	X	135
105	X+1	1,000
207	2X−1	334
209	2X+1	204
311	3X−1	84
313	3X+1	42
415	4X−1	22
417	4X+1	19
519	5X−1	19
521	5X+1	19
623	6X−1	24
727	7X−1	20
831	8X−1	10
935	9X−1	0.7

[a] X denotes the monomer unit $CH_2 \cdot C_6H_4 \cdot CH_2$ of mass 104.

mass spectrometer it gave a complicated but repetitive mass-spectrum pattern extending to mass 935. Table 5 gives the larger peaks in the spectrum obtained at 310° C. These peaks come at multiples of 104 ±1 mass units. That is, the larger peaks fall at odd mass numbers. The xylene molecule ion of mass 106 is small, but xylene amounts to only 3 percent of the degradation products [6]. The large peak at mass 105 must come from the ionization of heavier molecules. The complete spectrum includes other less abundant ions with 1 or 2 CH_2 radicals added to or subtracted from the chain of xylylene units. Evidently the polymer breaks preferentially at the beta bond between the two CH_2 radicals, but it can also break at the alpha bonds.

3.5. Polyphenyl

The polyphenyl was an experimental polymer synthesized by Max Hellmann of the NBS Polymer Structure Section from diiodobiphenyl heated in contact with copper. The product was partially soluble in benzene, and the lighter soluble fraction was estimated to have a mean molecular weight of 1,460, corresponding to 19 phenyl rings in each chain. The molecular weight of the insoluble fraction is unknown but is presumably much heavier than this.

When the insoluble fraction was slowly heated in the mass spectrometer to 500° C, only small impurity peaks were observed. The hydrogen mass range was not covered in any of these experiments. When the sample was removed it appeared to be completely carbonized. Apparently polyphenyl degrades by losing hydrogen atoms and not by breaking into smaller polyphenyl chains.

The soluble fraction of polyphenyl gave the results shown in table 6. Peak heights are given in scale divisions and many small peaks are omitted. The mass range below 230 was not covered in spectra obtained at 195° C and at 230° C. At the lowest temperature the sample gave off large amounts of unpolymerized biphenyl. (The ion of mass 163 is unidentified.) With increasing temperature heavier molecules appeared, but ion currents were always

TABLE 6. *Mass spectra of the soluble fraction of polyphenyl*

Mass	Ion	Ion current in scale divisions					
		80° C	195° C	230° C	290° C	346° C	390° C
77	C_6H_5	20	.....	.....	14	9	13.0
91	$C_6H_5.CH_2$	5	.....	.....	24	23	29.0
154	$(C_6H_4)_2H_2$	206	.....	.....	4	2.5	7.0
163	.....	11.5	.....	.....	19	12.0	9.0
230	$(C_6H_4)_3H_2$	.....	2	3	12	3.5	5.0
306	$(C_6H_4)_4H_2$	.....	13.5	4	9	3.5	3.5
382	$(C_6H_4)_5H_2$	.....	.....	15	43	1.5	1.5
458	$(C_6H_4)_6H_2$	.....	.....	2	29	.....	.....
534	$(C_6H_4)_7H_2$	.....	.....	1.5	8	1.0	.....
610	$(C_6H_4)_8H_2$	.....	.....	.....	1.5	4.0	2.0
686	$(C_6H_4)_9H_2$	.....	.....	.....	1.0	2.5	4.0
762	$(C_6H_4)_{10}H_2$	.....	.....	.....	.....	0.5	2.5
838	$(C_6H_4)_{11}H_2$	.....	.....	.....	.....	.....	0.5

relatively small. At 195° C, molecules with 4 phenyl rings are predominant, and at 230° C, molecules with 5 rings are most abundant, and the 4 ring molecules are diminished. At 346° C and at 390° C increasingly heavier molecules appear, but at the higher temperature rapid carbonization terminates the evaporation.

4. Summary and Conclusions

The experimental results with polyethylene are consistent with previous work on polyethylene degradation, except that the upper mass limit 684 of table 1 is somewhat less than expected. The average molecular weight of the heavy fraction had been estimated as 690.

Results on degradation of polyvinyl chloride should clarify existing uncertainty as to the mechanism of degradation [7]. There are two distinct stages in the degradation, with loss of HCl and benzene predominant at low temperatures and random breaking of the resulting CH chain occurring above 300° C. The CH chain evidently degrades in a complicated manner above 300° C, taking up hydrogen atoms from the residue to form hydrocarbons with all degrees of saturation. There is no evidence of evaporation of chlorinated hydrocarbons.

The experiment on direct degradation of crepe rubber gave a range of molecular weights much smaller than expected, but this may be ascribed to inadequate sensitivity. The experiment on evaporation of the heavy fraction recovered from rubber degradation showed a range of molecular weights consistent with previous estimates. There are molecules ranging in molecular weight from 204 (3 monomer units) to 1,088 (16 units) and molecules with 9, 10, 11, and 12 monomer units are abundant. The average molecular weight [2] based on the melting point of a camphor solution was 616 or about 9 units.

Polyxylylene seems to break at random into fragments containing up to 9 monomer units. The range of molecular weights is entirely consistent with the average molecular weight, 661, of the nonvolatile

fraction. An interesting point, however, is that it has been assumed that polyxylylene actually degrades into monomer and dimer units and that these repolymerize on condensation [6]. The present experiment gives no support to this theory, for degradation products are evaporated at pressures below 10^{-4} mm, and molecular interaction is negligible.

The experiments with polyphenyl indicate that it does not degrade by breaking into shorter chains but loses hydrogen and carbonizes. A published research [5] on perfluoropolyphenyl shows that it too degrades by carbonizing. Low polymers with up to 11 rings evaporate without degradation, and the same upper limit is found for both the hydrocarbon and the fluorocarbon.

The upper limits of molecular weights observed in mass spectra of four of the polymers are listed in table 7. These limits are presumably set by the consideration that heavier molecules will degrade at the evaporation temperature. A variable intensity factor also enters into consideration. The aromatic polymers are favored in this respect, as their molecule ions are relatively abundant. These are the heaviest hydrocarbons ever reported in mass spectra. The simple recurring pattern of these polymers leaves little doubt as to the molecular formulas of the heavy molecules. The polyvinyl chloride product is an exception in that the degradation product is hopelessly complicated.

Three different types of experiments have been reported: (1) the direct evaporation of degradation products into the mass spectrometer, (2) the reevaporation of degradation products recovered in a separate experiment (table 4), (3) the evaporation of low polymers without degradation (table 6). In the second and third types of experiments the complicated mixture is fractionated as the temperature is gradually increased, and this simplifies the resulting spectra. The results afford a basis for observing the distribution of molecular weights in the material. Results are not quantitative, as there is no possibility of calibrating the sensitivity of the mass spectrometer in terms of pure chemical compounds. However, these experimental results are, in general, consistent with values of the average molecular weight of the degradation products as measured by the NBS Polymer Structure Section. There is no evidence that the condensed degradation products repolymerize to form larger molecules, but results on the degradation of rubber are inconclusive on this point and deserve further study.

TABLE 7. *Upper mass limits of polymer mass spectra*

Polymer	Temperature	Ion	Mass
	°C		
Polyethylene	386	$C_{49}H_{98}$	684
Rubber	264	$C_{80}H_{137}$	1,087
Polyxylylene	310	$C_{72}H_{72}$	935
Polyphenyl	390	$C_{66}H_{42}$	838

5. References

[1] S. L. Madorsky, S. Straus, Dorothy Thompson, and Laura Williamson, J. Research NBS **42,** 499 (1949) RP1989.

[2] S. Straus and S. L. Madorsky, J. Research NBS **50,** 165 (1953) RP2405.

[3] S. L. Madorsky and S. Straus, J. Research NBS **53,** 361 (1954) RP2553.

[4] Paul Bradt, Vernon H. Dibeler, and Fred L. Mohler, J. Research NBS **50,** 201 (1953) RP2410.

[5] Paul Bradt and Fred L. Mohler, Anal. Chem. **27,** 875 (1955).

[6] S. L. Madorsky and S. Straus, J. Research NBS **55,** 223 (1955) RP2624.

[7] Symposium on polymer degradation mechanisms, NBS Circular 525 (1953).

[8] American Petroleum Institute Catalog of Mass Spectral Data.

WASHINGTON, July 26, 1955.

Journal of Research of the National Bureau of Standards Vol. 55, No. 6, December 1955 Research Paper 2638

Heats of Combustion of Liquid *n*-Hexadecane, 1-Hexadecene, *n*-Decylbenzene, *n*-Decylcyclohexane, *n*-Decylcyclopentane, and the Variation of Heat of Combustion With Chain Length[1]

Frances Maron Fraser and Edward J. Prosen

The heats of combustion of five highly purified long-chain liquid hydrocarbons were measured with a bomb calorimeter. The calorimetric data yield the following values for the heats of combustion, $-\Delta Hc°(25° C)$, of the liquid hydrocarbon with gaseous oxygen to form gaseous carbon dioxide and liquid water; 1 kilocalorie = 4.1840 kilojoule.

n-Decylbenzene = 2340.58 ± 0.42 kcal/mole
1-Hexadecene = 2519.17 ± 0.44
n-Hexadecane = 2557.15 ± 0.42
n-Decylcyclohexane = 2497.90 ± 0.43
n-Decylcyclopentane = 2347.54 ± 0.46

It is shown that, in the liquid as well as in the gaseous state, the increment in the heat of combustion (and hence in the heat of formation) per CH_2 group added in the *n*-alkyl side chain is a constant except for the first two members of the series, and that this increment has the same value for each of these series of compounds.

1. Introduction

This investigation is a continuation of the program [1, 2, 3, 4][2] on the determination of some of the thermodynamic properties of compounds of importance in the national synthetic rubber program. In the study of the processes of polymerization and depolymerization, it is important to have thermodynamic data for the compounds in the liquid as well as in the gaseous state, and data on the variation of these properties with carbon chain length. Previous studies [5, 6] have shown that for several homologous series of gaseous hydrocarbons the heat of combustion increases by a constant amount upon the addition of each CH_2 group in the *n*-alkyl side chain; the first few members of each series are anomalous. In an earlier paper [5] the variation, with chain length, in the heat of combustion was studied for the liquid normal paraffins. The increment 156.26 kcal per CH_2 group was calculated, by the method of least squares, from these experimental data. This increment, together with previously reported values for the heats of combustion of the 1-alkenes [2, 22, 23, 24] alkylbenzenes [19, 20] *n*-alkylcyclopentanes [21], and *n*-alkylcyclohexanes [21] was used to calculate values for the heats of combustion of higher members of these series. Up to the present time there has been no experimental check on the validity of this extrapolation. Therefore, it seemed desirable to measure the heat of combustion of a higher member of each series. In this investigation the heats of combustion of 1-hexadecene, *n*-decylbenzene, *n*-decylcyclopentane, *n*-decylcyclohexane, and *n*-hexadecane were measured. It was found that the measured heats agree, within the limits of experimental error, with those calculated using the increment 156.26 per CH_2 group added in the *n*-alkyl side chain.

This agreement shows that the heats of combustion of liquid hydrocarbons may be expressed by an equation of the form $\Delta H_c = A + Bm$, $m > 1$. A is a constant characteristic of the homologous series; B is the constant for the increase in the heat of combustion per CH_2 group added in the *n*-alkyl side chain, and is the same for all these series; and m is the number of carbon atoms in the side chain.

2. Units of Energy and Molecular Weights

The unit of energy upon which values reported in this paper are based is the absolute joule (j). For conversion to the conventional thermochemical calorie, the relation, 1 cal = 4.1840 j, is used.

The molecular weight of carbon dioxide, the mass of which was used to determine the amount of reaction, was taken as 44.010, from the 1952 table of international atomic weights [7].[3]

3. Method and Apparatus

The heats of combustion of the compounds were determined by burning the liquid samples in oxygen in a bomb, at constant volume. The procedure is similar to that used in previous investigations [9,10,

[1] The work discussed herein was performed as a part of the research project sponsored by the Federal Facilities Corp., Office of Synthetic Rubber, in connection with the Government Synthetic Rubber Program.

[2] Figures in brackets indicate the literature references at the end of this paper.

[3] The value for the atomic weight of carbon has recently been changed from 12.010 [7] to 12.011 [8]. The molecular weight of carbon dioxide was taken as 44.010 in this paper to retain consistency with values previously reported by the Thermochemical Laboratory for the heats of formation of other hydrocarbons and of carbon dioxide. The values of the heats of combustion per mole of hydrocarbon reported here can be corrected for the effect of the change to the new atomic weight of carbon by multiplication by the factor 44.011/44.010.

11,12]. The samples were sealed in weighed glass ampoules to prevent evaporation before the combustion period. The filled ampoules were weighed and placed in a platinum crucible in the bomb, 1 ml of water was added to the bomb, and the bomb was flushed and filled with purified oxygen to 30-atm pressure at 25° C. The internal volume of the bomb was 385 ml. The sample was ignited by means of an iron wire fuse, 0.012 cm in diameter and 5 cm long, coiled above the bulb. The amount of reaction was determined from the mass of carbon dioxide formed in the combustion. The heat of reaction was referred to the final calorimeter temperature of 28° C. Corrections were made for deviations from the standard calorimeter system, for the heat contributed by the ignition process of heating and burning the iron wire fuse, and for the heat produced by the formation of nitric acid during the combustion.

A series of calorimetric combustion experiments was made with each of the following substances: 1-hexadecene, *n*-decylbenzene, *n*-hexadecane, *n*-decylcyclohexane, *n*-decylcyclopentane, and benzoic acid (NBS Standard Sample 39g). All of the experiments were performed in as much the same manner as possible. The same calorimeter system, platinum resistance thermometer (NBS No. 485), and Mueller resistance bridge (NBS No. 24530) were used for all of the experiments. The experiments with standard benzoic acid were carried out to determine the energy equivalent of the calorimeter system. Some of these combustion experiments on benzoic acid were performed before and some after the experiments on the hydrocarbons, to allow for any errors which might result from changes in the calorimeter system with time.

The heat of combustion of *n*-hexadecane had been previously determined [10] in the Thermochemical Laboratory. The measurement was repeated as a general check on the procedure.

In several experiments, tests for completeness of combustion were made by analyzing samples of the product gases for carbon monoxide by the colorimetric method described by Shepherd [13].[4] In no case was a significant amount of carbon monoxide found. A further check on the completeness of reaction was afforded by the ratio, r, of carbon dioxide produced in the combustion to the stoichiometric amount of carbon dioxide calculated from the mass of sample used. The following average values of r were obtained in the experiments; the number in parenthesis is the number of experiments for which the value of r was determined, and the uncertainty is the standard deviation of the mean:

1-hexadecene (5)	0.99982 ±0.00011
n-decylbenzene (5)	0.99990 ±0.00008
n-hexadecane (3)	1.00003 ±0.00005
n-decylcyclohexane (4)	1.00019 ±0.00012
n-decylcyclopentane (5)	1.00006 ±0.00009
benzoic acid (5)	1.00008 ±0.00003

[4] These analyses were made by the Gas Chemistry Section of the Bureau.

4. Materials

The hydrocarbons were from the API–NBS series of purified hydrocarbons. The assigned purities of these compounds in mole percent, as determined from measurements of freezing points, were: 1-hexadecene, 99.84 ±0.18; *n*-decylbenzene, 99.88 ±0.10; *n*-hexadecane, 99.96 ±0.04; *n*-decylcyclohexane, 99.86 ±0.11; *n*-decylcyclopentane 99.80 ±0.18.

The impurities in each compound are believed to be isomeric and present in such small amounts that their effect on the heat of combustion is less than the estimated uncertainty assigned.

5. Experimental Results

Table 1 lists the following data for the calibration experiments: The experiment number; the mass of benzoic acid; Δe_1, the deviation from the standard calorimeter system; ΔR_c, the corrected increase in temperature of the calorimeter system; q_i, the correction for ignition energy; q_n, the correction for the formation of nitric acid; and E_s, the energy equivalent of the standard calorimeter system.

TABLE 1. *Calibration experiments*

Experiment No.	Mass of benzoic acid	Δe_1	ΔR_c	q_i	q_n	E_s
	g	*j/ohm*	*ohms*	*j*	*j*	*j/ohm*
1[a]	1.51226	15.1	0.286180	34.1	6.3	139799.7
2[a]	1.51221	16.5	.286084	34.3	5.7	139838.9
3[a]	1.51426	14.3	.286475	35.0	4.9	139839.1
4[b]	1.51471	5.5	.286751	36.1	21.0	139814.8
5[b]	1.51346	5.6	.286515	36.1	22.5	139819.9
6[b]	1.51315	5.6	.286432	35.9	22.0	139829.3
7[b]	1.51227	5.4	.286292	35.5	22.2	139815.8
8[b]	1.51279	5.5	.286390	35.0	22.0	139813.6
Mean						139821.4
Standard deviation of the mean						±4.8

[a] Experiments performed before the combustion experiments on the hydrocarbons.
[b] Experiments performed after the combustion experiments on the hydrocarbons.

The standard calorimeter system was considered to be the actual calorimeter as it existed just prior to the start of the first calibration experiment except that the sample to be burned was not considered a part of the system. Thus Δe_1, the deviation from the standard calorimeter, was computed from the heat capacity of the benzoic acid, 1.21 j/g° C at 26.5° C (minus the heat capacity, 0.03 j/° C ml, of that amount of oxygen at 30 atm and 28° C which was displaced by the benzoic acid) and the heat capacity of any parts of the calorimeter which were changed during the course of this investigation. Also included in Δe_1 are minor corrections for deviations of the average temperature of the experiment from the standard average temperature of 26.50° C (computed from the calculated change of heat capacity of the calorimeter with temperature) and for variations in the heat of the calibrating reaction due to deviations of the final temperature of the experiment from the standard final temperature of 28.00° C.

TABLE 2. *Calorimetric combustion experiments*

Experiment No.	Mass of carbon dioxide	Δe_2	ΔR_c	Q(28° C)	q_i	q_n	$-\Delta U_B$(28° C)	Mean value of $-\Delta U_B$ with its standard deviation
				n-Decylbenzene				
	g	*j/ohm*	*Ohms*	*j*	*j*	*j*	*j/g* CO_2	*j/g* CO_2
1	2.85874	11.8	0.284165	39735.7	31.5	4.9	13887.0	
2	2.84816	10.4	.283114	39588.3	35.7	5.6	13885.1	
3	2.86925	10.6	.285230	39884.3	35.4	4.8	13886.6	13886.8
4	2.87300	10.4	.285654	39943.5	35.4	5.0	13889.0	±0.6
5	2.77388	10.2	.275735	38556.5	35.2	5.2	13885.3	
6	2.91076	10.9	.289374	40463.8	35.2	5.0	13887.6	
				1-Hexadecene				
1	2.67126	10.9	0.285683	39947.7	35.8	6.0	14939.0	
2	2.72788	10.2	.291792	40801.7	35.9	6.0	14941.9	
3	2.66637	9.5	.285222	39882.8	36.2	5.7	14942.0	14941.1
4	2.65190	7.3	.283676	39666.0	35.7	5.9	14941.9	±0.6
5	2.60973	7.2	.279126	39029.8	36.4	5.7	14939.4	
6	2.68706	7.3	.287441	40192.5	35.8	6.0	14942.2	
				n-Hexadecane				
1	2.73431	5.6	0.296839	41506.1	35.9	6.2	15164.3	
2	2.67456	6.8	.290381	40603.5	36.1	6.3	15165.5	
3	2.65107	6.1	.287786	40240.4	35.2	5.7	15163.5	15164.5
4	2.63905	5.1	.286517	40062.7	36.1	6.2	15164.7	±0.4
5	2.77207	5.0	.300919	42076.4	34.8	6.4	15163.8	
6	2.43637	5.0	.264537	36989.3	36.1	5.0	15165.3	
				n-Decylcyclohexane				
1	2.71781	4.1	0.288249	40304.6	35.7	3.6	14815.3	
2	2.63256	3.7	.279230	39043.4	35.7	5.3	14815.4	
3	2.59134	3.6	.274887	38436.1	35.7	6.6	14816.2	14814.7
4	2.69554	6.0	.285858	39970.8	35.9	5.6	14813.1	±0.5
5	2.59597	3.5	.275319	38496.5	35.1	5.5	14813.7	
				n-Decylcyclopentane				
1	2.48540	3.4	0.264257	36949.7	34.8	6.4	14850.1	
2	2.61842	3.5	.278461	38935.8	36.2	7.1	14853.4	
3	2.73536	1.9	.290933	40679.2	36.2	23.5	14848.3	14851.2
4	2.73981	1.8	.291485	40756.4	35.8	23.8	14853.9	±0.9
5	2.56356	0.5	.272715	38131.5	35.4	26.2	14850.4	
6	2.64616	.6	.281489	39358.4	35.5	24.6	14851.1	

The energy equivalent, E_s, was computed by:

$$E_s=[(Q'_B m_s+q_i+q_n)/\Delta R_c]-\Delta e_1,$$

where $Q'_B=\Delta U_B$ (28° C) is the heat of combustion of benzoic acid under the actual bomb conditions used in this investigation expressed in joules per gram of benzoic acid and m_s is the mass of benzoic acid. The value used for the heat of combustion of standard benzoic acid under standard conditions at 25° C is Q_B (25° C)=26434.7 ±2.2 j/g.[5]

Under the actual bomb conditions and at 28° C, this value becomes Q'_B (28° C)=26431.8±2.2 j/g.

Table 2 lists the following data for the calorimetric combustion experiments on the five compounds: The experiment number; the mass of carbon dioxide formed; Δe_2, the deviation from the standard calorimeter system; ΔR_c; Q (28° C)=$(E_s+\Delta e_2)\Delta R_c$, the isothermal heat liberated by the process which took place in the bomb; q_i; q_n; and ΔU_B (28° C)=[Q (28° C)$-q_i-q_n$]/g CO_2, the heat of combustion in the bomb process expressed in joules per gram of carbon dioxide formed.

In table 3 the following quantities are given for each of the compounds: The mean value of $-\Delta U_B$ (28° C) expressed in joules per gram carbon dioxide from table 2, and in kilojoules per mole of hydrocarbon; $-\Delta U°$ (28° C), the decrement in internal energy in the ideal bomb process [10]; $-\Delta Hc°$ (28° C), the heat of combustion at constant pressure at 28° C; $-\Delta Hc°$ (25° C), the heat of combustion at constant pressure at 25° C; and $\Delta H_f°$, the heat of formation at constant pressure at 25° C. The uncertainties in the heats of combustion assigned to the values in table 3 were calculated using the relation,

$$\text{uncertainty}=[(0.0083)^2+(2\sigma E_s)^2+(2\sigma\Delta U_B)^2+(0.01)^2]^{1/2}$$

where σ represents the standard deviation of the mean for the specified measurement, and all de-

[5] This value for benzoic acid, which is based on electrical calibration experiments made in the Thermochemical Laboratory [11], was used to maintain consistency with values previously reported [10] for the lower hydrocarbons, which were based on electrical calibrations. This value differs slightly from the value certified for benzoic acid, Q_B (25° C)=26433.8±2.2 j/g [14, 15]. However, the uncertainty thus introduced is within the estimated over-all uncertainty.

TABLE 3. *Heats of combustion and formation of the liquid hydrocarbons at 25° C*

Compound (liquid)	$-\Delta U_B$ at 28° C		$-\Delta U°$ at 28° C	$-\Delta Hc°$			$\Delta Hf°$ at 25° C	
				at 28° C	at 25° C			
	j/g CO_2	*kj/mole*	*kj/mole*	*kj/mole*	*kj/mole*	*kcal/mole*	*kj/mole*	*kcal/mole*
n-Decylbenzene	13886.8 ±2.5	9778.5 ±1.76	9775.1 ±1.76	9791.3 ±1.76	9793.0 ±1.76	2340.58 ±0.42	−219.12 ±1.97	−52.37 ±0.47
1-Hexadecene	14941.1 ±2.6	10520.9 ±1.85	10518.0 ±1.85	10538.0 ±1.85	10540.2 ±1.85	2519.17 ±0.44	−329.41 ±2.09	−78.73 ±0.50
n-Hexadecane	15164.5 ±2.5	10678.2 ±1.74	10675.5 ±1.74	10696.8 ±1.74	10699.1 ±1.74	2557.15 ±0.42	−456.35 ±2.00	−109.07 ±0.48
n-Decylcyclohexane	14814.7 ±2.6	10431.9 ±1.82	10429.0 ±1.82	10449.0 ±1.82	10451.2 ±1.82	2497.90 ±0.43	−418.39 ±2.06	−100.00 ±0.49
n-Decylcyclopentane	14851.2 ±2.7	9804.0 ±1.92	9801.3 ±1.92	9820.1 ±1.92	9822.1 ±1.92	2347.54 ±0.46	−368.19 ±2.12	−88.00 ±0.51

viations are expressed as percent of the measured quantity. The term 0.0083 percent is the assigned uncertainty in Q'_B; the term 0.01 percent is arbitrarily assigned to allow for systematic errors in the measurements.

The heats of combustion refer to the reaction:

$$C_aH_b(\text{liq})+(b+4a)/4\ O_2(\text{gas})$$
$$=aCO_2\ (\text{gas})+b/2\ H_2O\ (\text{liq}).$$

The heats of formation refer to the reaction:

$$a\text{C(graphite)}+b/2\ H_2\ (\text{gas})=C_aH_b\ (\text{liq}).$$

The heats of formation were calculated from the heats of combustion using the values −68.317 ±0.010 kcal/mole [16] for the heat of formation of liquid water and −94.052 ±0.011 kcal/mole [14] for the heat of formation of carbon dioxide.

The value obtained for the heat of combustion of *n*-hexadecane (liquid), $-\Delta Hc°(25°\ C)=2557.15 \pm 0.42$, is in good agreement with the value previously reported [10] by the Thermochemical Laboratory, $-\Delta Hc°(25°\ C)=2557.58 \pm 0.68$ kcal/mole. The agreement of this value with those of other investigators has been described in a previous publication [5]. No previous measurements have been reported for 1-hexadecene, *n*-decylbenzene, *n*-decylcyclohexane, or *n*-decylcyclopentane.

6. Heats of Combustion of Homologous Compounds

The increment in the heat of combustion per CH_2 group added to the chain in the *n*-paraffins in the gaseous state has been shown [5] to have the constant value 157.44±0.05 kcal/mole. This increment is constant beginning with the third member of the series, propane. From a study of the heats of isomerization of branched-chain paraffin hydrocarbons, it has been shown that the average bond energy of a particular bond between two atoms is affected, within experimental error, only by the other bonds (or atoms) attached to these atoms. Bonds (or atoms) further removed have no measurable effect on this bond energy unless major steric effects are present (such as are revealed by the difficulty in making a Fisher-Hirschfelder model of the molecule). The constancy in the increment per CH_2 group for members of the series above propane is in accord with this observation, since the addition of a CH_2 group to propane to form *n*-butane forms the same kind of bond and neighboring bonds as do further CH_2 additions. In later reports [6,18,19] the increment of 157.44 was applied to other homologous series of hydrocarbons with *n*-alkyl side chains to obtain heats of combustion for higher members of these series in the gaseous state.

A constant increment per CH_2 group for numbers above propane was also found [5] for the *n*-paraffins

TABLE 4.—*Comparison of experimental values of* $-\Delta Hc°$ *with calculated values using the equation* $-\Delta Hc°=A+Bm$

Series Structure	1-Alkenes Vinyl-$(CH_2)_m$−H		Normal alkylbenzenes Phenyl-$(CH_2)_m$−H		Normal alkylcyclopentanes Cyclopentyl-$(CH_2)_m$−H		Normal alkylcyclohexanes Cyclohexyl-$(CH_2)_m$−H	
	Experimental $-\Delta Hc°$ (liq)	Deviation experimental −calculated	Experimental $-\Delta Hc°$ (liq)	Deviation experimental −calculated	Experimental $-\Delta Hc°$ (liq)	Deviation experimental −calculated	Experimental $-\Delta Hc°$ (liq)	Deviation experimental −calculated
	kcal/mole	*kcal/mole*	*kcal/mole*	*kcal/mole*	*kcal/mole*	*kcal/mole*	*kcal/mole*	*kcal/mole*
$m=0$	.....	.....	780.98 ±0.10	(+2.49)	786.54 ±0.17	(+1.49)	936.88 ±0.17	(+1.19)
$m=1$	.....	.....	934.50 ±0.12	(−0.23)	941.14 ±0.18	(−0.15)	1091.13 ±0.23	(−0.80)
$m=2$	644.46[a] ±0.18	+0.10	1091.03 ±0.17	+.06	1097.50 ±0.22	−.03	1248.23 ±0.35	+.06
$m=3$	800.61 ±0.26	+.01	1247.19 ±0.16	−.02	1253.74 ±0.28	−.03	1404.34 ±0.27	−.07
$m=4$	956.72 ±0.33	−.12	1403.46 ±0.27	+.01	.....	.....	1560.78 ±0.29	+.13
$m=5$	1112.87 ±0.38	−.21	.....	.....	.....	.....	.....	.....
$m=10$	.....	.....	2340.58 ±0.42	−.31	2347.54 ±0.46	+.09	2497.90 ±0.43	−.19
$m=14$	2519.17 ±0.44	−.07	.....	.....	.....	.....	.....	.....
A	.....	331.88	.....	778.49	.....	785.05	.....	935.69
B	.....	156.24	.....	156.24	.....	156.24	.....	156.24

[a] At saturation pressure.

in the liquid state. The value of this increment is 156.26 $\pm$0.05 kcal/mole. Because of possible variations in intermolecular forces, it was not evident that this increment could be applied to other homologous series of hydrocarbons with *n*-alkyl side chains in the liquid state. The values obtained here for the heats of combustion of some higher members of such series, together with values previously reported for the lower members in the liquid state, show that this value of 156.26 can be applied to these series as well. The constancy begins with the ethyl side chain.

The constant B was re-evaluated, by the method of least squares, utilizing all of the available experimental data from the Bureau. The new value of B, 156.24, is in agreement with the value 156.26 calculated from the *n*-paraffin series alone.

In table 4 are given the experimental values for the heats of combustion of compounds of several series in the liquid state. These data were obtained from the following sources: the heats of combustion of benzene, toluene, ethylbenzene, *n*-propylbenzene, and *n*-butylbenzene in the liquid state [19, 20]; the heats of combustion of cyclopentane, methylcyclopentane, ethylcyclopentane, *n*-propylcyclopentane, cyclohexane, methylcyclohexane, ethylcyclohexane, *n*-propylcyclohexane, and *n*-butylcyclohexane in the liquid state [21]; the heats of combustion of 1-butene [2] and 1-pentene [22] in the gaseous state together with heats of vaporization of 1-butene [23] and 1-pentene [24]; the heats of combustion of 1-hexene and 1-heptene in the liquid state [25]; and the heats of combustion of 1-hexadecene, *n*-decylbenzene, *n*-decylcyclohexane, *n*-decylcyclopentane, and *n*-hexadecane in the liquid state from the present investigation.

In table 4 are also given the deviations of these experimental data from the heats of combustion calculated using the equation $-\Delta Hc^\circ = A + Bm$ where A is the constant characteristic of the homologous series, B is the constant 156.24 kcal/mole for each series, and m is the number of carbon atoms in the *n*-alkyl side chain. The values of A were calculated weighting the value of ΔHc°, for each compound measured, inversely as the square of its assigned uncertainty.

7. References

[1] E. J. Prosen, F. W. Maron, and F. D. Rossini, J. Research NBS **42**, 269 (1949) RP1968.
[2] E. J. Prosen, F. W. Maron, and F. D. Rossini, J. Research NBS **46**, 106 (1951) RP2181.
[3] F. M. Fraser and E. J. Prosen, J. Research NBS (in preparation).
[4] F. M. Fraser and E. J. Prosen, J. Research NBS **54**, 143 (1955) RP2575.
[5] E. J. Prosen and F. D. Rossini, J. Research NBS **34**, 263 (1945) RP1642.
[6] E. J. Prosen, W. H. Johnson, and F. D. Rossini, J. Research NBS **37**, 51 (1946) RP1728.
[7] E. Wichers, J. Am. Chem. Soc. **74**, 2447 (1952).
[8] E. Wichers, J. Am. Chem. Soc. **76**, 2033 (1954).
[9] E. J. Prosen and F. D. Rossini, J. Research NBS **27**, 289 (1941) RP1420.
[10] E. J. Prosen and F. D. Rossini, J. Research NBS **33**, 255 (1944) RP1607.
[11] E. J. Prosen and F. D. Rossini, J. Research NBS **33**, 439 (1944) RP1619.
[12] W. H. Johnson, E. J. Prosen, and F. D. Rossini, J. Research NBS **42**, 251 (1949) RP1966.
[13] M. Shepherd, Anal. Chem. **19**, 77 (1947).
[14] R. S. Jessup, J. Research NBS **29**, 247 (1942) RP1499.
[15] R. S. Jessup, J. Research NBS **36**, 421 (1946) RP1711.
[16] D. D. Wagman, J. E. Kilpatrick, W. J. Taylor, K. S. Pitzer, and F. D. Rossini, J. Research NBS **34**, 143 (1945) RP1634.
[17] E. J. Prosen, R. S. Jessup, and D. F. Rossini, J. Research NBS **33**, 447 (1944) RP1620.
[18] E. J. Prosen and F. D. Rossini, J. Research NBS **36**, 269 (1946) RP1702.
[19] E. J. Prosen, W. H. Johnson, and F. D. Rossini, J. Research NBS **36**, 455 (1946) RP1714.
[20] E. J. Prosen, R. Gilmont, and F. D. Rossini, J. Research NBS **34**, 65 (1945) RP1629.
[21] W. H. Johnson, E. J. Prosen, and F. D. Rossini, J. Research NBS **36**, 463 (1946) RP1715.
[22] F. M. Fraser, R. G. Miller, and E. J. Prosen, J. Research NBS (in preparation).
[23] Selected values of properties of hydrocarbons, NBS Circular C461 (U. S. Government Printing Office, Washington 25, D. C., 1947).
[24] D. W. Scott, G. Waddington, and H. M. Huffman, J. Am. Chem. Soc. **71**, 2767 (1949).
[25] I. Jaffe and E. J. Prosen, J. Research NBS (in preparation).

WASHINGTON, August 12, 1955.

Journal of Research of the National Bureau of Standards Vol. 55, No. 6, December 1955 Research Paper 2639

Computation of Atomic Energy Levels: Spectrum of Singly-Ionized Tantalum (Ta II)

Richard E. Trees, W. F. Cahill, and P. Rabinowitz [1]

Energies and wave functions of atomic systems can be calculated as the characteristic values and vectors of matrices in accordance with long-established procedures. Coding for carrying out these computations on the Standards Eastern Automatic Computer is described. Some preliminary values are given for the energy levels of the spectrum of singly-ionized tantalum (Ta II).

1. Introduction

Calculations of atomic energy levels have been helpful in expediting the analysis of experimental data.[2,3] However, except in the simplest cases, the numerical work is excessive for hand computation, and the calculations have had very limited applicability. It is possible to overcome this limitation by utilizing digital computers. A calculation of the levels of the low even configurations in the spectrum of singly-ionized tantalum (Ta II) is given. This is a typical example of a calculation that is too difficult for hand computation, although fairly simple as compared with others in the field of complex spectra.

2. Statement of Problem

Spectra in which configuration interaction and spin-orbit coupling are both important are considered; the basic theory for these spectra is well established.[4,5] According to this theory, energies of levels with the same total angular momentum (i. e., the same "J-value") are the eigenvalues of a matrix, which is here designated by (a_{ij}). The J-value is omitted for brevity, but there will be one of these matrices for each J-value that is allowed, in the configurations of the spectrum under consideration. The configurations occurring in Ta II are d^4, d^3s, and d^2s^2; these give rise to matrices of orders 9×9, 12×12, 21×21, 15×15, 15×15, 6×6, and 3×3 for the allowed J-values 0, 1, 2, 3, 4, 5, and 6, respectively.

Each matrix element is a linear combination of a limited number of "parameters", $p^{(k)}$, multiplied by known "coefficients" $c_{ij}^{(k)}$ (the parameters are the same for all J-values).

$$a_{ij}=\sum_k c_{ij}^{(k)}\,p^{(k)}. \tag{1}$$

These linear forms can be derived in a straightforward manner by use of methods developed by Racah (see footnote 5). For commonly occurring configurations, the calculation of any one element of the "coefficient matrix" $(c_{ij}^{(k)})$ involves at most the multiplication of a few factors, which are given in readily available tables.[6] The parameter associated with a given coefficient matrix is defined in theory as a radial integral (Slater integral, spin-orbit integral, etc.) (see footnote 4). This can be evaluated if radial wave functions are determined by the method of self-consistent fields, but the work involved in this procedure is great. In the present calculations, the parameters are adjusted by least-squares to get best agreement with levels that have already been identified experimentally. This limits the use of the theory to spectra in which the analysis of the experimental data is already well started. This limitation may also be removed when computers are used to carry out self-consistent field calculations for complex spectra such as Ta II.

The coefficient matrices for the electrostatic interaction in the configurations of Ta II are given in R II and R III. For each J-value there are 16 of these associated with parameters identified by the letters A, B, C, G_2, H_2, and α (see table 2).[7] In addition to these, there are three parameters ζ associated with the coefficient matrices of the spin-orbit interaction. The latter coefficient matrices have been given for the configurations d^2s^2 (see footnote 4) and for d^4 also.[8] The matrices for d^3s have been computed by Trees; for the sake of brevity, the results are not given here.

Recapitulating, there are 19 different parameters, and for each of the seven J-values there are 19 coefficient matrices, one associated with each parameter.[9] Though the orders of the coefficient matrices

[1] Present address: Weizmann Institute of Science, Rehovot, Israel.
[2] R. E. Trees and M. M. Harvey, J. Research NBS **49**, 397 (1952) RP2378
[3] M. Gehatiah, Phys. Rev. **94**, 618 (1954).
W. F. Meggers has recently located the $c\,^1D(3/2)$ level of Hf II at 30595, less than 100 K away from Gehatiah's calculated position of 30692.
[4] E. U. Condon and G. H.Shortley, The theory of atomic spectra (Cambridge University Press, London, 1951).
[5] G. Racah, Phys. Rev. **62**, 438 (1942); **63**, 367 (1943); **76**, 1352 (1949). Referred to as R II, R III, and R IV, respectively.
[6] Because there are often many elements, it will nevertheless require much time and effort to set up these coefficient matrices correctly; probably automatic computers can be utilized in this phase of the work.
[7] For a discussion of the parameter α and other advances in atomic theory not covered in footnotes 4 and 5, see G. Racah, Kungl. Fysiografiska Sällskapets Handlingar N. F. **65**, 31 (1955). (Proceedings of the Rydberg Centennial Conference on Atomic Spectroscopy).
[8] H. Greyber, Ph. D. thesis, University of Pennsylvania, 1953 (unpublished).
[9] It is convenient to use the code of section 6 to calculate the g-values; to do this the LS-coupling g-values are included as an extra coefficient matrix, the "parameter" associated with the g-value always being zero. Therefore, 20 parameters were actually used for Ta II.

are the same as those already given for the appropriate J-value, there are very few nonzero elements in most of the coefficient matrices; the only coefficient matrices with large numbers of nonzero elements are those associated with the two parameters $\zeta(d^1)$ and $\zeta(d^3\ s)$.

3. Eigenvalues and Eigenvectors of Real Symmetric Matrices

Preliminary estimates of the parameters $p^{(k)}$ are made by using methods given in section 7.1., and the matrix elements are then calculated according to formula (1). This can be done by hand computation; or the coding described in section 5 can be used to generate the matrices on the National Bureau of Standards Eastern Automatic Computer (SEAC). The eigenvalues and eigenvectors of the matrices are then to be determined.

A SEAC code that will do this is based on the Duncan-Collar iteration procedure.[10] The use of this code with matrices up to order 12×12 has been briefly reported.[11] The code can handle matrices with orders up to 25×25. The major disadvantage of this code is that it requires too much machine time for regular use when all eigenvalues of several high-order matrices are desired.[12] Because of this, no effort was made to determine all the eigenvectors and eigenvalues for the matrices of Ta II set up with the preliminary values of the parameters. No matrices were set up with the final values obtained for the parameters.[13]

4. Least-Squares Adjustment of Parameters

The matrices set up with preliminary values of the parameters $p^{(k)}$ have the eigenvalues $\lambda^{(m)}$ and the eigenvectors $X^{(m)}$ determined (the components of a vector will be indicated by $x_i^{(m)}$) as described in section 3. The eigenvalues are approximated as a function of the parameters by the following linear formula, which will be accurate to first order, in the difference between the parameters and their preliminary values:

$$\lambda^{(m)} = \sum_k d_{(k)}^{(m)} p^{(k)}, \tag{2}$$

where

$$d_{(k)}^{(m)} = \sum_{ij} x_i^{(m)} c_{ij}^{(k)} x_j^{(m)} \tag{3}$$

The coefficients $c_{ij}^{(k)}$ are the ones already used in (1). The linear formulas (2) can be set up by hand; or the coding described in section 6 can be used to generate them on SEAC. A least-squares adjustment can then be made to find new values of the parameters $p^{(k)}$, which will make the linear forms (2) agree best with a corresponding set of observed experimental values.

A general-purpose orthonormalizing code has been set up for SEAC,[14] and it can be used to carry out least-squares calculations. The coefficients $d_{(k)}^{(m)}$, for fixed "k", are regarded as components of a vector in a space with the same dimensionality as the number of observations to be fitted. For successive k-values, each vector is orthogonalized to all preceding vectors with smaller k-values. The observed values, regarded as an additional vector, are then expanded in terms of this set, and the residues that remain after the expansion will be the least-squares deviations. The process can be interrupted before the orthonormalization is completed for all k-values, so that the least-squares calculation can be carried out, say, first by omitting and then by including the last parameter, without making two separate calculations. As many sets of observations may be fitted as desired in a single calculation. Consequently, different possibilities for correlating observations with theory may be tested. An observation may be omitted from the calculation by inserting a new "weight vector" in which the component corresponding to the deleted observation is given the weight zero. The vectors must be "augmented" in these applications (see footnote 14), so that the least-squares values of the parameters will be recorded by SEAC (along with the deviations between theory and experiment). This augmentation reduces the capacity of the code when used with the high-speed memory; with 18 adjustable parameters, a maximum of 22 observations could be fitted, whereas with 9 adjustable parameters, 63 observations could be fitted. However, an alternative slightly slower code is available if external tapes are used, and in this the only limitation is that the sum of the number of observations and the number of parameters be less than 256.

The Ta II problem was worked in an approximation where first 8 and then 9 parameters were adjusted (i. e., results were obtained with and without the final parameter α included). There were 39 observed values, but the number of these was reduced in successive calculations. As a check, both the observed values and the original deviations from these values were fitted. It required about 20 min of machine time for each of these calculations as compared to about 9 hr required in an earlier hand computation, where the normal equations were first obtained and then solved by elimination. The results are described in section 7.3.

[10] The matrix is modified to obtain successive values by the method given by W. M. Kincaid, Quart. Appl. Math. **5**, 320 (1947).

[11] D. E. Mann, L. Fano, W. F. Cahill, and T. Shimanouchi, J. Chem. Phys. **22**, 764 (1954).

[12] Appreciation is expressed to W. G. Hall for running SEAC to get the energy values in Ta II reported in section 7.2. He also obtained values in the first spectrum of tungsten (W I) for G. Racah; a report on the latter work, which involved matrices with orders up to 25×25, has been given in footnote 7. On the basis of his work, Hall has estimated that the average time required to iterate for one eigenvalue and eigenvector is about 5 min for a 10×10 matrix, 20 min for a 20×20 matrix, and 50 min for a 25×25 matrix.

[13] K. Goldberg has a code that determines only the eigenvalues; this code is similar to that described by W. Givens, ORNL 1574 (1954). It can determine the eigenvalues of matrices up to order 30×30; the time required for a 30×30 matrix is 25 min. About 10 min are needed for a 20×20 matrix. This code is being extended to give the vectors; it is expected that the extended code will be able to handle matrices of orders up to 23×23.

[14] P. Davis and P. Rabinowitz, J. Assoc. Comp. Mach. **1**, 183 (1954).

5. Data Preparation—Matrix Inputs

A code has been set up that will generate all matrices with a single input of the parameter values. It uses the internal memory and can generate matrices of order up to 38×38. Checks in the code insure that the matrix generated is correct on wire and ready as an input for the coding described in section 3. For the Ta II work, all matrices could be generated in 30 to 60 min of machine time.

When a problem is first started, it is necessary to type many coefficient matrices (20 for the Ta II work) for each final matrix generated, and it would seem simpler to evaluate the elements (1) with a desk computer and type the final matrix directly.[15] However, only the nonzero coefficients need be typed, and as there are usually very few of these, the total work involved is about the same.[16] Once the coefficient matrices are typed, final matrices can be generated for as many sets of parameter values as desired. In any one problem, matrices must be set up with at least two sets of parameter values, so an appreciable amount of time will be saved.[17] The same coefficient matrices are used to generate the linear formulas (2) with the coding described in section 6, and in relation to this work, the time required to type the coefficient matrices is a negligible factor.

The coefficient matrices used with this code must have no more than 56 nonzero elements, but larger coefficient matrices can be inserted piecemeal by associating extra parameters (which will be given the same value) with each part. To allow for this possibility, the code has been written for 24 parameters, which is probably a larger number than would ever be needed. The largest coefficient matrix encountered in the Ta II problem had only 36 nonzero elements.

6. Data Preparation—Least-Squares Inputs

A code has been set up that will generate the coefficients, formula (3), that enter into the linear formula for the eigenvalue, formula (2). Instructions that determine the number of independent parameters desired in the linear formula outputs are first fed in; frequently, as here, parameters having the same symbol are regarded as identical in all configurations in which they occur, but other approximations are also used. All vectors for which linear formulas are desired are then fed into the internal memory; there is space for 582 vector components (all vectors of a 24×24 matrix).[18] The coefficient matrices are then fed in, and for each one fed in (or for each group of consecutive matrices, depending on the instructions), as many coefficients of linear formulas print out as there are vectors in the vector input (the maximum number of possible outputs is 24). For the Ta II work, the 39 linear formulas in nine parameters were computed in less than 60 min of machine time; originally this work was carried out with a desk computer, and the time required was of the order of 60 hr.

The coding just described groups coefficients of the same parameter only if they are in the same matrix. For use in the least-squares code of section 4, coefficients of the same parameter must be grouped together without regard to the J-value of the matrix in which they occur. The second part of this code sorts out the preceding coefficient outputs. A remaining uncorrected deficiency is that it does not give an output ready to be used as an input for the orthonormalization code of section 4; the augmenting and check sums were inadvertently overlooked, so the results had to be outscribed, amplified, and reinscribed to get the correct input. This sorting can be carried out only for problems where the number of coefficients, formula (3), is less than 672. With 15 parameters (which may be the least number that can give good agreement in Ta II) only 44 observations can be handled (and 39 of 81 possible levels have already been observed in Ta II). This limitation is a very difficult one to overcome without altering the construction of the computer itself. However, it is always possible to combine two partial sortings and set up by hand the final input for the least-squares code.

It would be convenient at this point to carry out a few manipulations with the sorted linear formulas, but the potentialities for doing this have not yet been fully explored. However, supplemental coding has been made that will evaluate the linear formulas, and also the differences between the formulas and a set of observed values, for as many sets of parameters as desired.

7. Results for Ta II

7.1. Preliminary Estimates of Parameters

The spectrum of Ta II is very complicated because of the presence of the three overlapping configurations of $5d^4$, $5d^3\,6s$, and $5d^2\,6s^2$. The analysis of the experimental data [19] is far from complete, as only 39 of 81 possible levels in these configurations have been identified. J-values are assigned to all identified levels, but the configuration and LS-coupling desig-

[15] The time required to set up the code was naturally far in excess of the time needed to do the work with hand computers. The expenditure of this time is justified only because it is expected that the same coding will be used subsequently in many similar problems.

[16] The last four digits of each coefficient are used to specify the position in the matrix; this leaves seven digits for the coefficient itself. In the present work only four significant figures were retained after the decimal point, because a result theoretically correct to within 1 kayser was considered adequate with a mean deviation between theory and experiment more than a hundred times as great.

[17] The same set of coefficient matrices can often be used to generate final matrices for other spectra that have the same, or related, configurations. The coefficient matrices used in the Ta II work also apply to the configurations d^3, $d^7\,s$, and $d^6\,s^2$, and they have been used to generate the matrices for the first spectrum of ruthenium (Ru I) as a start toward assisting with the analysis of this spectrum.

[18] With some amplification, the coding could be used to obtain nondiagonal elements of the transformed coefficient matrices (as well as the diagonal elements, formula (3)); it is estimated that matrices of order up to 18 × 18 might be transformed with this amplified code. Such a code would be useful in solving the problem referred to in footnote 6 because it is sometimes easiest to set up coefficient matrices in a scheme that does not correspond to observed behavior, and then to use a simple transformation to arrive at a labeling that is more nearly approached in nature.

[19] C. C. Kiess, G. R. Harrison, and W. J. Hitchcock, J. Research NBS **44**, 245 (1950) RP2075.

nations have been made for only 26 of them. However, the configuration assignments of six of the lowest levels have been uncertain. Kiess (see footnote 19) had assigned these levels to the ^{3}F and ^{3}P terms of the $5d^2\ 6s^2$ configuration, but this assignment put the ^{3}P term below the ^{3}F term, whereas it would be expected to be much higher on the basis of a simple LS-coupling theory. It would have been reasonable to assign the ^{3}F term to the $5d^3\ 6s$ configuration, but this would leave the ^{3}F term in $5d^2\ 6s^2$ still unidentified and force one to conclude that the lowest levels of this spectrum, corresponding to the $5d^2\ 6s^2\ ^3$F term, were completely unknown.[20] In any case, it was certain that configuration and LS-coupling assignments would be approximations at best, so that it would be very hard to decide what experimental values should be correlated with theory in estimating preliminary values for the parameters.

Because of this, the theory was first applied to the experimental values [21] in the simpler, almost completely analyzed spectrum of singly-ionized hafnium (Hf II), to get some idea of the values that would be expected for the parameters in spectra with $5d$-electrons; no calculations had been published for these spectra at that time. The Hf II parameters were not evaluated by least-squares, but the values obtained agreed well with those recently published by Gehatiah (see footnote 3).[22]

Preliminary parameter values were then estimated for Ta II by adjusting the Hf II values to get rough agreement with a few of the best identified levels of the Ta II spectrum. The magnitude of the readjustment was kept reasonably consistent with what would be expected from the known behavior of the parameters in spectra with $3d$- and $4d$-electrons. However, some of the parameters were poorly adjusted, and acceptable preliminary values of the parameters were still obtained, so it is likely that this readjustment is not critical. Some details of the procedure will be given, however, mainly to bring out significant features of the parameter behavior. The preliminary parameter values are given in calculation I of table 1, and the final least-squares-adjusted values of the parameters are given in calculation II.

The preliminary values for parameters B and C were assumed to be 20 percent greater than the values in Hf II, although an increase of only about 15 percent would be expected from analogy with $3d$-electron spectra. Calculation II shows not only that this overestimated B and C, but also what is more important, that the final ratio of B to C in Ta II is about 8 percent smaller than the ratio in Hf II (it is 25 percent greater than the ratio for the W I parameters (see footnote 22). This ratio has a more constant value in spectra with $3d$- and $4d$-electrons (see footnote 22). The ratio may vary in spectra with $5d$-electrons, but it is also possible that a nearly constant ratio would be obtained in these spectra if a higher-order approximation were used, as suggested at the end of this paper.

The preliminary estimate $G_2=2{,}000$ was made to favor the assumption that the lowest identified ^{3}F term belonged to the $5d^3\ 6s$ configuration, even though this assumption was not considered correct. Calculation II shows that G_2 should have been given the value found in Hf II. Analogy with $3d$-electron spectra indicates that G_2 should be slightly larger in Ta II than in Hf II, but the increase is much less than expected for B and C.

The value $\zeta=2{,}100$ is a considerable overestimate; calculation II indicates that a value slightly larger than the value applicable in Ta I should have been used (see footnote 22), which is what would be expected from analogy with $3d$-electron spectra.

To estimate the interaction parameter H_2, the ^{3}F and ^{3}P matrices were set up in LS-coupling by using all the preceding preliminary parameter evaluations. The lowest terms of these matrices were expected to be very sensitive to the value of the parameter H_2, so that errors in estimating the other parameters would not be too important. A value of 500 was assumed for H_2, as it was expected that the parameter would have a value in Ta II that would nearly equal that in Hf II. Analogy with the behavior shown in the $3d$-electron spectra would lead one to expect that the value in Ta II might be smaller than in Hf II, but as this integral depends strongly on the overlapping of d- and s-wave functions, the analogy would not be very reliable. The eigenvalues of the two 5×5 matrices were obtained on SEAC with the coding described in section 3. The lowest ^{3}P term was found to be 800 K above the ^{3}F term, instead of 1800 K below as observed. It was decided that an extra 10-percent increase in the value of H_2 would be justified, and that this, together with the inclusion of second-order spin-orbit effects, would explain the observations with reasonable parameter values.

---

[20] In commenting on this, Kiess noted that too few strong transitions were left unidentified in his line list to give much weight to this possibility (private communication). The assignment made by Kiess was originally made also by P. F. A. Klinkenberg, G. J. van den Berg, and J. C. van den Bosch, Physica **16,** 861 (1950), but they later favored the second possibility that the lowest levels had not yet been identified (Physica **17,** 167 (1951)); theory was used to demonstrate the validity of the second alternative by van den Berg (Ph. D. Thesis, University of Amsterdam, 1951 (unpublished)). His calculation is much too simplified to decide the point, however, and the calculation given here shows conclusively that the first alternative is the correct one.

[21] W. F. Meggers and B. F. Scribner, J. Research NBS **13,** 625 (1934) RP732.

[22] Gehatiah's parameter values for Hf II are:

$$B=435,\ C=1{,}530,\ G_2=2{,}818,\ H_2=482,\ \text{and}\ \zeta=1{,}336.$$

Analogy with results for $3d$- and $4d$-electrons suggests that the Ta II parameters should more nearly equal to the parameters of Ta I or W I (excepting the spin-orbit parameter ζ for the latter spectrum) than to those of Hf II. Some recent unpublished evaluations of parameters in these two first spectra are interesting. Racah has given the final parameter values that he obtained in the $5d^4\ 6s^2$ and $5d^5\ 6s$ configurations of W I:

$$B=371,\ C=1{,}900,\ G_2=2{,}700,\ H_2=434,\ \zeta=2{,}089\ \text{and}\ \alpha=46.$$

His calculations are briefly described in footnote 7. The Ta I calculations are for the $5d^3\ 6s^2$ configuration and neglect configuration interaction; they have been carried out with and without the $L\ (L+1)$ correction (see R. E. Trees, Phys. Rev. **92,** 308 (1953) and also T. Kamei, Phys. Rev. **99,** 789 (1955):

$$B=345,\ \mathrm{C}=1{,}289,\ \zeta=1{,}657,\ \alpha=112.$$

$$B=278,\ \mathrm{C}=2{,}100,\ \zeta=1{,}650.$$

The neglect of configuration interaction in the Ta I calculations is probably not fully justified, which may account for the value of α being larger than expected.

TABLE 1. *Configurations $d^2 s^2$, $d^3 s$, and d^4 of* Ta II *in intermediate coupling*

Levels are identified by their J-values and by the label number, which is the order in energy sequence.
Calculation I: Solutions of matrices for preliminary values of the parameters.
Calculation II: Solution from linear formulas; parameters evaluated by least-squares, with the levels 18500 and 23295 omitted.

J-value	Label	Observed energy	Obs. g	Calculation I			Calculation II	
				Calc. energy	Calc.−obs.	Calc. g	Calc. energy	Calc.−obs.
6	1	4125	.....	3798	−327	.....	4046	−79
	2	12601	.....	11591	−1010	.....	12547	−54
	3	.....	.....	15240	.....	.....	.....	.....
	4	23381	.....	23317	−64	.....	23084	−297
	5	.....	.....	25860	.....	.....	.....	.....
	6	.....	.....	33923	.....	.....	.....	.....
1	1	0	0.000	−292	−292	0.058	−53	−53
	2	5331	1.550	5316	−15	1.537	5216	−115
	3	10713	2.374	11351	638	2.128	10982	269
	4	13475	1.510	13111	−364	1.654	13331	−144
	5	14628	0.850	13651	−977	1.119	14156	−472
	6	17375	1.171	17014	−361	1.007	17175	−200
	7	.....	.....	22412	.....	.....	.....	.....
	8	.....	.....	26426	.....	.....	.....	.....
	9	.....	.....	30446	.....	.....	.....	.....
2	1	1031	1.008	853	−178	1.009	1139	108
	2	3180	0.750	2607	−573	0.767	3532	352
	3	5658	1.390	5045	−613	1.126	5872	214
	4	9690	1.063	7865	−1825	1.039	9469	−221
	5	11875	1.48	11706	−169	1.210	11653	−222
	6	13560	1.11	13892	332	1.495	13246	−314
	7	14494	1.472	14794	300	1.485	14375	−120
	8	16424	1.405	16576	152	1.392	17227	803
	9	17168	1.211	17966	798	1.289	17886	718
	10	18500	1.462	22389	3889	1.094	22836	(4335)
	11	22928	0.700	23128	200	0.732	22866	−63
	12	.....	.....	28091	.....	.....	.....	.....
	13	.....	.....	30795	.....	.....	.....	.....
3	1	2642	1.250	2980	338	1.244	2663	21
	2	6831	1.098	6598	−233	1.080	6820	−11
	3	11767	0.915	9876	−1891	0.996	11793	23
	4	12435	1.614	13679	1244	1.467	12730	295
	5	14581	1.004	13322	−1259	1.048	13293	−1288
	6	15726	1.476	16197	471	1.460	15898	172
	7	23295	1.120	19144	−4151	1.348	18863	(−4932)
	8	23620	1.076	23976	356	1.080	23464	−156
	9	24870	0.995	24563	−307	1.006	24656	−214
	10	26829	0.855	27699	870	0.852	27054	225
	11	.....	.....	32217	.....	.....	.....	.....
4	1	4416	1.350	5068	652	1.329	4434	18
	2	9746	1.225	9421	−325	1.174	9651	−95
	3	.....	.....	11206	.....	1.110	.....	.....
	4	12705	1.021	12375	−330	1.061	12685	−20
	5	.....	.....	14675	.....	1.072	.....	.....
	6	17231	1.23	17597	366	1.050	16968	−263
	7	.....	.....	18354	.....	1.358	.....	.....
	8	23083	1.026	23372	289	1.042	22841	−242
	9	24433	0.978	24479	46	0.949	24535	102
	10	.....	.....	25409	.....	1.155	.....	.....
	11	.....	.....	29577	.....	.....	.....	.....
	12	.....	.....	31925	.....	.....	.....	.....
5	1	6187	1.33	6967	780	1.362	6224	37
	2	12831	1.280	13958	1127	1.148	13778	947
	3	.....	.....	18538	.....	1.102	.....	.....
	4	.....	.....	22392	.....	1.020	.....	.....
	5	25414	1.052	26448	1034	1.059	25754	340

Parameters		
$A(d^2 s)$	19215	20272
$A(d^2 s^2)$	13615	13744
$A(d^4)$	28365	26777
B	530	483
C	1860	1841
ζ	2100	1776
H_2	550	538
G_2	2000	2872

7.2. Preliminary Calculation of Energy Levels

By using these preliminary values for the parameters, matrices were set up for the Ta II problem, as outlined in section 2. (The coding in section 5 was not then available.) The eigenvalues and eigenvectors of these matrices were then calculated on SEAC, as described in section 3. The results are given in calculation I of table 1. Partly because the eigenvectors obtained in this calculation are based on preliminary values for the parameters, no attempt has been made to give the conventional LS-coupling designation for the levels, and the levels have been identified by the J-values alone; the assignments given to some of these levels by Kiess (see footnote 19) are, however, roughly confirmed.

366278—56——4

Although the preliminary parameters were estimated without making any effort to assign the majority of the observed levels to any theoretical state, a good correlation can be established between observed energy levels and calculated eigenvalues, and between the corresponding observed and calculated g-values. There are, however, three observed levels with $J=2$ (16424, 17168, and 18500) in a region where there are only two calculated (16576, 17966); the g-values indicate that the level which cannot be correlated with theory is the one observed at 18500. Similarly, there are three observed levels with $J=3$ (23295, 23620, and 24870) in a region where two are calculated (23976 and 24563); in this case the g-values indicate that the level which cannot be correlated with theory is the one observed at 23295. The levels with $J=3$ observed at 12435 and 14581 were correlated with the respective calculated values 13679 and 13322. This is the only instance where the calculated and observed values were not correlated in the same sequence with respect to energy. This correlation was made when it was found with better parameter estimates that the linear formulas for the eigenvalues indicated that their energies would cross. This correlation could have been made more easily by noting that it makes the g-values agree much better, but this criterion would also call for reversing the correlations of the fifth and sixth levels with $J=2$, and this was not done. Within the limits of accuracy of this preliminary calculation, the only other correlations that seem uncertain are the ones connecting the level observed at 12705 with the level calculated at 12375, rather than the ones calculated at 11206 or 14675, and also the correlation of 17231 with 17597 rather than with 18354. Both these correlations worked well in subsequent least-squares calculations. However, the least-squares calculations show that agreement would be improved if the level observed at 16424 were disregarded, rather than the one at 18500. It is likely that other possibilities still remain, that might give better agreement.

7.3. Least-Squares Estimates of Parameters

Linear formulas for the eigenvalues were set up by hand (the coding of section 6 was not then available) in an approximation with nine adjustable parameters; the parameter α, which was neglected for the preliminary estimates, is the additional parameter. Least-squares calculations were then carried out on SEAC, with and without the parameter α, as described in section 4. These calculations will be described briefly; the parameter values that were obtained are given in successive columns of table 2, labeled to correspond to the descriptions.

(I) The parameters were determined by using all 39 observed levels with the correspondence between theory and observation the same as that already given in calculation I of table 1. The purpose was to verify, what was already fairly certain, that no readjustment of the parameters would give a good fit for all 39 observations. In this calculation the level at 18500 had a deviation of 3817, and the deviation for the level at 23295 was −4294. The level at 12831 had the next largest deviation of 1316, which is an order of magnitude smaller. The mean deviation was ±1048; the mean deviation, exclusive of the two badly fitting levels, was ±515.

TABLE 2. Least-squares evaluations of the parameters of $d^2\,s^2$, $d^3\,s$, and d^4 of Ta II

The parameters A determine the centers of gravity of the three configurations; B, C, ζ, and α would be specified independently in all three configurations in higher approximations than the one given here. The interaction parameter, $G_2(d^4-d^2\,s^2)$, has been taken equal to the exchange integral $G_2(d^3\,s)$ and designated G_2; the two interaction integrals $H_2(d^4-d^3\,s)$ and $H_2(d^3\,s-d^2\,s^2)$ are taken equal and designated H_2.

The first of a pair of determinations grouped together omits the $L(L+1)$ correction, the second includes it. A correspondingly numbered section of the text specifies the observations included in making each pair of calculation.

Parameter	Calculation—							
	I		II		III		IV	
$A(d^3\,s)$	19505	19303	20272	20168	20188	20140	20446	20388
$A(d^2\,s^2)$	12843	12892	13744	13785	13614	13641	13636	13957
$A(d^4)$	26563	26095	26777	26498	26468	26341	26830	26356
B	461	424	483	462	474	464	479	447
C	1915	2088	1841	1945	1897	1947	1824	2012
G_2	2496	2476	2872	2863	2859	2856	2924	2918
ζ	1980	2008	1776	1800	1786	1798	1843	1874
H_2	497	502	538	541	538	539	521	544
α	—	−35	—	−19	—	−10	—	−35

The inclusion of the $L(L+1)$ correction produced a negligible improvement in the mean deviations, and the correction was negative ($\alpha=-35$), whereas all the evidence so far accumulated indicates that it should be positive. With the $L(L+1)$ correction the mean deviation for all levels was reduced to ±1,038, and the deviation, excluding the two badly fitting levels, was ±510.

(II) The levels at 18500 and 23295 were omitted from the least-squares calculation; the deviations for this calculation are given in calculation II of table 1. The mean deviation of this calculation is ±371: As this is considerably less than the value ±515 for calculation (I), described in the previous paragraph, it indicates that the parameters of the latter calculation were influenced by the inclusion of the two badly fitting levels. Comparison of the parameters themselves also indicates this. In this calculation there are three deviations (for the levels 16424, 14581, and 12831) that exceed twice the mean deviation of all levels fitted.

Again, when the $L(L+1)$ correction is included, the mean deviation is reduced only slightly (to the value ±364) and the correction is negative ($\alpha=-19$). Most of the improvement produced by including the $L(L+1)$ correction can be attributed to the slightly better agreement obtained for the badly fitting level 12831, which has its deviation reduced to 858; if the mean deviation is computed without this level the value ±371 would be replaced by ±341, and the value ±364 replaced by ±340. The inclusion of the $L(L+1)$ correction is therefore not justified.

As calculations III and IV indicate, the inclusion of three badly fitting levels has not had much effect on the agreement obtained for the other levels. Also, there seems to be no possibility of including

the $L(L+1)$ correction and getting an appreciable improvement. The best calculation that can be offered at this time is that in calculation II of table 1. Possibilities for improving this calculation will be given in the discussion.

(III) The levels 18500, 23295, and 12831 were omitted from the least-squares calculation. The mean deviation was ± 335, which is only a little less than the value ± 341 obtained in (II). Inclusion of the $L(L+1)$ correction produced negligible improvement, as the deviation was reduced only to ± 333; the correction was still negative ($\alpha = -10$). It would have been difficult to justify the omission of the level 12831 if this calculation had given much better agreement.

(IV) Eleven levels were omitted in this calculation. These omissions consist of the two pairs, 18500 and 22928, and 12435 and 14581, omitted partly because the calculated eigenvalues were close and it seemed possible, therefore, that the linear formulas might not apply; the two triplet groups 23295, 23620, and 24870, and 16424, 17168, and 18500, which were omitted because of uncertainties in the correspondence between theory and experiment; and the levels 23381 and 12831, omitted because they had rather large deviations that tended to be improved by a negative $L(L+1)$ correction. The mean deviation of this calculation was ± 170 (the mean deviation of the same terms in calculation (II) is ± 200). The only large deviation was -491 for the level 14628. With the $L(L+1)$ correction included, the mean deviation was reduced to ± 151, due mainly to a decrease in the deviation for the level 14628 to -306. Again the sign of the correction was negative ($\alpha = -35$).

8. Discussion

Results obtained in spectra with $3d$- and $4d$-electrons indicate that when the $L(L+1)$ correction is used the mean deviation between theory and experiment will generally be less than 200 K, and that the sign of the correction will be positive.[23] Calculation (II) of table 1 should therefore be improved because a better significant agreement between theory and experiment can probably be obtained.

It is fortunate that the experimental analysis of the Ta II spectrum will be extended by members of the NBS Spectroscopy Section. The calculation given is already accurate enough to furnish considerable help. This analysis may, in turn, help solve the problem of the two excess levels pointed out previously. In a preliminary survey, the switching of J-values has been ruled out, as none of the levels concerned are poorly identified. The identification of new levels will help to eliminate some of the arbitrariness involved in correlating the observed and calculated values. With more observations a calculation with extra adjustable parameters (suggested below) will also be better justified.

Eigenvalues and eigenvectors of the matrices set up with least-squares values of the parameters will be obtained on SEAC after the coding now underway is completed (see footnote 13). The g-values obtained should be much more accurate than those already calculated, and if this is so, the uncertainties in making correlations may be resolved. Knowledge of the exact eigenvalues will show whether or not any of the large errors of the calculation are due to limitations on the validity of linear formulas for the eigenvalues. The linear formulas obtained from these new solutions should be accurate enough so that eigenvalues can be redetermined from them for any additional small changes that are made in the parameters, without setting up new matrices.

The agreement between theory and experiment may also be improved by using more adjustable parameters; B, C, and ζ can be adjusted independently in all three configurations, thus increasing the number of adjustable parameters from 9 to 15. Theoretically, this should be done, as the effect of differences in these parameters is likely to have the same order of magnitude as the $L(L+1)$ correction.[24] The difficulty of carrying out least-squares calculations with this number of parameters is great, even with SEAC. Some coding improvements and more experience in the behavior of the codes with this type of problem are required.

[23] Racah (see footnote 7) reports a mean error of 411 without the $L(L+1)$ correction, and an error of 229 with the $L(L+1)$ correction in W I; as indicated in footnote 22, the sign of the $L(L+1)$ correction is positive. By coincidence, the mean error of calculation II, table 1 is 412 K, nearly identical with the corresponding W I value; however, no appreciable improvement was obtained by the use of the $L(L+1)$ correction. In Hf II, Gehatiah (see footnote 3) obtains a mean error of 257 without the use of this correction.

[24] See section 4.2 of the reference in footnote 2, or section 2 of the reference in footnote 7.

WASHINGTON, September 9, 1955.

Journal of Research of the National Bureau of Standards Vol. 55, No. 6, December 1955 Research Paper 2640

Reflection and Transmission of Gamma Radiation by Barriers: Monte Carlo Calculation by a Collision-Density Method[1,2]

Martin J. Berger

The collision density of photons in an infinite Compton-scattering medium was calculated by random sampling. The intensity, spectral composition, and angular distribution were then determined for radiation reflected and transmitted by plane-parallel barriers by carrying out appropriate integrations over the collision density, taking into account the absorbing properties of the medium and the effect of boundaries. All numerical work was done on the National Bureau of Standards automatic computer (SEAC). Sample results are presented for 0.66-Mev radiation incident on water barriers of various thicknesses.

1. Introduction

The Problem. The results of an investigation of the following boundary problem in gamma-ray diffusion are presented: A beam of monoenergetic gamma rays is incident at a given angle on a plane-parallel barrier that has a finite thickness in one dimension but is infinite in the other two dimensions. What are the intensities and spectral compositions of the reflected and transmitted beam?

Method of Solution. An analytical attack on this problem by the solution of the relevant transport equation leads to great mathematical difficulty. So far such an approach has been successfully carried out for homogenous infinitely extended media [1],[3] but boundary problems remain unsolved. In order to bypass these difficulties, explore the problem, and obtain at least an approximate solution, this investigation employed the Monte Carlo (random sampling) method. All numerical work was carried out on the automatic computer of the National Bureau of Standards (SEAC).

The calculation was divided, in regard to both method and execution, into two rather distinct parts: (1) a stochastic part, in which photon random walks are generated by random sampling in an infinite nonabsorbing scatterer, whereby a collision density is obtained, and (2) a calculation of the reflected and transmitted radiation obtained by summations over collision densities, taking into account boundary conditions and absorption characteristics of the barrier. There were a number of reasons for this division. For one thing, it reduced the required computer memory capacity. More importantly, the random walks have a "universal" character, i. e., they can be used for the calculation of different boundary problems involving different geometries as well as different scattering and absorbing media. Not only will the repeated use of the same set of random walks often lead to computing economy, but it may also increase the accuracy of a calculation. Suppose, for example, that we wish to determine the difference in transmission for two beams incident on a barrier at different angles but otherwise identical. It will then be to our advantage to base the comparison on the same set of random walks because irrelevant differences resulting from statistical fluctuations will thereby be largely eliminated.

2. Gamma-Ray Random Walks in an Infinite Compton Scatterer

2.1. Definitions

The state S of a photon can be specified by a set of six quantities:

$$S=(E,\theta,\varphi,x,y,z),$$

where E is the photon energy, θ and φ are angular coordinates describing the direction of motion (in a spherical coordinate system with the z-axis as polar axis), and x, y, and z are Cartesian coordinates of position. Let the state of the photon immediately after the nth scattering event occurring in a given random walk be denoted by $S_n(n=1,2,\cdots)$, and let S_0 denote the state in which it was introduced into the scattering medium. A random walk is then described by a sequence

$$S_0,\ S_1,\ S_2,\ \cdots,\ S_L,$$

each term (except S_0) depending stochastically on its immediate predecessor only (Markov process). The length, L, of such a sequence would be infinite, but in the present work the random walks are terminated when the energy, E, drops below 30 kev. This arbitrary cutoff[4] results in an average value $\langle L\rangle=18$ for an initial energy $E_0=660$ kev. A

[1] This work was supported by the Office of Naval Research and the Atomic Energy Commission Reactor Division.

[2] Some of the results of this paper were presented at a symposium on Monte Carlo methods at the University of Florida in March 1954.

[3] Figures in brackets indicate the literature references at the end of this paper.

[4] The cutoff is justified on physical grounds because radiation at energies below 30 kev is always so heavily absorbed that it makes only a negligible contribution to the emergent radiation flux.

set of random walks constitutes a Monte Carlo estimate of the collision density resulting from the diffusion of radiation in an infinite homogenous Compton scatterer.

It will be observed that for the problem of transmission and reflection by plane-parallel barriers, only the variables E, θ and one space variable, say z, are required. Nevertheless, it is worthwhile to calculate the other three variables also. The random walks are thus made applicable to other boundary problems with different geometrical conditions. Moreover, we can use the same set of random walks for barrier problems with different angles of incidence. We always set $\theta_0=0$ and rotate the boundaries as required by using, instead of cos θ and z,

$$\cos\theta' = \cos\theta\cos\alpha + \sin\theta\sin\alpha\cos\varphi$$

$$z' = x\sin\alpha + z\cos\alpha,$$

where $\alpha=\theta_0'$ is the angle of incidence.

2.2. Random Sampling

Next the sampling scheme is described, by which successive states S_n are selected, the initial state being specified as $S_0=(E_0,0,0,0,0,0)$. Calculations of a set of random walks with this initial condition will serve for the solution of problems involving monoenergetic beams of energy E_0 and arbitrary direction of incidence α. Because of the linearity of the gamma-ray diffusion equation, it is possible to obtain solutions for incident beams of specified energetic and angular composition by superposition of the results obtained with different E_0's and α's.

Prior to the discussion of the detailed steps in the sampling process, some comment is in order concerning the required random numbers. With a high-speed computer the use of tables of random numbers is clearly impractical. Instead, so-called pseudo-random numbers $r_m (0\le r_m\le 1)$ were used, and which were generated as required in the course of the computation by a method developed by O. Taussky-Todd [2]. They are defined by the relations

$$r_m = 2^{-42} R_m \tag{2}$$

$$R_{m+1} = 5^{17} R_m \text{ modulo } 2^{42}, \qquad R_0 = 1.$$

It may be shown that the period of r_m is 2^{40}, i. e., that a sequence of 2^{40} different numbers will be obtained before repetition occurs. Extensive testing carried out at the National Bureau of Standards has shown that these pseudorandom numbers satisfy the various accepted statistical criteria of randomness. It is an advantageous feature of this method that identical random walks may be recreated repeatedly for checking purposes, provided the initial random number used for the walk is recorded.

The various steps in the calculation of S_{n+1}, given S_n, follow.

a. Energy Change

The energy E_{n+1} after a scattering is determined by

$$\left[\int_{E_{n+1}}^{E_n} k(E_n,E)dE \Big/ \int_0^{E_n} k(E_n,E)dE\right] = r, \tag{3}$$

where r is a random number, and $k(E_n,E)$ is the Klein-Nishina differential coefficient (per unit path length) for Compton scattering with energy change from E_n to E.

It was found convenient to carry out the random sampling for the wavelength $\lambda=mc^2/E$, where mc^2 is the electron rest mass, rather than for the energy directly. If we make this change of variable, substitute the explicit formula for the Klein-Nishina differential coefficient, and carry out the indicated integrations, eq (3) is transformed into

$$\left\{[1-2\lambda_n(\lambda_n+1)]\log\frac{\lambda_{n+1}}{\lambda_n} + \lambda_n(\lambda_n+2)\frac{\lambda_{n+1}-\lambda_n}{\lambda_{n+1}} + \lambda_n(\lambda_{n+1}-\lambda_n) + \frac{\lambda_{n+1}^2-\lambda_n^2}{2\lambda_{n+1}^2}\right\} \Big/ \left\{[1-2\lambda_n(\lambda_n+1)]\log\frac{\lambda_n+2}{\lambda_n} + 2\frac{1+\lambda_n}{(2+\lambda_n)^2}\right\}^{-1} = r. \tag{4}$$

To use this equation to find λ_{n+1}, given λ_n and r, would be intolerably cumbersome, even when an automatic computer is used. Latter and Kahn [3] evaluated eq (4) numerically and presented a table of $\lambda_{n+1}=\lambda_{n+1}(\lambda_n,r)$ for a grid of values in the range $0\le r\le 1$, $0.05\le\lambda_n\le 10$. The tabulation has been extended to $\lambda_n=16$ and used to obtain a polynomial representation

$$\lambda_{n+1} = \sum_{i=0}^{I}\sum_{j=0}^{J} A_{ij}(\lambda_n)^i r^j. \tag{5}$$

This required extensive bivariate interpolation, which was carried out by a convenient matrix technique. This technique is described in the appendix because it does not appear in the standard literature on numerical analysis.

The following coefficient-matrices, A_{ij}, were found to give representations of λ_{i+1} accurate to 1 percent:

$0.05\le\lambda_n<0.5$

i \ j	0	1	2	3	4	5
0	0	0.1180	−0.9844	4.683	−6.896	5.079
1	1.0	.07930	20.57	−69.56	117.2	−68.29
2	0	2.124	−63.66	209.7	−342.3	194.1
3	0	−3.418	70.31	−227.8	359.2	−198.3

$0.5\le\lambda_n<10.0$

i \ j	0	1	2	3	4	5
0	0	0.04100	2.851	−8.346	13.37	−5.916
1	1.0	.4779	−1.502	4.863	−5.168	1.330
2	0	−.05409	0.07590	−0.1713	−0.02945	0.1789
3	0	.002153	.0008490	−.0077	.02359	−.01891

$10 \leq \lambda_n \leq 16$				
i	j			
	0	1	2	3
0	0	27.4295	−96.6375	71.2080
1	1.0	−6.173625	23.35	−17.17
2	0	0.4584375	−1.763	1.304
3	0	−.01106	0.04342	0.03233

b. Change of Direction

Deflection and wavelength shift are related by the Compton equation

$$\cos \omega_n = 1 - \lambda_{n+1} + \lambda_n, \tag{6}$$

where ω_n is the angle between the directions of motion immediately before and after the $n+1$st scattering.

The direction of the scattered photon depends on ω_n and on an azimuth angle χ_n, which is a random quantity distributed uniformly between 0 and 2π. We need the sine and cosine of χ_n rather than χ_n itself. Hence we take advantage of the following convenient computational scheme suggested by Von Neumann [4]. Choose random numbers a and b satisfying the condition $a^2+b^2 \leq 1$, and let c be a random number that is equal to ± 1 with probability 1/2. Then

$$\cos \chi_n = \frac{2abc}{a^2+b^2} \text{ and } \sin \chi_n = \frac{a^2-b^2}{a^2+b^2}. \tag{7}$$

From the deflections ω_n and χ_n, the new angular coordinates are then determined by the following trigonometric relationships:

$$\left.\begin{aligned} \cos \theta_{n+1} &= \cos \theta_n \cos \omega_n + \sin \theta_n \sin \omega_n \cos \chi_n \\ \sin (\phi_{n+1} - \phi_n) &= \frac{\sin \chi_n \sin \omega_n}{\sin \theta_{n+1}} \\ \cos (\phi_{n+1} - \phi_n) &= \frac{\cos \omega_n - \cos \theta_n \cos \theta_{n+1}}{\sin \theta_n \sin \theta_{n+1}}. \end{aligned}\right\} \tag{8}$$

c. Displacement

The position of the $(n+1)$st scattering is defined by

$$\left.\begin{aligned} x_{n+1} &= x_n - \frac{\sin \theta_n \cos \varphi_n}{\mu_s(E_n)} \log r \\ y_{n+1} &= y_n - \frac{\sin \theta_n \sin \varphi_n}{\mu_s(E_n)} \log r \\ z_{n+1} &= z_n - \frac{\cos \theta_n}{\mu_s(E_n)} \log r \end{aligned}\right\}, \tag{9}$$

where r is a random number, and

$$\mu_s(E_n) = \int_0^{E_n} k(E_n, E) dE.$$

3. The Transmission-Reflection Boundary Problem

3.1. Summation Over the Collision Density [5]

The information obtained by sampling J photon random walks is contained in the set of state vectors $S_n(j)(n=0,1,\cdots L_j; j=1,2,\cdots J)$, which describe the state of the jth photon immediately after its nth scattering. We consider these vectors to form a set of representative points (a sample collision density) in a six-dimensional collision-density space. The solution of boundary problems can be obtained by performing appropriate sums over the collision density.

In the reflection-transmission problem, one considers a plane-parallel barrier between the planes $z=0$ and $z=t$. A beam of photons is assumed to be incident on the face $z=0$.

Reflected and transmitted radiation will be classified according to energy and direction.[6] Let R_{ik} denote the average number of photons per incident photon that are reflected from the face $z=0$ with energies in the ith interval and directions in the kth interval. Similarly, let T_{ik} denote the average number of photons transmitted through the face $z=t$. R_{ik} and T_{ik} are obtained by summations over the sample collision density as follows:

$$R_{ik} = \frac{1}{J} \sum_{j=1}^{J} \sum_{n=0}^{L_j} B_n(j) P_n(j) Q_n(j,0) f_n^{ik}(j). \tag{10}$$

The factors in this formula have the following meaning:

(a) The factor $B_n(j)$ takes into account the boundary conditions. It is equal to unity when the inequalities $0 \leq z_m(j) \leq t$ are satisfied for $m=0,1,\cdots n$, and zero otherwise. In other words, a contribution to the reflected radiation is obtained only if the photon in the state under consideration has not previously gone out of the barrier.

(b) The factor

$$P_n(j) = \prod_{m=0}^{n-1} \exp \left\{ - \frac{\sec \theta_m(j)}{\mu_A[E_m(j)]} [z_{m+1}(j) - z_m(j)] \right\} \tag{11}$$

is the probability that the photon has not been absorbed in the jth history prior to reaching state $S_n(j)$. (μ_A is the absorption coefficient.)

(c) The quantity $Q_n(j,z')$ denotes the probability that a photon starting from state $S_n(j)$ will cross the plane $z=z'$ without further scattering or absorption. It is defined as follows:

$Q_n(j,z')$ vanishes except when $\sec \theta_n(j)[z'-z_n(j)] \geq 0$, in which case

$$Q_n(j,z') \exp \left\{ - \frac{\sec \theta_n(j)}{\mu[E_n(j)]} [z'-z_n(j)] \right\} \tag{12}$$

[5] The method described in this section is closely related to suggestions by H. Kahn, [3].

[6] 32 energy intervals and 10 angular intervals have been used.

$\mu = \mu_A + \mu_s$ is the total linear attenuation coefficient).

(d) $f_n^{ik}(j)$ is the energy-angle classification factor. It is equal to unity when $E_n(j)$ is in the ith energy interval and $\theta_n(j)$ in the kth angular interval, and zero otherwise.

Transmitted radiation T_{ik} is calculated by a formula similar to eq (10) but with $Q_n(j,0)$ replaced by $Q_n(j,t)$.

We shall use the collision density also for the evaluation of the flux in an infinite medium in which a plane source is embedded in the plane $z=0$. By comparing the results for this problem with those for the barrier, the nature of the boundary effect can be established. Moreover, the Monte Carlo results for the infinite medium can be checked against those obtained by systematic moment-method calculations. Such a comparison is of use in establishing the validity and accuracy of the random-sampling approach. Let $B_{ik}(z')$ denote the average number of photons crossing the plane $z=z'$ from both directions (our main interest will be in the planes that form the barrier boundaries: $z'=0$ and $z'=t$). The necessary summation over the collision density is similar to formula (10), except that the boundary factor $B_n(j)$ is omitted.

When the sampled collision density is used for the simultaneous determination of R_{ik}, T_{ik}, $B_{ik}(0)$, and $B_{ik}(t)$, all states $S_n(j)$ make a contribution to the final score except those for which $z_n(j)<0$ and $\cos\theta_n(j)<0$, or $z_n(j)>t$ and $\cos\theta_n(j)>0$. This is in contrast to a direct stochastic analogue method, which would allow only those sections of the random walks containing an actual crossing of the boundaries to contribute to the score. The more elaborate scoring procedure gives proper credit for "near misses," i. e., collisions taking place close to a boundary, for which the factor $Q_n(j,z')$ is very close to unity.

3.2. Fluxes and Buildup Factors

The SEAC calculation is designed to yield the quantities R_{ik}, T_{ik}, and B_{ik}, which represent the average number of photons crossing the planes $z=0$ and $z=t$ per unit area (the number flux). Radiation detectors often do not measure the number flux directly, so that it is desirable to calculate various related types of flux. These can all be obtained from the number flux through multiplication by suitable weight factors, depending on the energy and direction of the photons. For example, multiplication of the number flux by the average energy, $\langle E_i\rangle$, yields the energy flux, division by the average value, absolute value $|\langle\cos\theta_k\rangle|$, yields fluxes through a unit area whose normal is in the direction of motion of the radiation. This is the flux that a nondirectional detector would measure. Some inaccuracy is introduced into these flux-conversions because the averages $\langle E_i\rangle$ and $\langle\cos\theta_k\rangle$ are to some extent arbitrary. Arithmetic means have been used.

According to the usage common in shielding calculations the results for the total flux (integrated over-all directions and spectral energies) are presented in the form of buildup factors, defined as the ratio of the total to the unscattered flux [5]. For the various types of flux described above, the buildup factors for an infinite homogenous medium have the following form:

Number buildup factors

$$B_N = \sum_{ik} B_{ik} / \exp(-\mu_0 z/\cos\alpha)$$

$$B'_N = \sum_{ik} \frac{B_{ik}}{|\langle\cos\theta_k\rangle|} \Big/ \frac{\exp(-\mu_0 z/\cos\alpha)}{\cos\alpha} \qquad (13)$$

Energy buildup factors

$$B_E = (\sum_{ik} \langle E_i\rangle B_{ik}/E_0 \exp(-\mu_0 z/\cos\alpha)$$

$$B'_E = \sum_{ik} \langle E_i\rangle \frac{B_{ik}}{|\langle\cos\theta_k\rangle|} \Big/ \frac{E_0}{\cos\alpha} \exp(-\mu_0 z/\cos\alpha), \quad (14)$$

where μ_0 is the total attenuation coefficient of the source radiation, and z is the distance between the source plane and the plane of observation. In order to obtain the corresponding buildup factors T_N, T'_N, T_E, and T'_E, one replaces B_{ik} in eq (13) and (14) by T_{ik}, and z by the barrier thickness, t. The reflection buildup factors R_N, R'_N, R_E, and R'_E are obtained by using R_{ik} and setting $z=0$.

4. Results[7]

4.1. Energy Spectra

In figures 1, a, b, c, and d, energy spectra are shown in histogram form for the number flux of photons reflected and transmitted by barriers, reflected by a semi-infinite medium, and for the flux in an infinite medium through planes that correspond to the barrier boundary planes. The histograms pertain to scattered radiation only.[8] Spectra are shown for normal incidences ($\alpha=0°$) and for oblique incidence ($\alpha=60°$). The oblique barrier thickness is the same for both cases: $(\mu_0 t/\cos\alpha)=2$. The shaded areas between the "finite slab" and the "infinite medium" histograms are a measure of the boundary effect. It can be seen that the boundaries greatly reduce the amount of soft radiation below 200 kev. The reason for this is that in an infinite medium soft radiation is mainly due to photons that have overshot the boundary plane and have been turned around in a collision in the close vicinity of the boundary, making their second passage through the boundary with resultant low energy.

[7] Based on the analysis of 400 random walks for each problem.

[8] To obtain the scattered flux only, one must begin the sum in eq (10) with $n=1$.

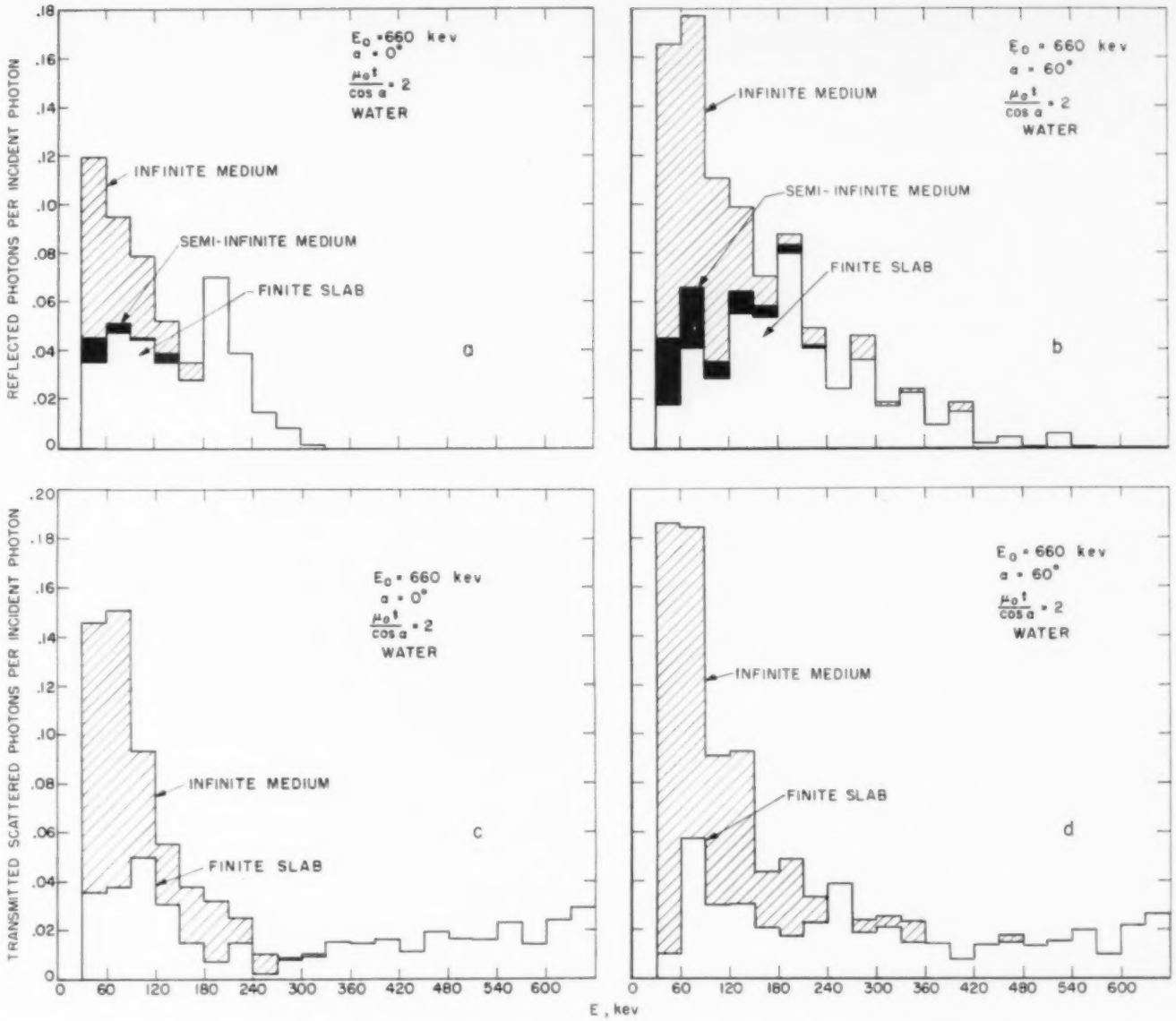

FIGURE 1. *Energy spectra of photons reflected and transmitted by water barriers and of photons in an infinite homogenous medium crossing planes corresponding to the barrier boundaries.*

The spectra pertain to a monodirectional beam of 0.66-Mev photons incident on the barrier (or released within a semi-infinite medium) with obliquity α. a, Reflection; obliquity $\alpha=0°$ (normal incidence); b, Reflection; obliquity $\alpha=60°$; c, Transmission; obliquity $\alpha=0°$ (normal incidence); d, Transmission; obliquity $\alpha=60°$.

4.2. Angular Distributions

Figure 2, a, shows the angular distribution of the reflected number flux from a barrier with oblique thickness $\mu_0 t=1$, and from a semi-infinite medium for obliquity angles of incidence $\alpha=0°$ and $\alpha=60°$. Figure 2, b, shows the angular spectra of transmitted scattered photons for normal incidence and barrier thickness $\mu_0 t=1$ and $\mu_0 t=4$.

4.3. Buildup Factors

The various buildup factors for transmission, reflection, and an infinite medium (as defined in section 3.1 and 3.2) are listed in table 1 for the number flux, and in table 2 for the energy flux for 0.66-Mev radiation in water. Estimated standard deviations are indicated, which were obtained by dividing the 400 photon histories into groups of 50 each and computing the dispersion of the buildup factors obtained for the various groups.

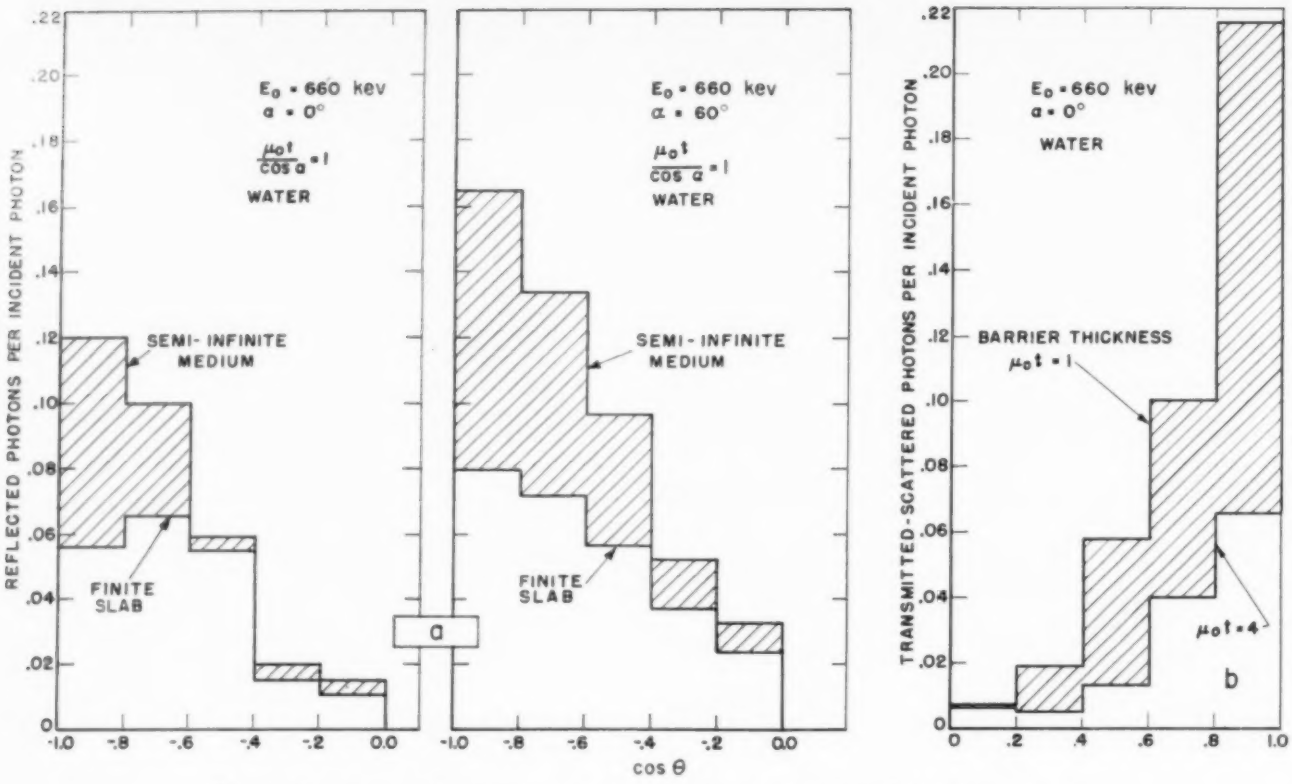

FIGURE 2. *Angular distributions of photons reflected and transmitted by water barriers.*

The distributions pertain to a monodirectional beam of 0.66-Mev photons incident on the barrier with obliquity α.
a, Reflection; obliquities $\alpha = 0°$ and 60°; b, Transmission; obliquity $\alpha = 0°$ (normal incidence).

TABLE 1. *Number buildup factors for 0.66-Mev radiation in water*

α	$\frac{\mu d}{\cos \alpha}$	P_N	P'_N	T_N	T'_N	B_N	B'_N
°							
0	0	.....	.....	.....	.....	1.61 ±0.09	2.30 ±0.16
0	1	1.18 ±0.03	1.36 ±0.05	2.09 ±0.16	2.73 ±0.18	3.69 ±0.26	6.24 ±0.35
0	2	1.29 ±0.03	1.55 ±0.06	3.94 ±0.45	6.02 ±0.55	7.11 ±0.64	12.3 ±1.3
0	4	1.31 ±0.05	1.59 ±0.07	8.21 ±1.75	13.5 ±2.2	13.3 ±2.8	24.3 ±4.2
0	∞	1.31 ±0.05	1.61 ±0.07	.....	.....	.....	.....
60	0	.....	.....	.....	.....	1.85 ±0.11	1.97 ±0.13
60	1	1.27 ±0.05	1.30 ±0.06	2.00 ±0.13	2.17 ±0.13	4.13 ±0.25	4.41 ±0.28
60	2	1.41 ±0.06	1.48 ±0.07	4.13 ±0.46	3.90 ±0.50	8.89 ±0.95	8.21 ±0.98
60	4	1.47 ±0.06	1.53 ±0.07	15.4 ±2.0	14.2 ±2.5	29.3 ±4.9	30.2 ±5.3
60	∞	1.48 ±0.06	1.53 ±0.07	.....	.....	.....	.....

TABLE 2. *Energy buildup factors for 0.66-Mev radiation in water*

α	$\frac{\mu d}{\cos \alpha}$	P_E	P'_E	T_E	T'_E	B_E	B'_E
°							
0	0	.....	.....	.....	.....	1.10 ±0.02	1.23 ±0.04
0	1	1.05 ±0.01	1.10 ±0.02	1.62 ±0.06	1.89 ±0.09	1.87 ±0.07	2.48 ±0.10
0	2	1.07 ±0.02	1.14 ±0.03	2.50 ±0.20	3.21 ±0.30	2.97 ±0.22	4.07 ±0.31
0	4	1.07 ±0.02	1.15 ±0.03	3.62 ±0.39	5.64 ±0.65	4.33 ±0.39	6.98 ±0.72
0	∞	1.07 ±0.02	1.15 ±0.03	.....	.....	.....	.....
60	0	.....	.....	.....	.....	1.19 ±0.03	1.23 ±0.04
60	1	1.10 ±0.03	1.11 ±0.05	1.57 ±0.07	1.65 ±0.09	1.98 ±0.09	2.15 ±0.10
60	2	1.13 ±0.03	1.17 ±0.05	2.43 ±0.22	2.37 ±0.20	3.24 ±0.25	3.48 ±0.29
60	4	1.14 ±0.03	1.18 ±0.05	5.92 ±0.68	5.40 ±0.73	7.61 ±0.91	6.21 ±1.05
60	∞	1.14 ±0.03	1.18 ±0.05	.....	.....	.....	.....

5. Discussion

The results presented have a preliminary character. Greater sample sizes are desirable, as well as the extension of the calculation to other energies and media. Moreover, the scoring method used is not expected to be very successful for penetrations of depth $\mu_0 t > 4$ because excessively large sample sizes would be required. Prior to extending the calculations by the collision-density method, other Monte Carlo approaches have been explored, including a semianalytic method designed for dealing with deep as well as shallow penetrations [6]. Table 3 gives a comparison of the buildup factors obtained in this investigation (a) with those found by the semianalytical Monte Carlo method, (b) with the Monte Carlo results of a group at the Naval Research Laboratory [7], and (c), for an infinite medium, with calculations carried out according to the moment method of Spencer and Fano [1, 8]. The agreement is generally good, indicating that the shallow penetration of gamma radiation, in the presence of boundaries, can be calculated accurately by the Monte Carlo method. The results for R_N and R_E at 0.66 Mev are consistent with the results of a Monte Carlo calculation at 1 Mev by Hayward and Hubbell [9].

TABLE 3. *Comparison of buildup factors obtained in various calculations for 0.66-Mev radiation in water*

Column 1, this paper; 2, semianalytic Monte Carlo method [6]; 3, Monte Carlo, NRL [7]; 4, Spencer-Fano moment method [8].

	α	$\frac{\mu_0 t}{\cos\alpha}$	Method 1	2	3	4
B'_N	0°	∞	1.53	.....	1.59	.....
T'_N		1	2.73	.....	2.74	.....
		2	6.02	.....	6.60	.....
		4	13.5	.....	13.0	.....
B'_N		1	6.24	.....	6.0	.....
		2	12.3	.....	12.3	.....
		4	24.3	.....	25.0	.....
B'_E		∞	1.15	1.15	1.14	.....
T'_E		1	1.89	1.96	1.92	.....
		2	3.21	3.06	3.30	.....
		4	5.64	5.99	5.55	.....
B'_E		0	1.23	.....	.....	1.30
		1	2.48	2.44	2.43	2.43
		2	4.07	4.02	3.75	3.89
		4	6.98	7.15	6.55	7.37
B'_E	60°	0	1.23	.....	.....	1.27
		1	2.15	.....	.....	2.05
		2	3.48	.....	.....	3.28
		4	6.21	.....	.....	7.82

6. References

[1] L. V. Spencer and U. Fano, J. Research, NBS **46,** 446 (1951) RP2213.
[2] H. A. Meyer, L. S. Gephart, and N. L. Rasmussen, On the generation and testing of random digits, WADC Technical Report 54–55 (1954).
[3] R. Latter and H. Kahn, Rand Report R–170 (1949).
[4] Monte Carlo Methods, NBS Applied Math. Series (1951) AMS12.
[5] H. Goldstein and J. E. Wilkins, Jr., AEC Report NYO–3075, (June 1954).
[6] M. J. Berger and J. Doggett, J. Research NBS (publication pending).
[7] L. A. Beach, R. B. Theus, J. D. Plawchan, and W. R. Faust, NRL Report 4412 (1954).
[8] M. J. Berger, J. Research NBS (publication pending).
[9] E. Hayward and J. Hubbell, Phys. Rev. **93,** 955 (1954).
[10] A. C. Aitken, Determinants and matrices, p. 118, (Interscience Publishers, Inc., New York, N. Y., 1951).

7. Appendix. A Method of Bivariate Interpolation

Suppose we know a bivariate function $f(p,q)$ at $(M+1)(N+1)$ gridpoints (p_s,q_t) $(s=0,1, \cdots, M;$ $t=0,1, \ldots, N)$. The problem is to use this knowledge for determining the expansion coefficients in a polynomial expansion

$$f(p, q)=\sum_{i=0}^{M}\sum_{j=0}^{N} A_{ij}p^i q^j. \tag{17}$$

Let $F=f(p_s,q_t)$ be the known matrix of functional values, and $A=(A_{ij})$ the desired coefficient matrix. From the variables p and q we form the matrices $P=(p_s)^i$ and $Q=(q_t)^i$. In matrix form, eq (17) becomes

$$F=PAQ', \tag{18}$$

where Q′ is the transpose of Q. Hence

$$A=P^{-1}F(Q^{-1})'. \tag{19}$$

P and Q are so-called alternant matrices whose inverse is well known [10]. The prescription for obtaining the inverse is simplest to describe by means of an example. When P has rank 3

$$\begin{pmatrix} 1 & p_0 & p_0^2 \\ 1 & p_1 & p_1^2 \\ 1 & p_2 & p_2^2 \end{pmatrix}^{-1} = \begin{pmatrix} \frac{p_1p_2}{(p_0-p_1)(p_0-p_2)} & \frac{p_0p_2}{(p_1-p_0)(p_1-p_2)} & \frac{p_0p_1}{(p_2-p_0)(p_2-p_1)} \\ \frac{-(p_1+p_2)}{(p_0-p_1)(p_0-p_2)} & \frac{(p_0+p_2)}{(p_1-p_0)(p_1-p_2)} & \frac{-(p_0+p_1)}{(p_2-p_0)(p_2-p_1)} \\ \frac{1}{(p_0-p_1)(p_0-p_2)} & \frac{1}{(p_1-p_0)(p_1-p_2)} & \frac{1}{(p_2-p_0)(p_2-p_1)} \end{pmatrix}. \tag{20}$$

The numerators of of the elements in the respective columns are elementary symmetric functions in the arguments p_0, p_1, and p_2, with one argument omitted each time. The arrangement of the denominators is obvious.

When the grid points are equidistant, one can, without loss of generality, set $p_s=s$. The inverses P^{-1} for this case are listed below for the first few alternant matrices:

$$\begin{pmatrix} 1 & 0 \\ -1 & 1 \end{pmatrix} \qquad \frac{1}{2}\begin{pmatrix} 2 & 0 & 0 \\ -3 & 4 & 1 \\ 1 & -2 & 1 \end{pmatrix} \qquad \frac{1}{6}\begin{pmatrix} 6 & 0 & 0 & 0 \\ -11 & 18 & -9 & 2 \\ 6 & -15 & 12 & -3 \\ -1 & 3 & -3 & 1 \end{pmatrix} \qquad \frac{1}{24}\begin{pmatrix} 24 & 0 & 0 & 0 & 0 \\ -50 & 96 & -72 & 32 & -6 \\ 35 & -104 & 114 & -56 & 11 \\ -10 & 36 & -48 & 28 & -6 \\ 1 & -4 & 6 & -4 & 1 \end{pmatrix}$$

$$\frac{1}{120}\begin{pmatrix} 120 & 0 & 0 & 0 & 0 & 0 \\ -274 & 600 & -600 & 400 & -150 & 24 \\ 225 & -770 & 1070 & -780 & 305 & -50 \\ -85 & 355 & -590 & 490 & -205 & 35 \\ 15 & -70 & 130 & -120 & 55 & -10 \\ 1 & 5 & -10 & 10 & -5 & 1 \end{pmatrix}$$

The sum of the elements in the first row of each inverse matrix is 1, and the sum of the elements in each other row is zero. This is also true for the case of nonequidistant grid points, and provides a useful arithmetical check.

The author thanks Frank Stockmal for his help in coding the problem for SEAC, and Mary Orr and John Doggett for their assistance with the hand computations.

WASHINGTON, May 10, 1955.

INDEX TO VOLUME 55

July to December 1955—Research Papers 2599 to 2640

A

Page

Absolute calibration of National Bureau of Standards photoneutron standard: I, in water bath: II, in manganese sulfate bath:
RP2605 ... 63
RP2635 ... 311
Adsorption of nitrogen on carbon adsorbents at low pressures between 69° and 90° K, RP2600 ... 11
Alkali metals, thermodynamic properties of, RP2608 ... 83
Alloys, cobalt-iron-chromium, thermal expansion and phase transformations, RP2602 ... 29
Anthophyllite, fluoro, synthesis, RP2622 ... 215
Arc and spark spectra of ruthenium, RP2609 ... 97
Armstrong, G. T., F. G. Brickwedde, R. G. Scott, Vapor pressures of the methanes, RP2603 ... 39
—, *J. M. Goldstein, D. E. Roberts,* Liquid-vapor phase equilibrium in solutions of oxygen and nitrogen at pressures below one atmosphere, RP2629 ... 265
Atomic energy levels, computation: Spectrum of singly-ionized tantalum, RP2639 ... 335
Atomic form factor, data on: Computation and survey, RP2604 ... 53
Atomic negative-ion-photodetachment cross-section and affinity measurements, RP2615 ... 165
Austenite to martensite transformation in SAE 1050 steel, RP2616 ... 177

B

Barium, first spectrum, RP2633 ... 299
Bates, R. G., V. E. Bower, pH values of the Clark and Lubs buffer solutions at 25° C, RP2619 ... 197
Berger, M. J., Reflection and transmission of gamma radiation by barriers: Monte Carlo calculation by a collision-density method, RP2640 ... 343
Black, M. H., J. M. Florence, F. W. Glaze, Infrared transmittance of some calcium aluminate and germinate glasses, RP2625 ... 231
Blaine, L. R., E. K. Plyler, E. D. Tidwell, Infrared absorption and emission spectra of carbon monoxide in the region from 4 to 6 microns, RP2617 ... 183
—, —, —, Precise measurement of wavelengths in infrared spectra, RP2630 ... 279
Bower, V. E., R. G. Bates, pH values of the Clark and Lubs buffer solutions at 25° C, RP2619 ... 197
Bradley, J. C., L. Haar, A. S. Friedman, Ideal gas thermodynamic functions of the isotopic hydrogen sulfides, RP2631 ... 285
Bradt, P., F. L. Mohler, Mass spectra of thermal degradation products of polymers, RP2637 ... 323
Branscomb, L. M., S. J. Smith, Atomic negative-ion-photodetachment cross-section and affinity measurements, RP2615 ... 165
Brauer, G. M., H. I. Copeland, Jr., W. T. Sweeney, A. F. Forziati, Setting reaction of zinc oxide and eugenol, RP2611 ... 133
Brickwedde, F. G., G. T. Armstrong, R. B. Scott, Vapor pressures of the methanes, RP2603 ... 39
Bromine, thermodynamic properties of, RP2614 ... 147
Buffer solutions, pH control, RP2619 ... 197
Bunsen-type calorimeter, a new, RP2636 ... 317
Butadiene-styrene copolymers, heat capacity of, RP2610 ... 127

C

Cahill, W. F., R. E. Trees, P. Rabinowitz, Computation of atomic energy levels. The spectrum of singly-ionized tantalum, RP2639 ... 335
Calcium aluminate and germinate glasses, infrared transmittance of, RP2625 ... 231
Calorimeter, a new Bunsen-type, RP2636 ... 317
Carbon monoxide, infrared absorption and emission spectra, RP2617 ... 183
Carbon, oxygen, iron, arsenic, and mercury, computation of form factors, RP2604 ... 53
Carpenter, F. G., J. Lopez-Gonzalez, V. R. Deitz, Adsorption of nitrogen on carbon adsorbents at low pressures between 69° and 90° K, RP2600 ... 11
Ceramics, piezoelectric, properties of, RP2626 ... 239
Cesium, thermodynamic properties of, RP2608 ... 83
Chin, J., J. De Juren, Absolute calibration of the National Bureau of Standards photoneutron standard: II. Absorption in manganese sulfate, RP2635 ... 311
Chlorine, thermodynamic properties of, RP2614 ... 147
Chrysotile, fluoro, synthesis, RP2622 ... 215
Clabaugh, W. S., R. T. Leslie, R. Gilchrist, Preparation of titanium tetrachloride of high purity, RP2628 ... 261
Clark and Lubs buffer solutions, pH values of, RP2619 ... 197
Cobalt-iron-chromium alloys, thermal expansion and phase transformations, RP2602 ... 29
Collagen and leather, specific heats of, RP2618 ... 191
Computation of atomic energy levels. The spectrum of singly-ionized tantalum, RP2639 ... 335
Copeland, H. I., Jr., G. M. Brauer, W. T. Sweeney, A. F. Forziati, Setting reaction of zinc oxide and eugenol, RP2611 ... 133
Copolymers, butadiene-styrene, heat capacity of, RP2610 ... 127
Compressibilities of long-chain normal hydrocarbons, RP2634 ... 307
Coughanour, L. W., R. S. Roth, Phase equilibrium relations in the systems titania-niobia and zirconia-niobia, RP2621 ... 209
Cryostat, low-temperature adsorption of nitrogen, RP2600 ... 11
Curtiss, L. F., J. A. De Juren, D. W. Padgett, Absolute calibration of the National Bureau of Standards photoneutron standard: I., RP2605 ... 63

D

Page

Davis, R., C. I. Pope, Development of a photoresist for etching designs in glass, RP2612 ... 139
Decaborane, heat capacity, heats of fusion and vaporization, and vapor pressure of, RP2627 ... 255
n-Decylbenzene, heat of combustion of, RP2638 ... 329
n-Decylcyclohexane, heat of combustion of, RP2638 ... 329
n-Decylcyclopentane, heat of combustion of, RP2638 ... 329
Degradation, thermal, of polychlorotrifluoroethylene, poly-α, β, β-trifluorostyrene, and poly-*p*-xylene in a vacuum, RP2624 ... 223
Deitz, V. R., J. Lopez-Gonzalez, F. G. Carpenter, Adsorption of nitrogen on carbon adsorbents at low pressures between 69° and 90° K, RP2600 ... 11
De Juren, J., J. Chin, Absolute calibration of the National Bureau of Standards photoneutron standard: II. Absorption in manganese sulfate, RP2635 ... 311
—, *D. W. Padgett, L. F. Curtiss,* Absolute calibration of the National Bureau of Standards photoneutron standard: I., RP2605 ... 63
N-Dimethylaminodiborane, heat capacity; heats of fusion, vaporization, and transition of, RP2620 ... 201
Diphenyl ether calorimeter, RP2636 ... 317

E

Electric hygrometer, fast responding, RP2606 ... 71
Electron affinity measurements, atomic negative-ion-photodetachment, RP2615 ... 165
Eugenol and zinc oxide, setting reaction of, RP2611 ... 133
Evans, W. H., R. Jacobson, T. R. Munson, D. D. Wagman, Thermodynamic properties of the alkali metals, RP2608 ... 83
—, *T. R. Munson, D. D. Wagman,* Thermodynamic properties of some gaseous halogen compounds, RP2614 ... 147
Expansion, thermal, cobalt-iron-chromium alloys, RP2602 ... 29

F

Fibers, properties and behavior of, when impacted at high velocities, RP2601 ... 19
Field distortion in free-air ionization chambers, measurement, RP2632 ... 291
Florence, J. M., F. W. Glaze, M. H. Black, Infrared transmittance of some calcium aluminate and germanate glasses, RP2625 ... 231
Fluorine, thermodynamic properties of, RP2614 ... 147
Fluoro talc, chrysotile, and anthophyllite, synthesis, RP2622 ... 215
Form factor, atomic, computation and survey, RP2604 ... 53
Forziati, A. F., H. I. Copeland, Jr., G. M. Brauer, W. T. Sweeney, Setting reaction of zinc oxide and eugenol, RP2611 ... 133
Fraser, F. M., E. J. Prosen, Heats of combustion of liquid *n*-hexadecane, 1-hexadecene, *n*-decylbenzene, *n*-decylcyclohexane, *n*-decylcyclopentane, and the variation heat of combustion with chain length, RP2638 ... 329
Friedman, A. S., L. Haar, J. C. Bradley, Ideal gas thermodynamic functions of the isotopic hydrogen sulfides, RP2631 ... 285
Furukawa, G. T., R. E. McCoskey, M. L. Reilly, A. W. Harman, Heat capacity; heats of fusion, vaporization, and transition; and vapor pressure of *N*-dimethylaminodiborane, $(CH_3)_2NB_2H_5$, RP2620 ... 201
—, —, —, Heat capacity of some butadiene-styrene copolymers from 0° to 330° K, RP2610 ... 127
—, *R. P. Park,* Heat capacity, heats of fusion and vaporization, and vapor pressure of decaborane ($B_{10}H_{14}$), RP2627 ... 255

G

Gamma radiation, penetration through and deflection from barriers, RP2640 ... 343
Garfinkel, S. R., A. Werler, F. E. Jones, S. Hasegawa, A. Krinsky, A fast responding electric hygrometer, RP2606 ... 71
Gaseous halogen compounds, thermodynamic properties, RP2614 ... 147
Germanate and calcium aluminate glasses, infrared transmittance of, RP2625 ... 231
Gilchrist, R., W. S. Clabaugh, R. T. Leslie, Preparation of titanium tetrachloride of high purity, RP2628 ... 261
Glass, photoresist for etching designs in, RP2612 ... 139
Glass used in paper manufacture, RP2599 ... 1
Glasses, calcium aluminate and germanate, infrared transmittance, RP2625 ... 231
Glaze, F. W., J. M. Florence, M. H. Black, Infrared transmittance of some calcium aluminate and germanate glasses, RP2625 ... 231
Goldstein, J. M., G. T. Armstrong, D. E. Roberts, Liquid-vapor phase equilibrium in solutions of oxygen and nitrogen at pressures below one atmosphere, RP2629 ... 265

H

Haar, L., J. C. Bradley, A. S. Friedman, Ideal gas thermodynamic functions of the isotopic hydrogen sulfides, RP2631 ... 285
Halogen compounds, gaseous, thermodynamic properties, RP2614 ... 147
Harman, A. W., G. T. Furukawa, R. E. McCoskey, M. L. Reilly, Heat capacity; heats of fusion, vaporization, and transition; and vapor pressures of *N*-dimethylaminodiborane, $(CH_3)_2NB_2H_5$, RP2620 ... 201
Hasegawa, S., A. Werler, S. R. Garfinkel, F. E. Jones, A. Krinsky, A fast responding electric hygrometer, RP2606 ... 71

Page

Heat capacity, heats of fusion and vaporization, and vapor pressure of decaborane, RP2627 ... 255
Heat capacity; heats of fusion, vaporization, and transition; and vapor pressure of *N*-dimethylaminodiborane, $(CH_3)_2NB_2H_5$, RP2620 ... 201
Heat capacity of some butadiene-styrene copolymers from 0° to 330° K, RP2610 ... 127
Heats of combustion of liquid *n*-hexadecane, l-hexadecene, *n*-decylbenzene, *n*-decylcyclopentane, and the variation of heat of combustion with chain length, RP2638 ... 329
l-Hexadecene, heat of combustion of, RP2638 ... 329
n-Hexadecane, heat of combustion of, RP2638 ... 329
Hidnert, P., R. K. Kirby, Thermal expansion and phase transformations of low-expanding cobalt-iron-chromium alloys, RP2602 ... 29
Hoffman, J. D., C. E. Weir, Compressibilities of long-chain normal hydrocarbons, RP2634 ... 307
Horowitz, E., M. Tryon, J. Mandel, Determination of natural rubber in GR–S—natural rubber vulcanizates by infrared spectroscopy, RP2623 ... 219
Hubbard, D., M. J. O'Leary, Some properties of a glass used in paper manufacture, RP2599 ... 1
Hydrocarbons, long-chain normal, compressibilities, RP2634 ... 307
Hydrogen sulfides, isotopic, ideal gas thermodynamic functions, RP2631 ... 285
Hygrometer, electric, fast responding, RP2606 ... 71

I

Ideal gas thermodynamic functions of the isotopic hydrogen sulfides, RP2631 ... 285
Infrared absorption and emission spectra of carbon monoxide in the region from 4 to 6 microns, RP2617 ... 183
Infrared spectroscopy determination of natural rubber in vulcanizates, RP2623 ... 219
Infrared transmittance of some calcium aluminate and germanate glasses, RP2625 ... 231
Infrared wavelength spectra, RP2630 ... 279
Iodine, thermodynamic properties of, RP2614 ... 147
Ionization chambers, free-air, measurement of field distortion, RP2632 ... 291

J

Jacobson, R., W. H. Evans, T. R. Munson, D. D. Wagman, Thermodynamic properties of the alkali metals, RP2608 ... 83
Jaffe, B., R. S. Roth, S. Marzullo, Properties of piezoelectric ceramics in the solid-solution series lead titanate-lead zirconate-lead oxide: tin oxide and lead titanate-lead hafnate, RP2626 ... 239
Jessup, R. S., A new Bunsen-type calorimeter, RP2636 ... 317
Jones, F. E., A. Wexler, S. P. Carfinkel, S. Hasegawa, A. Krinsky, A fast responding electric hygrometer, RP2606 ... 71

K

Kanagy, J. R., Specific heats of collagen and leather, RP2618 ... 191
Kennedy, R. J., W. Miller, Measurement of field distortion in free-air ionization chambers by analog method, RP2632 ... 291
Kessler, K. G., W. F. Meggers, Arc and spark spectra of ruthenium, RP2609 ... 97
Kirby, R. K., P. Hidnert, Thermal expansion and phase transformations of low-expanding cobalt-iron-chromium alloys, RP2602 ... 29
Krinsky, A., A. Wexler, S. P. Carfinkel, F. E. Jones, S. Hasegawa, A fast responding electric hygrometer, RP2606 ... 71

L

Lead titanate-lead zirconate-lead oxide, properties of piezoelectric ceramics in the solid-solution series, RP2626 ... 239
Leather and collagen, specific heats of, RP2618 ... 191
Lenses, spectacle, measuring marginal powers of, RP2607 ... 79
Leslie, R. T., W. S. Clabaugh, R. Gilchrist, Preparation of titanium tetrachloride of high purity, RP2628 ... 261
Liquid-vapor phase equilibrium in solutions of oxygen and nitrogen at pressures below one atmosphere, RP2629 ... 265
Lithium, thermodynamic properties of, RP2608 ... 83
Lopez-Gonzalez, J., F. C. Carpenter, V. R. Deitz, Adsorption of nitrogen on carbon adsorbents at low pressures between 69° and 90° K, RP2600 ... 11
Low-extanding alloys, thermal expansion and phase transformations, RP2602 ... 29
Low-temperature adsorption of nitrogen, RP2600 ... 11

M

Madorsky, S. L., S. Straus, Thermal degradation of polychlorotrifluoroethylene, poly-α, β, β-trifluorostyrene, and poly-*p*-xylylene in a vacuum, RP2624 ... 223
Mandel, J., M. Tryon, E. Horowitz, Determination of natural rubber in GR–S—natural rubber vulcanizates by infrared spectroscopy, RP2623 ... 219
Mandelkern, L., C. J. Newton, D. E. Roberts, Preferred orientation in stark rubber, RP2613 ... 143
Marginal powers of spectacle lenses, measuring, RP2607 ... 79
Marzullo, S., B. Jaffe, R. S. Roth, Properties of piezoelectric ceramics in the solid-solution series lead titanate-lead zirconate-lead oxide: tin oxide and lead titanate-lead hafnate, RP2626 ... 239
Mass spectra of thermal degradation products of polymers, RP2637 ... 323
McCoskey, R. E., G. T. Furukawa, M. L. Reilly, A. W. Harman, Heat capacity; heats of fusion, vaporization, and transition; and vapor pressure of *N*-dimethylaminodiborane, $(CH_3)_2NB_2H_5$, RP2620 ... 201
—, —, —, Heat capacity of some butadiene-styrene copolymers from 0° to 330° K, RP2610 ... 127
McCrackin, F. L., J. C. Smith, H. F. Schiefer, Stress-strain relationships in yarns subjected to rapid impact loading: 3. Effect of wave propagation, RP2601 ... 19
Measurement of wavelengths in infrared spectra, RP2630 ... 279
Meggers, W. F., K. G. Kessler, Arc and spark spectra of ruthenium, RP2609 ... 97
Metals, alkali, thermodynamic properties, RP2608 ... 83
Methanes, vapor pressure of, RP2603 ... 39

Page

Meyerson, M. R., S. J. Rosenberg, A study of the final stages of the austenite to martensite transformation in SAE 1050 steel, RP2616 ... 177
Miller, W., R. J. Kennedy, Measurement of field distortion in free-air ionization chambers by analog method, RP2632 ... 291
Mohler, F. L., P. Bradt, Mass spectra of thermal degradation products of polymers, RP2637 ... 323
Monte Carlo calculation of gamma ray diffusion by a collision-density method, RP2640 ... 343
Moore, C. E., H. N. Russell, First spectrum of barium, Ba I, RP2633 ... 299
Munson, T. R., W. H. Evans, R. Jacobson, D. D. Wagman, Thermodynamic properties of the alkali metals, RP2608 ... 83
—, —, *D. D. Wagman*, Thermodynamic properties of some gaseous halogen compounds, RP2614 ... 147

N

National Bureau of Standards neutron standard, absolute calibration:
RP2605 ... 63
RP2635 ... 311
Negative-ion-photodetachment cross-section and affinity measurements, atomic, RP2615 ... 165
Nelms, A. T., I. Oppenheim, Data on the atomic form factor: Computation and survey, RP2604 ... 53
Neutron standard, National Bureau of Standards, absolute calibration:
RP2605 ... 63
RP2635 ... 311
Newton, C. J., L. Mandelkern, D. E. Roberts, Preferred orientation in stark rubber, RP2613 ... 143
Niobia-titania and niobia-zirconia systems, phase equilibrium relations in, RP2621 ... 209
Nitrogen, adsorption of, on carbon adsorbents at low pressures, RP2600 ... 11
Nitrogen, binary solution with oxygen, RP2629 ... 265

O

O'Leary, M. J., D. Hubbard, Some properties of a glass used in paper manufacture, RP2599 ... 1
Oppenheim, I., A. T. Nelms, Data on the atomic form factor: Computation and survey, RP2604 ... 53
Orientation in stark rubber, RP2613 ... 143
Oxygen, binary solution with nitrogen, RP2629 ... 265

P

Padgett, D. W., J. A. De Juren, L. F. Curtiss, Absolute calibration of the National Bureau of Standards photoneutron standard: I., RP2605 ... 63
Paper manufacture, glass used in, RP2599 ... 1
Park, F. P., G. T. Furukawa, Heat capacity, heats of fusion and vaporization, and vapor pressure of decaborane ($B_{10}H_{14}$), RP2627 ... 255
*p*H values of the Clark and Lubs buffer solutions at 25° C, RP2619 ... 197
Phase equilibrium, liquid-vapor, in solutions of oxygen and nitrogen, RP2629 ... 265
Phase equilibrium relations in the systems titania-niobia and zirconia-niobia, RP2621 ... 209
Phase transformation in SAE 1050 steel, RP2616 ... 177
Photoneutron standard, National Bureau of Standards, absolute calibration:
RP2605 ... 63
RP2635 ... 311
Photoresist for etching designs in glass, RP2612 ... 139
Piezoelectric ceramics, properties of, RP2626 ... 239
Plyler, E. K., L. R. Blaine, E. D. Tidwell, Infrared absorption and emission spectra of carbon monoxide in the region from 4 to 6 microns, RP2617 ... 183
—, —, —, Precise measurement of wavelengths in infrared spectra, RP2630 ... 279
Pole figures in orientation study in stark rubber, RP2613 ... 143
Poly-α, β, β-trifluorostyrene, thermal degradation in a vacuum, RP2624 ... 223
Polychlorotrifluoroethylene, thermal degradation in a vacuum, RP2624 ... 223
Polymers, thermal degradation products of, RP2637 ... 323
Poly-*p*-xylylene, thermal degradation in a vacuum, RP2624 ... 223
Pope, C. L., F. Davis, Development of a photoresist for etching designs in glass, RP2612 ... 139
Potassium, thermodynamic properties of, RP2608 ... 83
Prosen, E. J., F. M. Fraser, Heats of combustion of liquid *n*-hexadecane, l-hexadecene, *n*-decylbenzene, *n*-decylcyclohexane, *n*-decylcyclopentane, and the variation of heat of combustion with chain length, RP2638 ... 329

R

Rabinowitz, P., R. E. Trees, W. F. Cahill, Computation of atomic energy levels. The spectrum of singly-ionized tantalum, RP2639 ... 335
Radiation, gamma, reflection and transmission by barriers, RP2640 ... 343
Raleigh scattering: Data on the atomic form factor: computation and survey, RP2604 ... 53
Reilly, M. L., G. T. Furukawa, R. E. McCoskey, A. W. Harman, Heat capacity; heats of fusion, vaporization, and transition; and vapor pressure of *N*-dimethylaminodiborane, $(CH_3)_2NB_2H_5$, RP2620 ... 201
—, —, —, Heat capacity of some butadiene-styrene copolymers from 0° to 330° K, RP2610 ... 127
Resin, light-sensitive, used as a resist for etching, RP2612 ... 139
Roberts, D. E., G. T. Armstrong, J. M. Goldstein, Liquid-vapor phase equilibrium in solutions of oxygen and nitrogen at pressures below one atmosphere, RP2629 ... 265
—, *C. J. Newton, L. Mandelkern*, Preferred orientation in stark rubber, RP2613 ... 143
Rosenberg, S. J., M. R. Meyerson, A study of the final stages of the austenite to martensite transformation in SAE 1050 steel, RP2616 ... 177
Roth, R. S., L. W. Coughanour, Phase equilibrium relations in the systems titania-niobia and zirconia-niobia, RP2621 ... 209
—, *B. Jaffe, S. Marzullo*, Properties of piezoelectric ceramics in the solid-solution series lead titanate-lead zirconate-lead oxide: tin oxide and lead titanate-lead hafnate, RP2626 ... 239
Rubber, natural, in vulcanizates of GR–S and natural rubber, determination by infrared spectroscopy, RP2623 ... 219

Page

Rubber, stark, preferred orientation in, RP2613 143
Rubidium, thermodynamic properties of, RP2608 83
Russell, H. N., C. E. Moore, First spectrum of barium, Ba I, RP2633 299
Ruthenium, arc and spark spectra of, RP2609 97

S

SAE steel 1050, phase transformation, RP2616 177
Schiefer, H. F., J. C. Smith, F. L. McCrackin, Stress-strain relationships in yarns subjected to rapid impact loading: 3. Effect of wave propagation, RP2601 19
Scott, R. B., G. T. Armstrong, F. G. Brickwedde, Vapor pressures of the methanes, RP2603 39
Setting reaction of zinc oxide and eugenol, RP2611 133
Smith, J. C., F. L. McCrackin, H. F. Schiefer, Stress-strain relationships in yarns subjected to rapid impact loading: 3. Effect of wave propagation, RP2601 19
Smith, S. J., L. M. Branscomb, Atomic negative-ion-photodetachment cross-section and affinity measurements, RP2615 165
Sodium, thermodynamic properties of, RP2608 83
Spark and arc spectra of ruthenium, RP2609 97
Specific heats of collagen and leather, RP2618 191
Spectacle lenses, measuring marginal powers of, RP2607 79
Spectra, arc and spark, of ruthenium, RP2609 97
Spectra, atomic infrared, measurement of wavelengths, RP2630 279
Spectra, infrared absorption and emission, of carbon monoxide, RP2617 183
Spectroscopy, infrared, determination of natural rubber in vulcanizates, RP2623 219
Spectrum, first, of barium, RP2633 299
Spectrum of singly-ionized tantalum, RP2639 335
Standard neutron source, National Bureau of Standards, calibration: RP2605 63
RP2635 311
Stark rubber, preferred orientation in, RP2613 143
Steel, SAE 1050, study of final stages of the, RP2616 177
Straus, S., S. L. Madorsky, Thermal degradation of polychlorotrifluoroethylene, poly-α,β,β-trifluorostyrene, and poly-*p*-xylylene in a vacuum, RP2624 223
Stress-strain relationships in yarns subjected to rapid impact loading: 3. Effect of wave propagation, RP2601 19
Sweeney, W. T., H. I. Copeland, Jr., G. M. Brauer, A. F. Forziati, Setting reaction of zinc oxide and eugenol, RP2611 133
Synthesis of a fluoro talc and attempted synthesis of fluoro chrysotile and fluoro anthophyllite, RP2622 215

T

Talc, fluoro, synthesis, RP2622 215
Tantalum, spectrum of singly-ionized, RP2639 335
Tetrachloride, titanium, high-purity preparation, RP2626 239
Textile yarns, rapid impact testing of, RP2601 19
Thermal degradation of polychlorotrifluoroethylene, poly-α,β,β trifluorostyrene, and poly-*p*-xylylene in a vacuum, RP2624 223
Thermal degradation products of polymers, mass spectra of, RP2637 323
Thermal expansion and phase transformations of low-expanding cobalt-iron-chromium alloys, RP2602 29
Thermodynamic functions, ideal gas, of the isotopic hydrogen sulfides, RP2631 285
Thermodynamic properties of decaborane, RP2627 255
Thermodynamic properties of N-dimethylaminodiborane, RP2620 201

Page

Thermodynamic properties of *n*-hexadecane, 1-hexadecene, *n*-decylbenzene, *n*-decylcyclohexane, and *n*-decylcyclopentane, RP2638 329
Thermodynamic properties of some gaseous halogen compounds, RP2614 147
Thermodynamic properties of the alkali metals, RP2608 83
Thermomolecular diffusion of nitrogen, RP2600 11
Tidwell, E. D., E. K. Plyler, L. R. Blaine, Infrared absorption and emission spectra of carbon monoxide in the region from 4 to 6 microns, RP2617 183
—, —, —, Precise measurement of wavelengths in infrared spectra, RP2630 279
Tin oxide and lead titanate-lead hafnate, properties of piezoelectric ceramics in the solid-solution series, RP2626 239
Titanate-lead zirconate-lead oxide, properties of piezoelectric ceramics in the solid-solution series, RP2626 239
Titania-niobia and zirconia-niobia systems, phase equilibrium relations in, RP2621 209
Titanium tetrachloride of high purity, preparation, RP2628 261
Transformation, phase, of SAE 1050 steel, RP2616 177
Trees, R. E., W. F. Cahill, P. Rabinowitz, Computation of atomic energy levels. The spectrum of singly ionized tantalum, RP2639 335
Tryon, M., E. Horowitz, J. Mandel, Determination of natural rubber in GR-S—natural rubber vulcanizates by infrared spectroscopy, RP2623 219

V

Van Valkenburg, A., Jr., Synthesis of a fluoro talc and attempted synthesis of fluoro chrysotile and fluoro anthophyllite, RP2622 215
Vapor pressure and thermodynamic properties of *N*-dimethylaminodiborane, RP2620 201
Vapor pressure of decaborane, RP2627 255
Vapor pressure of oxygen and nitrogen solutions, RP2629 265
Vapor pressures of the methanes, RP2603 39
Vulcanizates, infrared spectroscopy determination of natural rubber in, RP2623 219

W

Wagman, D. D., W. H. Evans, R. Jacobson, T. R. Munson, Thermodynamic properties of the alkali metals, RP2608 83
—, —, *T. R. Munson*, Thermodynamic properties of some gaseous halogen compounds, RP2614 147
Washer, F. E., A simplified method of measuring the marginal powers of spectacle lenses, RP2607 79
Wavelengths in infrared spectra, precise measurement, RP2630 279
Weir, C. E., J. D. Hoffman, Compressibilities of long chain normal hydrocarbons, RP2634 307
Werler, A., S. B. Garfinkel, F. E. Jones, S. Hasegawa, A. Krinsky, A fast responding electric hygrometer, RP2606 71

Y

Yarns, stress-strain relationships in, RP2601 19

Z

Zinc oxide and eugenol, setting reaction of, RP2611 133
Zirconate-lead titanate-lead oxide, properties of piezoelectric ceramics in the solid-solution series, RP2626 239
Zirconia-niobia and titania-niobia systems, phase equilibrium relations in, RP2621 209

Recent Publications of the National Bureau of Standards

Journal of Research of the National Bureau of Standards, volume **55**, No. 4, October 1955 (RP2617 to RP2625, incl.). 60 cents. Annual subscription $4.00.

Technical News Bulletin, volume **39**, No. 10, October 1955. 10 cents. Annual subscription $1.00.

Basic Radio Propagation Predictions for January 1956. Three months in advance. CRPL 134. Issued October 1955. 10 cents. Annual subscription $1.00.

Research Papers

*Journal of Research, volume **55**, No. 4, October 1955. Single copies of the Journal vary in price. Single copies of Research Papers appearing in the Journal are not available for sale. The Superintendent of Documents, U. S. Government Printing Office, Washington 25, D. C., will reprint 100 or more copies of a Research Paper. Request for the purchase price should be mailed promptly to that office.*

RP2617. Infrared absorption and emission spectra of carbon monoxide in the region from 4 to 6 microns. Earle K. Plyer, Lamdin R. Blaine, and Eugene D. Tidwell.

RP2618. Specfic heats of collagen and leather. Joseph R. Kanagy.

RP2619. *p*H values of the Clark and Lubs buffer solutions at 25° C. Vincent E. Bower and Roger G. Bates.

RP2620. Heat capacity; heats of fusion, vaporization, and transition; and vapor pressure of *N*-dimethylaminodiborane, $(CH_3)_2NB_2H_5$. George T. Furukawa, Robert E. McCoskey, Martin L. Reilly, and Ann W. Harman.

RP2621. Phase equilibrium relations in the systems titania-niobia and zirconia-niobia. R. S. Roth and L. W. Coughanour.

RP2622. Synthesis of a fluoro talc and attempted synthesis of fluoro chrysotile and fluoro anthophyllite. Alvin Van Valkenburg, Jr.

RP2623. Determination of natural rubber in GR–S—natural rubber vulcanizates by infrared spectroscopy. Max Tryon, Emanuel Horowitz, and John Mandel.

RP2624. Thermal degradation of polychlorotrifluoroethylene, poly-α,β,β-trifluorostyrene, and poly-*p*-xylylene in a vacuum. S. L. Madorsky and S. Straus.

RP2625. Infrared transmittance of some calcium aluminate and germanate glasses. Jack M. Florence, Francis W. Glaze, and Mason H. Black.

Circulars

C557. Worldwide radio noise levels expected in the frequency band 10 kilocycles to 100 megacycles. W. Q. Crichlow, D. F. Smith, R. N. Morton, and W. R. Corliss. 30 cents.

C565. Techniques for ruling and etching precise scales in glass and their reproduction by photoetching with a new light-sensitive resist. Raymond Davis and Chester I. Pope. 30 cents.

Publications in Other Journals

Indentation pressure of a smooth circular punch. E. Levin. Quart. Appl. Math. (Brown University, Providence 12, R. I.) **13**, No. 2, 133 (July 1955).

High-stability bridge-balancing oscillator. P. G. Sulzer. Proc. IRE (1 E. 79th St., New York 21, N. Y.) **43**, No. 6, 701 (June 1955).

Oxygen chemisorption on carbon adsorbents. William V. Loebenstein and Victor R. Deitz. J. Phys. Chem. (1155 16th St. NW., Washington 6, D. C.) **59**, 481 (June 1955).

Oil-soaked felt-pad lubrication of ball bearings at high speed & high temperature. H. S. White, J. F. Swindells, and Harriet V. Belcher. Lubrication Eng. (343 S. Dearborn St., Chicago 4, Ill.) **11**, No. 3, 182 (May–June 1955).

Mechanism of material transport during sintering. Raymond F. Walker. J. Am. Ceram. Soc. (2525 N. High St., Columbus 2, Ohio) **38**, No. 6, 187 (June 1955).

Experimental cross section for photodetachment of electrons from H^- and D^-. Lewis M. Branscomb and Stephen J. Smith. Phys. Rev. (57 E. 55th St., New York 22, N. Y.) **98**, No. 4, 1028 (May 1955).

Pores in collagen and leather. R. R. Stromberg and M. Swerdlow. J. Am. Leather Chemists' Assoc. (Univ. of Cincinnati, Cincinnati 21, Ohio) **50**, No. 7, 336 (July 1955).

Observations on field exposures of enameled gas stoves. James R. Crandall. Proc. Porcelain Enamel Inst. (1145 19th St. NW., Washington 6, D. C.) p. 27, Forum **18** (1954).

Observations in abrasion testing. J. H. Giles, Jr. Proc. Porcelain Enamel Inst. (1145 19th St. NW., Washington 6, D. C.) p. 136, Forum **16** (1954).

On moments of order statistics from the Weibull distribution. J. Lieblein. Ann. of Math. Statistics (c/o K. J. Arnold, Michigan State College, East Lansing, Mich.) **26**, No. 2, 330 (June 1955).

Low-capacitance power supply, J. H. Reaves. Radio-Electronic Eng. (64 E. Lake St., Chicago 1, Ill.) **24**, No. 5, 16 (May 1955).

Publications for which a price is indicated are available only from the Superintendent of Documents, U. S. Government Printing Office, Washington 25, D. C. (foreign postage, one-third additional). Reprints from outside journals are not available from the National Bureau of Standards but can often be obtained from the publishers.

UNITED STATES
GOVERNMENT PRINTING OFFICE
DIVISION OF PUBLIC DOCUMENTS
WASHINGTON 25, D. C.

OFFICIAL BUSINESS

PENALTY FOR PRIVATE USE TO AVOID PAYMENT OF POSTAGE, $300

Journal of Research of the National Bureau of Standards Vol. 55, No. 6 December 1955

Contents

		Page
The first spectrum of barium, Ba I. Henry Norris Russell and Charlotte E. Moore.	RP2633	299
Compressibilities of long-chain normal hydrocarbons. C. E. Weir and J. D. Hoffman.	RP2634	307
Absolute calibration of the National Bureau of Standards photoneutron standard: II. Absorption in manganese sulfate. James De Juren and Jack Chin.	RP2635	311
A new Bunsen-type calorimeter. Ralph S. Jessup.	RP2636	317
Mass spectra of thermal degradation products of polymers. Paul Bradt and Fred L. Mohler.	RP2637	323
Heats of combustion of liquid *n*–hexadecane, 1–hexadecene, *n*–decylbenzene, *n*–decylcyclohexane, *n*–decylcyclopentane, and the variation of heat of combustion with chain length. Frances Maron Fraser and Edward J. Prosen.	RP2638	329
Computation of atomic energy levels: Spectrum of singly-ionized tantalum (Ta II). R. E. Trees, W. F. Cahill, and P. Rabinowitz.	RP2639	335
Reflection and transmission of gamma radiation by barriers: Monte Carlo calculation by a collision-density method. Martin J. Berger.	RP2640	343
Index to volume 55 (July to December 1955, Research Papers RP2599 to RP2640).		351

Single copies of the above Research Papers are not available for sale, but the Superintendent of Documents, U. S. Government Printing Office, Washington 25, D. C., will reprint 100 or more copies, and request for the purchase price should be mailed promptly to that Office.

[A list of recent NBS publications is given on page 3 of the cover.]

For sale by the Superintendent of Documents, U. S. Government Printing Office, Washington 25, D. C. Price 60 cents (single copy) Subscription price: $4 a year; $1.25 additional for foreign mailing. Single copies vary in price.

UNITED STATES GOVERNMENT PRINTING OFFICE, WASHINGTON : 1955